Influence of tubulin tyrosination on the localization of microtubule plus end tracking proteins and microtubule dynamics

Von der Fakultät für Lebenswissenschaften

der Technischen Universität Carolo-Wilhelmina

zu Braunschweig

zur Erlangung des Grades eines

Doktors der Naturwissenschaften

(Dr. rer. nat.)

genehmigte

D i s s e r t a t i o n

von **Marcin Lukasz Ura**
aus Sandomierz / Polen

1. Referent: Prof. Dr. Jürgen Wehland
2. Referent: Prof. Dr. Martin Korte
eingereicht am: 31.03.2010
mündliche Prüfung (Disputation) am: 30.06.2010

Druckjahr 2010

Vorveröffentlichungen der Dissertation

Teilergebnisse aus dieser Arbeit wurden mit Genehmigung der Fakultät für Lebenswissenschaften, vertreten durch den Mentor der Arbeit, in folgenden Beiträgen vorab veröffentlicht:

Tagungsbeiträge

Marco van Ham, Andreas Fischer, **Marcin Ura**, Christian Erck and Jürgen Wehland (2008). Analysis of the tubulin tyrosination cycle in TTL-deficient cells. *23rd FEBS/ECF Workshop "Mechanics and dynamics of the cytoskeleton", June 22nd – 26th, 2008, Potsdam.*

Marco van Ham, Andreas Fischer, **Marcin Ura** and Jürgen Wehland (2008). Tubulin modifications and cytoskeleton dynamics. *Grant evaluation of the DFG-Research Group FOR629: Molecular mechanism of cellular motility, October 15th, 2008, Hannover.*

Marco van Ham, Andreas Fischer**, Marcin Ura**, Christian Erck and Jürgen Wehland (2009). Analysis of the tubulin tyrosination cycle in TTL-deficient cells. *32nd Annual Meeting of the German Society for Cell Biology, March 24th – 27th, 2009, Konstanz.*

Marcin Ura, Influence of tubulin tyrosination on cell differentiation. *International Graduate School Workshop, April 26th, 2009*, *Technische Universitaet, Braunschweig*, short talk

Marco van Ham, Andreas Fischer, **Marcin Ura**, Marcus Gereke, Ramona Baier, Christian Erck and Jürgen Wehland (2009). Analysis of the tubulin tyrosination cycle in TTL-deficient cells. *49th Annual Meeting of the American Society for Cell Biology, December 5th – 9th, 2009, San Diego (USA).*

Marco van Ham, Andreas Fischer, **Marcin Ura**, Marcus Gereke, Ramona Baier, Christian Erck and Jürgen Wehland (2010). Analysis of the tubulin tyrosination cycle in TTL-deficient cells. *33rd Annual Meeting of the German Society for Cell Biology, March 10th – 13th, 2010, Regensburg.*

Moim rodzicom

To my parents

Table of contents

Table of figures

Table of tables

1. Abstract

In eukaryotic cells, microtubules are one of the components of the cytoskeleton and are involved in vital processes like migration, cell polarity, mitosis, differentiation and intracellular trafficking. Alpha-tubulin, one of the building blocks of microtubules, is subjected to the tubulin tyrosination / detyrosination cycle, in which the C-terminal tyrosine residue of this protein is removed by a not yet characterized tubulin carboxy peptidase and subsequently re-added by tubulin tyrosine ligase (TTL). In this study, the influence of tubulin tyrosination on the localization of proteins that are specifically localized to the growing microtubule plus ends, the so-called microtubule plus end tracking proteins (+TIPs) was analyzed. By using RNAi knock-down of +TIPs in mouse embryonic fibroblasts (MEFs), we found that depletion of one of the most prominent +TIPs (i.e. EB1) leads to a TTL-dependent dislocalization of the CAP-Gly domain-containing proteins CLIP-115 and CLIP-170 from the microtubule plus ends (MT +ends). CLIP-170, the best studied member of the CLIPs, was removed from microtubule plus ends in both TTL wild type and *TTL* knock-out cells upon EB1 knock-down. In contrast, CLIP-115, a close homolog of CLIP-170 lacking the C-terminal zinc-binding domain, was found to be dislocalized from microtubule plus ends only in wild type and not in TTL-deficient EB1-depleted cells. This distinct CLIP-115 behavior could be rescued when TTL was reconstituted in *TTL* knock-out EB1-depleted MEFs. The observed difference in CLIP-115 MT +end binding is not caused by the lack of the C-terminal domain, since CLIP-170 mutant proteins lacking this domain localized to MT +ends similarly in both wild type and TTL-deficient MEFs. Analysis of microtubule binding of CLIP-115/170 hybrid proteins pointed to a possible role of coiled coil region in the apparent difference in CLIP-115 binding to microtubules. Furthermore, TTL deficiency leads to changes in dynamics of microtubules. By using mCherry-α-tubulin a decrease in microtubule shrinking speed as wells as an increase in the time microtubule spent pausing and a decrease in the time microtubule spent growing was observed. In addition TTL-deficiency resulted in increased levels of RhoA activity and a decrease of Rac1 and Cdc42 activity. Finally, the lack of TTL did not show any influence on the expression level of the RhoA effector mDia1.

Taken together, this study shed more light on the molecular mechanisms how microtubule plus end tracking proteins localize to microtubules and contributed to better understanding the role of the TTL cycle in microtubule dynamics.

2. Introduction

2.1. Cytoskeleton and Microtubules

The cytoskeleton is involved in many critical cellular processes, such as cell migration, mitosis, cell polarity and intracellular trafficking. There are three cytoskeleton components in eukaryotic cells – actin filaments, intermediate filaments and microtubules (Fig. 1). Whereas intermediate filaments mostly confer strength and a mechanical stress resistance in a cell, actin filaments and microtubules adapt and maintain cell shape. The assembly of cytoskeletal networks occurs via incorporation of small building molecules into filamentous or tubular polymers. Intermediate filaments polymerize through assembly of antiparallel dimers into oligomers that generate apolar filaments. The assembly of actin filaments and microtubules, in contrast, occurs by a head-to-tail incorporation of actin and respectively αβ-tubulin dimers, that results in polar fibres that hydrolyze phosphate bonds of ATP on actin filaments or GTP on microtubules. The polarized nature and dynamic properties of these two cytoskeletal systems allow cells to generate asymmetry, which can be recognized for instance in structurally different ends of both actin- and microtubule polymers.

In this work I have focused on microtubules (MTs), which are important for widely different processes, such as mitosis, cell migration, intracellular trafficking and neuronal differentiation. MTs are hollow cylindric tubes built from of α- and β-tubulin heterodimers (Fig. 1 and 2). Under *in vitro* conditions, growing MTs exhibit different behaviors. They can either polymerize or depolymerize on each end and the net growth depends on free tubulin concentrations (5). Above a certain tubulin concentration microtubules polymerize until most of the tubulin is in the form of a polymer, whereas below this concentration they undergo a switch-like behaviour known as dynamic instability, e.g. switching between phases of growth and shrinkage (1-4, 15). The transition from growth to shrinkage is called “catastrophe”, whereas the switch from shrinkage to growth is called “rescue”.

Basic microtubule bulding blocks are composed of a very stable tubulin heterodimers. The αβ–tubulin heterodimers assemble into protofilaments which form a hollow fibre of polar parallel protofilaments. Helical pitch of the 12 nm radius together with the 8

nm-long repeat between α- and β-tubulin subunits creates a lattice seam along the microtubule filament (3 – 5).

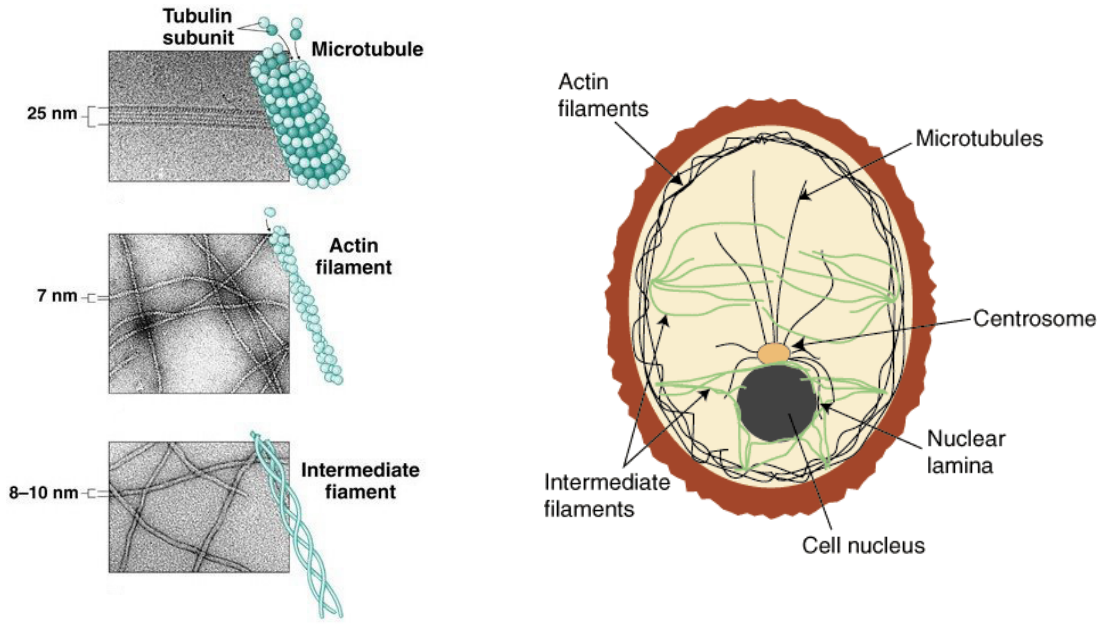

Figure 1. **Schematic representation and cellular distribution of the cytoskeleton.** Left panel – electron microscopic pictures and schematic drawings of three components of the cytoskeleton: microtubules, actin filaments and intermediate filaments, Right panel – intracellular organization of cytoskeleton in eukatyotic cells *(Adapted from the website available by following the enclosed links)*

Microtubule assembly and disassembly is a dynamic process that consumes and releases energy. It requires binding, hydrolysis and exchange of guanine nucleotide GTP on β-tubulin (note that GTP bound to α-tubulin is non-exchangeable and is not hydrolysed). GTP-β-tubulin is hydrolysed to GDP shortly after assembly and this is promoted by the locking of the partially exposed GTP nucleotide, as a result of the head-to-tail assembly of tubulin dimers (1, 3, 4). In this case, due to conformational changes, α-tubulin acts as a GTPase leading to GTP hydrolysis on the β-tubulin in the heterodimer (1, 3, 4). When the GTP dissociation rate is lower than a certain concentration of free GTP-β-tubulin, the addition of new GTP-β-tubulin subunits catches up and exceeds GTP dissociation leading to the formation of a so-called GTP-cap at the growing tip of the microtubule (1, 3, 4, 8). It has been postulated that GTP hydrolysis changes the conformation of the protofilament from a slightly curved GTP-tubulin to a more profoundly curved GDP-tubulin structure (6). This nucleotide-dependent, conformational model predicts that the curved GDP-tubulin stays straight

when it is part of the microtubule wall, thus growing microtubule sheets are believed to maintain the GTP-cap to stabilize straight tubulin conformation within the microtubule lattice. Under conditions when GTP-tubulin hydrolysis is higher than the cytoplasmic GTP-tubulin concentration, straight tubulin conformation is no longer maintained and the microtubule depolymerizes rapidly (1, 3, 4, 8).

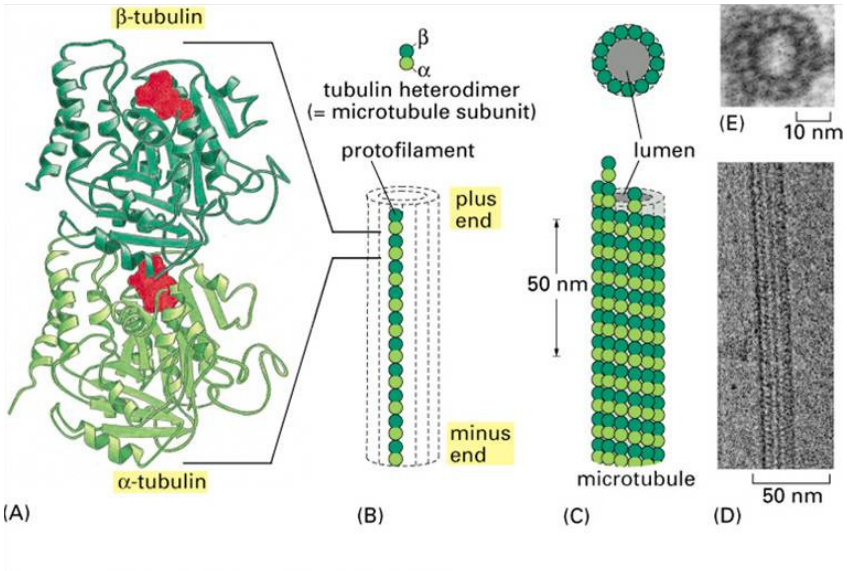

Figure 2. **Structural representation of a tubulin heterodimer and a microtubule filament.** α– and β-tubulin that bind GTP nucleotides (red) form stable heterodimers (A) that assemble in a head-to-tail fashion into protofilaments (B). 13 protofilaments build one microtubule (C). In panel (D) a transmission electron microscopic picture of an assembled microtubule is shown. (*Adapted from Molecular Biology Of The Cell, B. Alberts & others, 4th edition*)

Growing and shrinking microtubules, visualized by cryo-electron microscope have differently structured ends. Growing microtubules appear as curved sheets, whereas shrinking microtubules are characterized by fountain-like fraying arrays of protofilaments (9, 10, Fig. 3). When the assembled tubulin subunits are converted into GDP-tubulin, the new GTP-tubulin subunits can be incorporated at the plus end, so the already bound GDP-tubulin subunits undergo "treadmilling" through the microtubule (1, 3, 4, 8). Due to structural differences of both microtubule ends, rate constants that govern growth and shrinkage are different at the opposite ends. As a consequence, the addition of free tubulin subunits occurs preferentially at the plus end of microtubule. The minus end of microtubules is very often embedded in the

microtubule organizing centre (MTOC), a structure which is tightly linked to the centrosome (7) and prevents depolimerization from the minus end (8).

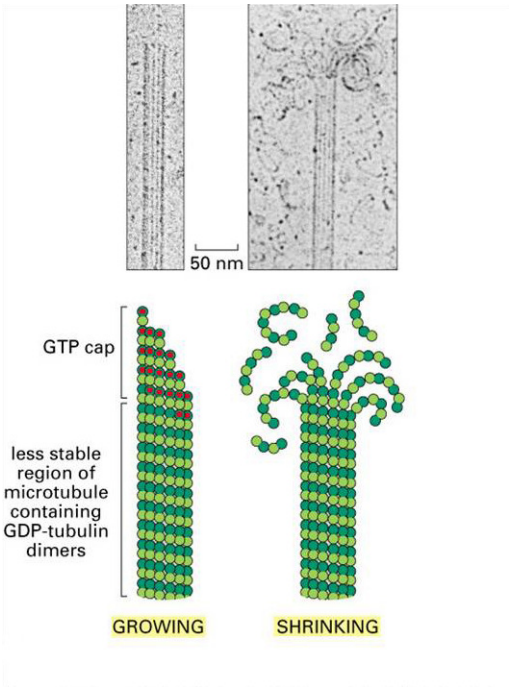

Figure 3. **Growing and shrinking microtubules.** Schematic structures (lower panels) and electron microscopic pictures (upper panel) of growing and shrinking microtubules. GTP bound tubulin (red) forms a GTP-cap which protects the microtubule from depolymerization. After loosing the GTP-cap, exposed GDP-bound tubulin leads to unstable polymer conformations resulting in microtubule depolymerization. (*Adapted from Molecular Biology Of The Cell, B. Alberts & others, 4th edition*)

An important component of the centrosome is γ-tubulin, which is an unusual form of tubulin, believed to initiate nucleation by forming rings that serve as templates for new microtubule growth (13, 14). If the minus end is not embedded, the dissociation of GDP-tubulin can take place also at these ends. Microtubules can be assembled in two structurally different polymers known as type A and B with different lateral contacts between the protofilaments. The typical lattice form, which is thought to be predominant in most of the cell types, is the B lattice containing lateral contacts of αα and ββ subunits resulting in one seam with αβ subunit contacts. There is however an increasing number of evidence showing that microtubule associated proteins could drive microtubules into the lattice A in which all lateral contacts are between αβ subunits (11).

2.2. Organization of cytoskeleton networks in different model systems

Microtubules in different model systems can be differently organized. This is related to unique cell morphologies in organisms varying from yeast to mammals. For instance in budding yeast, new daughter cells are formed from the mother cells at the so-called bud neck (Fig. 4a).

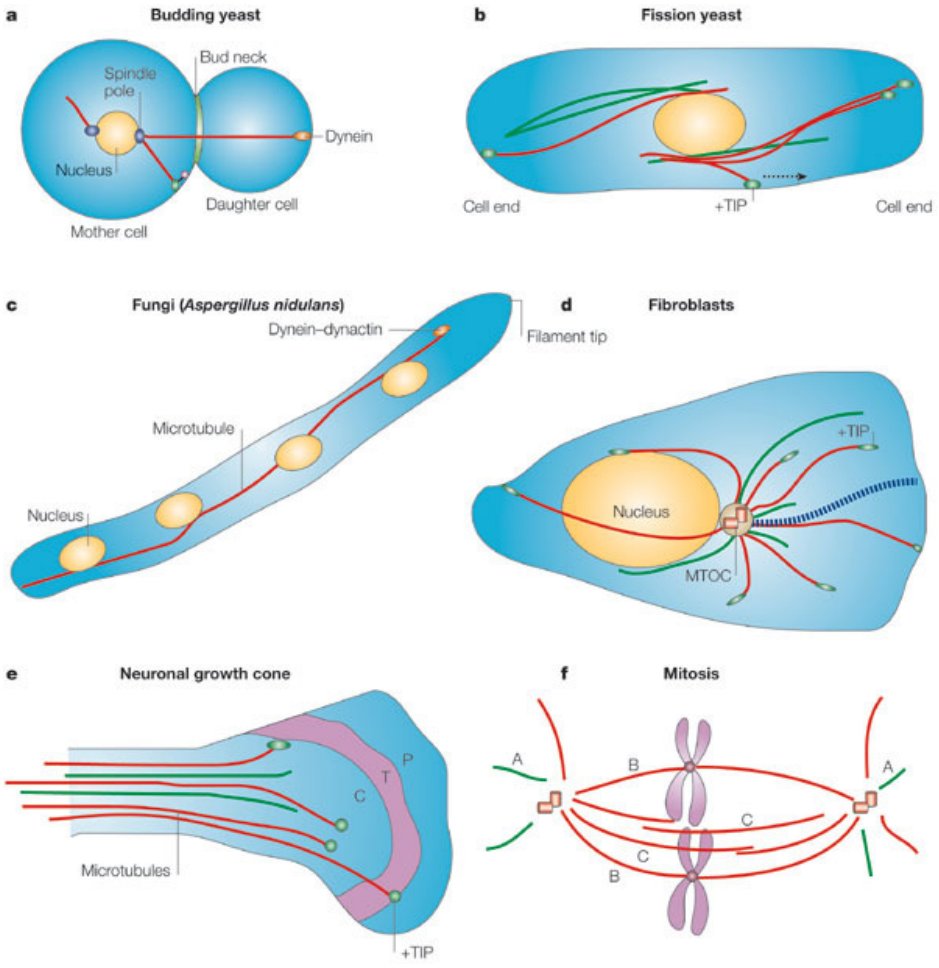

Figure 4. **Organization of microtubules in different model systems.** MTOC – microtubule organizing center, +TIP – microtubule plus end tracking proteins, C – central region, T – transition zone, P – peripheral region, A – astral microtubules, B – kinetochore microtubules, C – interpolar microtubules, growing microtubules shown in red, shrinking microtubules – green, stable microtubules – blue. For details see text. *(Adapted from Galjart 2005; Nature reviews, Molecular Cell Biology 6)*

Microtubules emanating from one spindle pole are guided by a Bim1-Kar9-myosin-dependent pathway into the bud. Dynein located at the microtubule plus end is important for "reeling in" the nucleus at the bud cortex (18). In fission yeast,

microtubule arrays grow out from the cell center (Fig. 4b). When microtubules approach the cell membrane, microtubule plus end tracking proteins (+TIPs) ensure that they grow until they reach the periphery of the cell, where they undergo catastrophe and shrink back (18).

Soil-born fungi such as *Aspergillus nidulans* represent a filamentous growth, meaning that in the multinucleated filament nuclei migrate towards the tip, in a process that depends on microtubules and the dynein-dynactin complex. Microtubules interconnect the nuclei along the entire length of the fungi filament and they reach the filament tip with their growing plus ends (18, Fig. 4c).

The polarity of migrating cells with a ruffling leading edge (e.g. the lamellipodium) and a contractile tail, is reflected by the polarized organization of the cytoskeleton. In most mammalian cells microtubules are usually arranged with the minus end located near the center of the cell or anchored at the MTOC, which is often positioned facing the leading edge. The plus ends of microtubules emanate radially towards the leading edge, where they explore the cell cortex (17, Fig. 4d). Actin filaments are arranged with growing plus "barbed" ends subadjacent to the plasma membrane and with the minus "pointed" ends directed towards the cell interior. In the lamellipodium, actin forms a dendritic network. In contrast, the tip of filopodium is devoid of microtubules and actin filaments are arranged in parallel bundles (19). Actin polymerization at the leading edge is balanced by a myosin-driven rearward movement of the lamellipodium actin network, called retrograde flow (20). Behind the lamellipodium, the actin meshwork moves in the direction of the cell front and creates so called "convergence zone" where retrograde and anterograde actin movements come across (21, 22) (Fig. 5). At this site, due to the presence of myosin-2, high contractility is observed (23) and actin filament disassembly prevails (21). To induce the movement of the cell, the traction through the contractile actin bundles is generated, which is accompanied by pulling on focal adhesion contacts attached to the substrate. Focal adhesions are then assembled at the cell front and disassembled at the rear-end of the cell (24).

Neurons are composed of the cell body, the axon and several shorter dendrites that all spread radially from the cell body. In dendrites the microtubules are organized in apolar bundles whereas in axons they are polar. The growth cones are formed at the tip of the axon and are divided into peripheral, transition and central regions (40). Microtubules emanate from the cell body through the axon and grow into the growth

cone (18, Fig. 4e). Large bundles of stable microtubules prevail in the central domain, whereas dynamic microtubules penetrate the peripheral region of the growth cone with their growing plus ends. The transition zone is located between the central and peripheral region and contains contractile actin bundles oriented perpendicular to filopodia. Like in migrating cells, actin retrograde flow occurs in lamellipodia at the leading edge of the growth cone (Fig. 6).

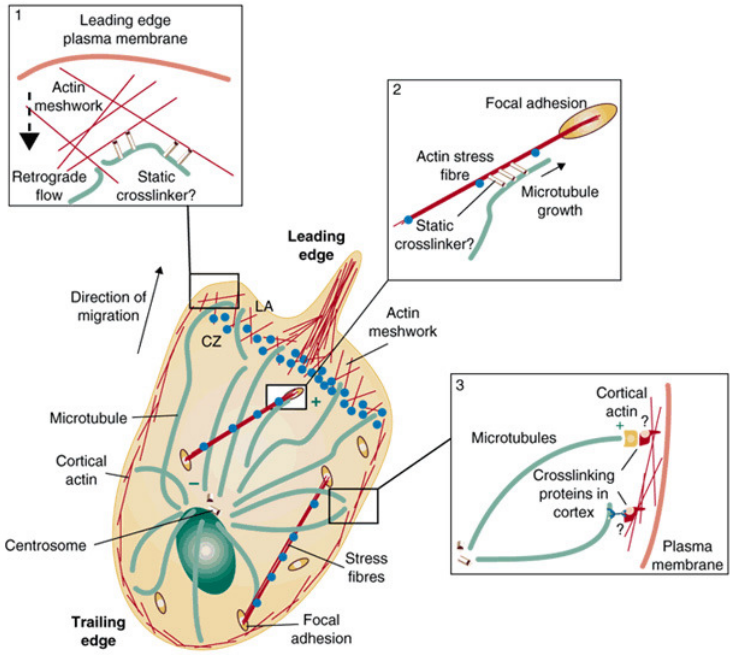

Figure 5. **Organization of microtubules and actin network in a migrating cell.** LA – lamellipodium, CZ – convergence zone. Microtubules shown in green, myosin – blue dots, F-actin – red. See text for details. *(Adapted from Rodriguez et al. 2003; Nature Cell Biology 5)*

Dynamic microtubules polymerize into the growth cone periphery where actin filaments serve as guides, along which microtubules grow into the growth cone extensions (41 – 43). Microtubules are at the same time cleared from the growth cone periphery by depolymerization or by coupling to actin retrograde flow, which enables microtubule turnover within the growth cone. Microtubles that are caught by the retrograde flow and move rearward, are very often buckled, they bend and finally break exposing unstable minus ends and new plus ends in the transition zone (41). Contractile actin bundles that predominate in the transition zone also interact with microtubules and by transverse movements, transport them into the central region of

the growth cone. The microtubules present in the transition zone are less dynamic than those associated with filopodia (21).

In dividing cells microtubules form the mitotic spindle which is composed of astral, kinetochore, and interpolar microtubules (Fig. 4f). Growing and shrinking microtubules can have various structures bound to their ends and this is thought to allow shrinking microtubules to exert forces on associated structures, such as kinetochores (12).

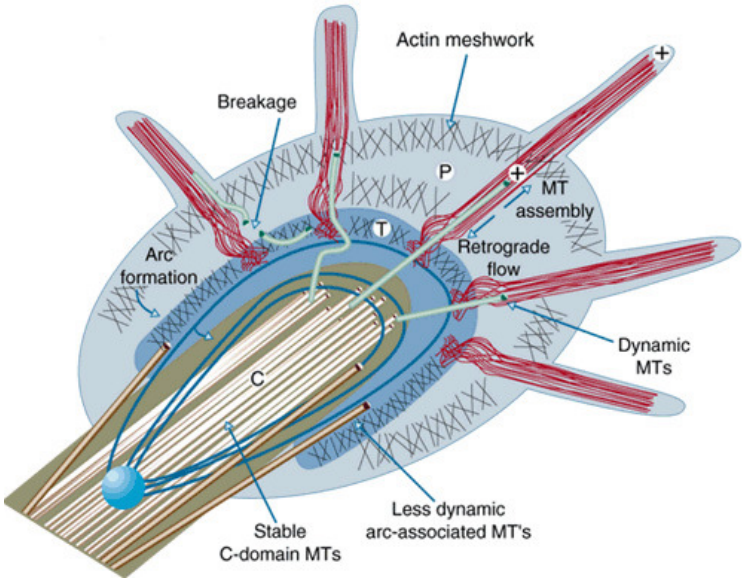

Figure 6. **Organization of microtubules and actin in the neuronal growth cone.** C-central region, T-transition zone, P-peripheral region. Filopodial parallel actin structures shown in red, actin meshwork in periphery – black, contractile actin bundles – blue, unbundled microtubules – green, less dynamic microtubules – brown, bundled microtubules – light brown. For details see text. *(Adapted from Rodriguez et al. 2003; Nature Cell Biology 5)*

Two microtubule asters that are organized by the sister MTOCs interlock themselves into an antiparallel array and connect with kinetochores on replicated sister chromosomes to separate them equally into daughter cells.

2.3. Interactions of microtubules with the actin cytoskeleton

In vitro and *in vivo* studies have already shown that in migrating cells the organization of microtubules is strongly influenced by the actin cytoskeleton. The first evidence came from the observation that microtubules are transported rearward in the lamella of the motile cells and that this is dependent on the actomyosin

machinery (25 – 27). Fluorescent Speckle Microscopy revealed that microtubules are coupled to actin retrograde flow in the lamella and to anterograde actin movement in the cell body (21, 23), and that microtubules can also grow along actin filaments and are often dragged through the cytoplasm by their connection to the moving actin bundles (21), (Fig. 5, panel 1). ACF7, a member of the spectraplakin family of cytoskeletal crosslinking proteins, that possesses both actin and microtubule binding domains, is proposed to be an essential integrator of microtubule-actin dynamics. Studies on ACF7 null endodermal cells showed that in the absence of ACF7 microtubules no longer grow along polarized actin bundles, nor do they pause and bind to actin-rich cortical sites (57). Microtubules can also target focal adhesions by crosslinking to and growing along focal adhesion associated actin bundles, leading to disassembly of focal adhesions, which is mediated by dynamin and focal adhesion kinase (FAK) (21, 44, Fig. 5, panel 2). The plus ends of microtubules might also be anchored at the cell cortex through the interactions between +TIPs and actin-binding proteins to orientate MTOC towards the direction of cell movement (Fig. 5, panel 3). Moreover, it is reported that MTOC reorientation is mediated by the small Rho GTPase, Cdc42 and the microtubule motor dynein. It has been suggested that microtubule plus ends are crosslinked to the actin cortex, at specific sites defined by Cdc42, leading to pulling forces and thereby moving the MTOC in front of the nucleus by cytoplasmic dynein (45 – 47).

Interactions between actin and microtubules can be controlled through diverse regulatory mechanisms. The mechanism involving the Rho family of small GTPases is so far best understood. RhoA for instance not only mediates the formation of contractile actin structures, the so-called stress fibres (28), but also promotes stabilization of microtubule sub-populations (29). Two key factors are known to act downstream of RhoA. One of them is Rho kinase, which promotes contractility by increasing phosphorylation of the regulatory light chain of myosin-2 (30). Secondly, mDia, a member of the formin protein family, promotes actin polymerization into bundles (31, 32) and additionally mediates microtubule stabilization (33). Specifically mDia1 appears as a coordinator of microtubules and the actin cytoskeleton. In HeLa cells it induces bipolar elongation, aligning microtubules in parallel to actin bundles along the longer axis of the cell (58). Another small GTPase, Rac1, also regulates both actin and microtubule polymerization, leading to promotion of lamellipodial protrusion (34, 35). Rac1 controls actin cytoskeleton dynamics through the

Scar/WASP protein pathway, which activates Arp2/3-dependent assembly of actin networks and through PAK kinases that regulate actin treadmilling on the leading edge via the ADF/cofilin pathway (30, 34, 35). PAK kinases can additionally promote microtubule growth by regulating the microtubule destabilizing protein Op18/stathmin (35, 36). Actin and microtubules can, in turn, also regulate the activity of small Rho GTPases. Microtubule and actin disassembly activates RhoA (37), whereas microtubule assembly stimulates Rac1 activity (38). Depolymerizing microtubules are believed to release the microtubule-bound Rho guanine nucleotide exchange factor (GEF) GEF-H1, which then activates RhoA (39). Although the pathway by which microtubule growth leads to Rac1 activation is still obscure, recent findings revealed the involvement of adenomatous polyposis coli (APC) protein in this process. APC protein is localized to growing microtubule ends in lamellipodial protrusions (49, 50) and binds the Rac1 specific GEF ASEF, which stimulates lamellipodia formation and cell migration (51, 52). Loss of APC results in disappearance of cellular protrusions and decreased cell migration (53). Another interesting candidate to mediate the microtubule growth-mediated Rac1 activation is IQGAP1, which forms a common complex together with Rac1, Cdc42, APC and actin and additionally binds to microtubule plus ends through CLIP-170 (54, 55). Moreover, disruption of the interactions between IQGAP1, Rac1 and Cdc42 leads to diminished lamellipodial activity (54).

2.4. Microtubules and intracellular transport

Due to their large size and complexity, eukaryotic cells need to ensure directional, effective transport and distribution of various kinds of cellular components to their proper destination in the cell. This is very important not only for cellular morphogenesis but also for proper targeting of organelles and proteins to distinct compartments within the cell, especially in highly polarized and differentiated cells, such as epithelial cells or neurons. Once assembled, polarized arrays of microtubules provide tracks for the transport of proteins, organelles and protein-containing vesicular cargoes (16). For this transport, eukaryotic cells use motor proteins that walk along microtubule tracks. There are two classes of microtubule associated motor proteins: kinesins (59) and dyneins (60). Kinesins (except for kinesin-14 family members) move in the direction of the microtubule plus end thereby ensuring anterograde transport which goes from the cell center to peripheral cellular regions.

All dyneins discovered so far move towards the microtubule minus end providing retrograde transport from the cell periphery to the cell interior.

Kinesins are present in all eukaryotic cells and are involved in fast axonal transport in neurons, in organization of the cytoplasm during interphase, in directional vesicle movement within the cell and in cell division. Kinesins are tetramers composed of two heavy and two light chains with typical molecular weights of ~ 110 – 130 and ~ 60 – 80 kDa, respectively (61). Kinesins are ATPases and most of them possess N-terminal motor domain that includes the ATP binding site and microtubule binding regions. They move towards microtubule plus ends with a velocity of about 1 μm/s making 8 nm long steps, that correspond to the spacing between tubulin dimers in protofilaments (62, 63). Some unconventional kinesins, like the above mentioned kinesin-14, have a C-terminal motor domains which enable minus end directed movement of the molecule (64). Finally, some kinesins do not move cargo but instead bind specifically to the microtubule plus ends resulting in microtubule destabilization (65).

Dyneins are microtubule motors that rely on energy from ATP hydrolysis to move along microtubules with velocities above 2 μm/s. The majority of vertebrate dyneins are axonemal motors involved in flagellar or ciliary movements, whereas the cytoplasmic dyneins are involved in retrograde transport of vesicles and organelles, mitotic spindle organization and chromosome segregation (60). Cytoplasmic dyneins move usually towards microtubule minus ends but they can also move laterally across the microtubule surface and even anterogradely. Dyneins consist of one to three heavy chains (~ 500 kDa), which possess the AAA-type ATPase motor domain and various intermediate domains and light chains. Although dyneins can directly interact with other proteins such as Lis1 (66), most of the interactions are mediated by accessory subunits. Dynein together with dynactin works as a part of a multiprotein complex, of which the main role is the orientation of the mitotic spindle and nuclear migration. Dynactin is a dynein cofactor, that increases dynein's processivity and is involved in most types of dynein activity (67). The dynein/dynactin complex has been resolved and showed to have the structure of a "shoulder-side arm", so that the "shoulder" provides binding to microtubules via the large dynactin subunit $p150^{Glued}$ and the "side arm" connects the entire complex to the transported vesicles (18).

2.5. Tubulin posttranslational modifications

In most eukaryotic cells, microtubules acquire several evolutionary conserved posttranslational modifications that principally affect the C-terminus of α-tubulin and in some cases β-tubulin. These modifications that include detyrosination, generation of Δ2-tubulin, acetylation, phosphorylation, palmitoylation, polyglutamylation and polyglycylation contribute to the generation of functional diversity of microtubules and may play a role in recruiting specific protein complexes. The precise generating mechanism and functional role of posttranslational modifications in regulation of microtubule structure are not yet fully understood, however it has been proven that most of these modifications occur on stable microtubules and they are thought to be involved in their stabilization.

2.5.1. Tyrosination / detyrosination

The reactions of tyrosination and detyrosination of microtubules are a part of the tyrosination / detyrosination cycle which is conserved in most eukaryotic cells (108, 109, Fig. 7). Since the C-terminal tyrosine is encoded by the α-tubulin messenger RNA, the primary modification in the tyrosination / detyrosination cycle to occur is α-tubulin detyrosiantion. This involves the enzymatic removal of the C-terminal tyrosine residue from α-tubulin by a so far poorly characterized tubulin tyrosine carboxypeptidase (TTCP) (110). Detyrosination takes place preferably on polymerized microtubules resulting in exposition of C-terminal glutamic acid on α-tubulin, that is often referred to as Glu-tubulin (111). Although the identity of the tubulin carboxypeptidase is still unknown, novel cytosolic carboxypeptidases have been identified. NNA1/CCP1 belongs to a family of six related genes and is present in tissues containing high amount of tubulin, such as testis and brain (112). Detyrosination seems to be important, as mice with deleted NNA1/CCP1 lack detyrosinated α-tubulin in the olfactory bulb and show degeneration of Purkinje cells. These mice also show notable movement disabilities (112).

The reverse reaction that converts soluble, depolymerized Glu-tubulin back to its tyrosinated status (Tyr-tubulin) is carried out by the tubulin tyrosine ligase (TTL), a globular monomeric enzyme with a molecular mass 43 kDa (113). TTL shows preference for free tubulin subunits and does not appear to tyrosinate tubulin within microtubules (114). *In vitro,* the enzyme can also catalyze the C-terminal

incorporation of phenyloalanine and modified tyrosines, such as fluoro- and iodo-tyrosine (133, 134). Purification of TTL was first described by Murofushi *et al.* (126) and after generation of monoclonal anti-TTL antibodies, sufficient amounts of the TTL enzyme were purified by immunoaffinity (113). Sequence analysis proved that TTL belongs to the group of glutathione-synthetase ADP-forming enzymes, which possess an ATP-dependent ligase activity (127). Interestingly, the TTL sequence appears to be present only in mammalian and trypanosome genomes, although detyrosination is widely spread among eukaryotes (115). In cell cultures Glu-tubulin is enriched in stable microtubules, whereas Tyr-tubulin is exclusively found in dynamic microtubules (119 – 121). Tubulin detyrosination however, is regarded to be rather a consequence and not the cause of microtubule stabilization (122). In cells with very long-lived microtubules, removal of the penultimate glutamic acid results in the formation of Δ2-tubulin, which is no longer a substrate for TTL and escapes the TTL cycle (116, 117). Since Δ2-tubulin is a marker for long-lived microtubules, stable Δ2-tubulin containing microtubules can principally be found in neurons but can also appear in cells lacking TTL activity (118). Furthermore, it has been described that most of the tyrosinated brain tubulin is polyglutamylated as well, and brain Δ2-tubulin is specifically polyglycylated suggesting a certain degree of coordination between distinct postranslational modifications (123).

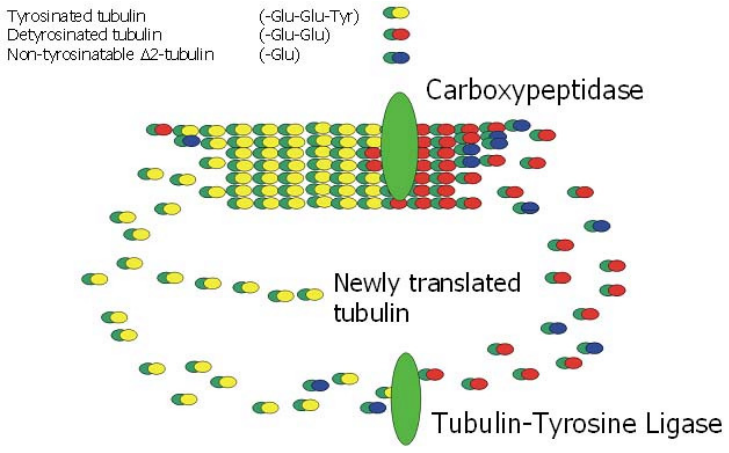

Figure 7. **The tubulin tyrosination / detyrosination cycle.** Newly translated tyrosinated tubulin dimers assembled in microtubules undergo detyrosiantion by a poorly characterized tubulin tyrosine carboxypeptidase (TTCP). After microtubule disassembly tubulin dimers are tyrosinated by tubulin tyrosine ligase (TTL). Δ2-tubulin, which additionally lacks the penultimate glutamic acid residue, can not be tyrosinated and escapes the cycle. *(Figure provided by Marco van Ham)*

Although a physiological significance of the tyrosination cycle has not been well demonstrated, in recent years some important functions of tubulin tyrosination have been discovered. In human and animal cancer models TTL happens to be often suppressed during tumor growth, giving an indication that TTL loss and tubulin detyrosination confers selective advantage for cancer cell proliferation (124). At least in mammals, TTL turns out to be essential for neuronal organization, as TTL suppression in mice leads to lethal disorganization of neuronal circuits (125). Brain anatomy investigation in TTL null mice showed blurring of cortical layers with a reduced number of cells in the cortical plate zone. Also a disruption of the cortico-thalamic loop in the brain of TTL null mouse embryos was noticed. This disruption most probably accounts for the early death of new-born mice. Accordingly, cultured TTL null neurons showed morphogenetic anomalies involving an accelerated and erratic time course of neurite and axon outgrowth, significantly higher axonal and neuritic growth rate, and premature axonal differentiation (125). It has also been published that tubulin tyrosination can have influence on different recruitment of microtubule plus end binding proteins (+TIPs) (see also chapter 2.6.). Proteins, such as CLIP-170, CLIP-115 and $p150^{Glued}$, +TIPs that contain a cytoskeleton-associated protein glycin-rich (CAP-Gly) microtubule binding domain, have been shown to be localized to the ends of tyrosinated microtubules but not to detyrosinated microtubules. The localization of other +TIPs, such as EB1, MCAK and CLASP2 was not affected by microtubule detyrosination. These changes in localization of +TIPs also correlated with defects in spindle positioning during cell division and with abnormal cell morphology during interphase (128). The tyrosination / detyrosination cycle is also reported to influence differential recruitment of the microtubule motor protein kinesin-1. It has been shown that kinesin-1 binds preferentially to detyrosinated microtubules and that this could enable a preferential movement of various cargoes, including vimentin filaments and transferin along detyrosinated microtubules (129 – 132). Very recently, tubulin tyrosination has been shown to drive motor-dependent microtubule disassembly. In fibroblasts, tubulin detyrosination inhibits MT disassembly and this inhibition is relieved by overexpression of the depolymerizing motor mitotic centromere-associated kinesin (MCAK). Suppression of MCAK expression prevents disassembly of tyrosinated microtbubules. Detyrosination of microtubules also suppresses MCAK activity *in vitro* (135). Some indications for the possible involvement of Glu-tubulin in the initiation of myogenic

differentiation are also apparent. Nitrotyrosine, which can also be incorporated into α-tubulin by TTL, has been used to suppress the detyrosiantion of microtubules and resulting in arrested differentiation of myoblasts into mytotubes (136 – 138). It is also proven that during muscle cell differentiation the plus end binding protein EB1, which is necessary for microtubule stabilization, is required for proper differentiation, elongation and fusion of myotubes (139). These processes are also accompanied by the appearance of Glu-tubulin in early events that precede differentiation, suggesting a possible role of stable microtubules in muscle differentiation processes (139, 140).

2.5.2. Glutamylation and glycylation

Glutamylation and glycylation occur both on α- and β-tubulin C-terminal ends (68, 69). Glutamylation is present in neurons, centriols, axonemes (cilia and flagella), and mitotic spindles, whereas glycylation prevails mostly in the axonemes. These two modifications can be present on the same C-terminal tail and a cross-talk between α- and β-tubulin tails that regulates the level and type of each modification is present (70, 71). Both modifications turned out to be reversible reactions, however, the enzymes responsible for the reverse reactions are poorly characterized.

In polyglutamylated microtubules, an up to 20 residues-long polyglutamylate side chain is added to the γ-carboxylate group of glutamate in the C-terminal tubulin tail via an isopeptide bond (72, 73). Biochemical studies have shown that polyglutamylation can involve multiple neighbouring amino acid residues (74, 75). The enzymes catalyzing tubulin glutamylation have been recently described. They belong to the tubulin tyrosine ligase-like (TTLL) family of enzymes containing a specific TTLL domain at the catalytic region, which is similar to the tubulin tyrosine ligase (TTL) domain. Some of the TTLL domain-containing enzymes have been reported to be glutamylases with different α- and β-tubulin specificities and different chain-initiating or chain-elongating activities (76 – 78). Many experiments have proven an essential role of polyglutamylation in the formation and maintenance of the axonemal structure (79). There is also an increasing number of evidence for polyglutamylation to influence the interactions between microtubules and microtubule associated proteins (MAPs). Kinesin and tau have been shown to exert stronger affinity for microtubules that are polyglutamylated with relatively short glutamic-acid side chains (80 – 82). Additionally centrioles in non-neuronal cells are

extensively polyglutamylated which has been found to occur on early stages of centriole genesis. Microinjection of specific antibodies recognizing polyglutamylated sites on microtubules in HeLa cells resulted in centriole disappearance and loss of the entire centrosome (83 – 84). These examples imply thus a main role of polyglutamylation in centriole maturation and stability.

In polyglycylated microtubules, similarly to polyglutamylation, a polyglycine side chain is covalently attached through an isopeptide bond to glutamate residues of the C-terminus of both α- and β-tubulin. This modification can involve the addition of an up to 34 glycine residue-long side chain and is mainly present in mammalian sperm tubulin (85, 86). Also, like in the case of polyglutamylation, multiple glutamate residues can be subjected to polyglycilation (87). The enzymes catalyzing polyglycylation are poorly described. Recently, it has been found that TTLL10, which is known as a polyglacylase for nucleosome assembly protein 1, can also perform tubulin glycylation (227). Another protein TTLL3 has also been identified as a tubulin glycine ligase which regulates the assembly of cilia (228). Polyglycylation occurs extensively and predominantly in axonemal tubulins in primitive eukaryotes, like *Tetrahymena*. This organism provided the most detailed functional analysis of polyglycylation so far. It has been shown that in this cialiate protozoa, polyglycylation is important for the axonemal organization, ciliary motility and cytokinesis (88).

2.5.3. Acetylation / deacetylation

Acetylation occurs only on the ε-amino group of the conserved lysine 40 residue at the N-terminus of α-tubulin (89, 90). This modification is present mostly in axonemal structures and on stable microtubules after microtubule assembly (91). Acetylation came into existence early during evolution and thus is present in most primitive eukaryotes. It is postulated, basing on electron-crystallographic structure, that the modified lysine residue resides on the luminal face of microtubules (92, 93). The enzyme which carries out the acetylation reaction has not been identified yet, however two enzymes have been shown to catalyze the reverse reaction both *in vivo* and *in vitro,* HDAC6 and SIRT2. HDAC6 belongs to the histone deacetylase family. SIRT2 has been described to play a role in transcriptional silencing in yeast. Knockdown of either HDAC6 or SIRT2 leads to hyperacetylation of tubulin,

suggesting an interdependence in action of each of them (94 – 96). There have been indications that acetylation is not essential for cell survival, however it has been proven that acetylation of α-tubulin plays a role in motor-based trafficking in mammals and that kinesin-1 binds with higher affinity to acetylated microtubules *in vitro* (97, 98). Acetylation is also suggested to be engaged in cell motility processes, as an overexpression of HDAC6 leads to increased chemotactic movement of NIH-3T3 cells and inhibition of HDAC6 abrogated cell migration (94, 99).

2.5.4. Other modifications

Phosphorylation

Tubulin phosphorylation is not wildely observed and its precise function is not well understood, however some indications for phosphorylation-dependent regulation of tubulins are noteworth. Phosphorylation of a serine residue in the C-terminus of β-tubulin has been reported to be essential in mouse neuroblastoma differentiation although the respective kinase at that time was unknown. Phosphorylation of class III β2-tubulin was accompanied by neurite outgrowth that depended on the level of phosphorylated β-tubulin in the polymer (100). β-tubulin can additionally be phosphorylated at serine 172 residue by Cdk1/cyclin B complex. This phosphorylation regulates the entry into mitosis (103). In B lymphocytes, a tyrosine residue in the C-terminus of α-tubulin is phosphorylated by the tyrosine kinase Syk, which is required for B-cell differentiation (101, 102). Several other kinases have been reported to phosphorylate tubulin *in vitro* but the physiological relevance of those events is so far unknown.

Palmitoylation

It has been shown that cysteine residue 376 on α-tubulin can incorporate radioactively labelled palmitate (105 – 107). It is suggested that palmitoylation could play a role in the positioning of astral microtubules and the interactions of microtubules with the cell cortex. Mutation of cysteine 376 to serine in the budding yeast *Saccharomyces cerevesiae* reduced the level of palmitoylation by 60% without affecting cell division, however some defects in the positioning of astral microtubules and an affected spindle translocation through the bud neck have been described (105 - 107).

Methylation

Recent mass spectrometry studies in the parasite *Toxoplasma gondii* have detected a novel posttranslational modification. Both α- and β-tubulins are C-terminally methylated which seems to be specific only for *T. gondii*, as this modification was not detected in the host cells (201).

2.6. Microtubule plus end tracking proteins

The dynamics and shape of microtubules are under control of multiple microtubules associated proteins (MAPs).

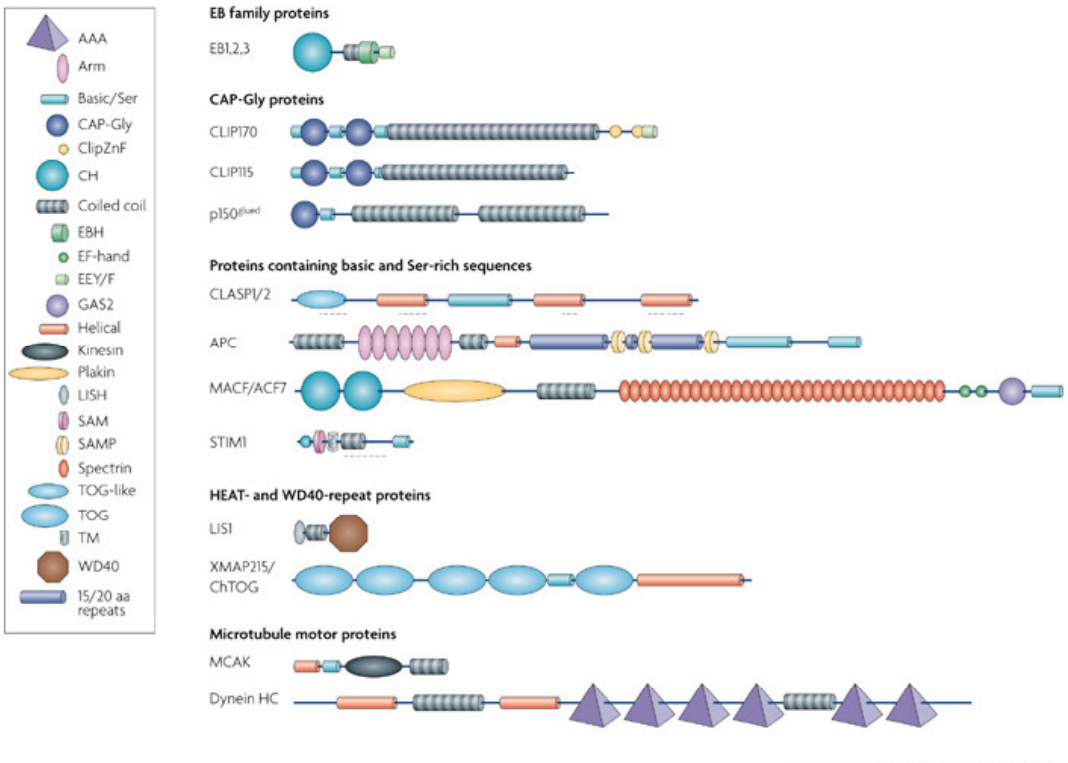

Figure 8. **Microtubule plus end tracking proteins (+TIPs).** Proteins are grouped according to structural elements involved in tracking microtubule plus ends. AAA – ATPase family associated with various cellular activities, Arm – armadillo repeats, Basic/Ser – basic/Serine-rich sequences, CAP-Gly – cytoskeleton associated protein Gly-rich domain, ClipZnF- C-terminal zinc binding domain, CH – calponin homology, EBH – end-binding protein homology, EF-hand – calcium binding motif, GAS2 – growth-arrest-specific protein-2 domain, LISH – Lis1 homology domain, SAM – sterile α motif domain, SAMP – Ser-Ala-Met-Pro repeat, TOG – tumour-overexpressed gene domain, TM – transmembrane domain, WD40 – motif of ~40 aminoacids, often terminating with Trp-Asp dipeptide. Predicted HEAT and TOR repeats in CLASP and ezrin-radixin-moesin domain of STIM1 are indicated by dotted lines. *(Adapted from Akhmanova & Steinmetz 2008; Nature reviews, Molecular Cell Biology)*

This large group of proteins embrace classic MAPs, which bind along the entire length of microtubules, such as molecular motors and non-motor proteins, and microtubule plus end tracking proteins (+TIPs). +TIPs are members of a family of evolutionary conserved and structurally unrelated proteins that specifically accumulate on the growing microtubules plus ends (Fig. 8).

+TIPs localize to a short stretch of the newly polymerized microtubule. They bind only weakly or are totally absent from the rest of the microtubule. All +TIPs possess characteristic structures and microtubule-binding regions (Fig. 8). They play roles in the regulation of microtubule dynamics, interactions of microtubules with the cell cortex and kinetochores, as well as in microtubule-mediated transport.

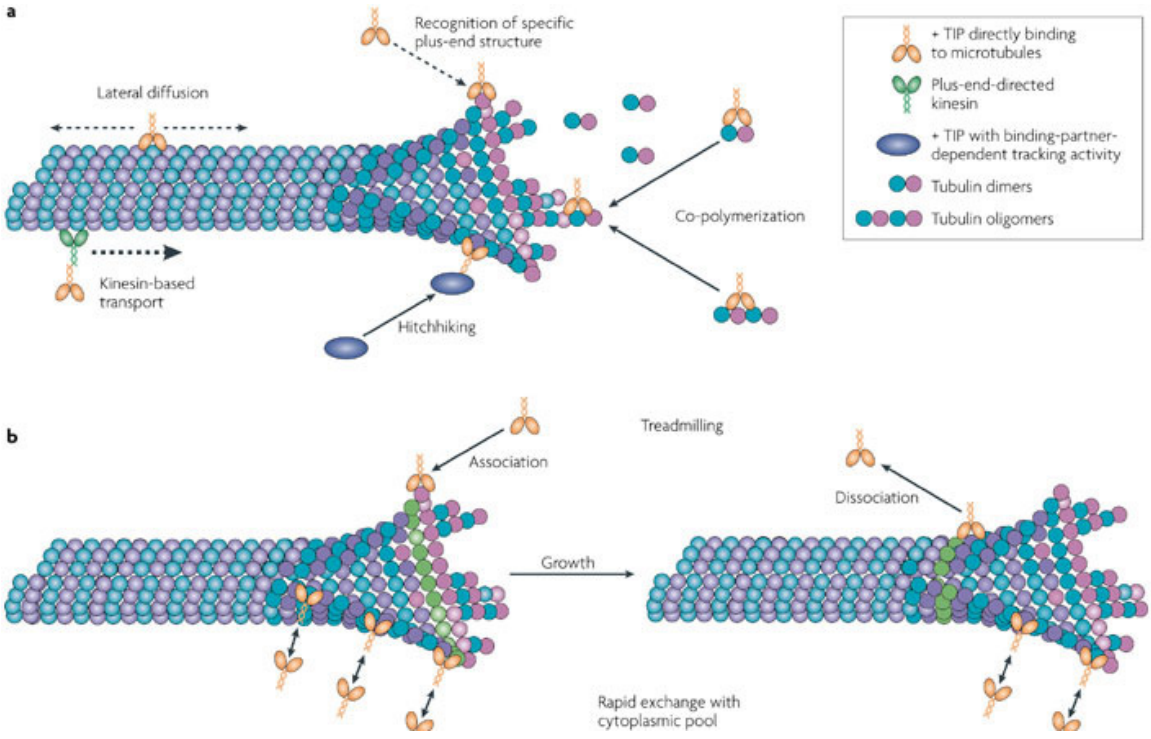

Figure 9. **Mechanisms of microtubule plus end tracking.** Schematic drawing of multiple mechanisms of microtubule plus end tracking: co-polymerization, lateral diffusion, kinesin based transport, hitchhiking and the recognition of specific structures are depicted in panel (a), treadmilling and the rapid exchange model are shown in (b). For details see text. *(Adapted from Akhmanova & Steinmetz 2008; Nature reviews, Molecular Cell Biology)*

Malfunction of these proteins leads to several human diseases, such as neurodevelopmental disorders and mental retardation. +TIPs, due to their specific

localization, turned out to be a useful tool for visualizing the dynamic behavior of microtubules in various cell types, like neurons and fibroblasts.

The molecular mechanisms leading to the specific targeting of +TIPs to growing microtubule plus ends and signaling pathways by which +TIPs regulate cellular dynamics are still poorly understood and are subject of intensive studies (196). The most current models predict that +TIPs recognize a specific structure at the growing microtubule end or copolymerize with tubulin (Fig. 9). After incorporation, +TIPs might be immobilized at the plus ends until the structure is shaped into the closed microtubule lattice and then +TIPs would be dissociated as microtubule treadmilling proceeds (152, see chapter 2.1.). Alternatively, +TIPs might undergo fast exchange at specific binding sites on microtubule ends. These binding sites would then disappear over time during microtubule lattice maturation (196, Fig. 9b).

There are different possibilities how +TIPs could reach the microtubule plus end. First, they could arrive at the plus ends by diffusion either in the cytoplasm or along the microtubule lattice. Secondly, +TIPs can be transported to microtubule plus ends by kinesins or by the other binding partners, a mechanism which is known as hitchkiking. Finally, +TIPs could also accumulate at the plus ends by co-polymerization with microtubule dimers or oligomers (152, Fig. 9a).

2.6.1. EB family of proteins

The evolutionary conserved EB family of end binding proteins encompasses three mammalian members EB1, EB2 (RP1), EB3. They share a conserved domain structure with high sequence homology and their orthologues are present in plants and fungi (141). All EB proteins play a common role in sustaining microtubule dynamics by increasing rescue frequencies and decreasing depolymerization rate, and the time microtubule spend pausing (142 – 144). Although functional analyses have been mostly restricted to EB1, it looks like distinct EBs can have different cellular functions. Recent findings proved that EB1 and EB3, but not EB2 promote persistent microtubule growth by suppressing catastrophes (145). Analysis of muscle cell differentiation pointed to a specific function of EB3 in regulation of microtubule dynamics at the cell cortex and its necessity for myoblast elongation and fusion (146). It has also been proven that the interactions discovered for EB1 can be replicated by EB3 but not EB2 (151).

EBs are small, dimeric proteins which contain an N-terminal calponin homology (CH) domain responsible for the interactions with microtubules (147), a linker region of unknown function, a C-terminal coiled coil domain required for dimerization (148, 149) and an acidic tail containing a C-terminal EEY/F sequence, which is important for autoinhibition and binding to various other partners (Fig. 8). The coiled coil domain of EBs partially overlaps with the unique EB1-like motif, which is referred to as the end-binding homology (EBH) domain (148, 149). Through a flexible C-terminal tail, which is strikingly similar to that of α-tubulin and CLIP-170, EB proteins can interact with almost all other known +TIPs recruiting them to growing microtubule plus ends (148 – 154).

EB1, which is the most detail studied member of the EB family was first identified as an APC interacting protein and was regarded as an accessory to APC function (155). When other interactions of EB1 emerged, it became clear that APC is rather one of many cofactors that competitively activate EB1 promoting microtubule growth and stability. Given the large variety of possible interactions between the C-terminus of EB1 and many other ligands, it is logical to place EB1 in the central core of the interactions with other +TIPs (48). Beside the microtubule growth promoting properties, EB1 has also been found to be involved in other cellular processes, such as cilia formation (156) and muscle cells differentiation (139, see chapter, 2.5.1.). The evolutionarily most conserved EB protein interactions take place during cell division. It is known that EB1 contributes to spindle positioning by capturing microtubules at the cell cortex (157, 158). EB1 is also involved in microtubule anchoring at the centrosome (159) and has been implicated in the interactions between microtubules and kinetochores (160). Reciprocal interactions between EB1, microtubules and other +TIPs will be described in detail in chapter 2.6.5.

2.6.2. Cytoskeleton-associated protein Gly-rich (CAP-Gly) proteins

CAP-Gly domain-containing proteins play an important role in many cellular processes including chromosome segregation, establishment and maintenance of cell polarity, intracellular transport, intracellular signaling and tumorgenesis. CLIP-170, CLIP-115 and the structurally related large subunit of the dynactin complex $p150^{Glued}$ contain a cytoskeleton-associated protein Gly-rich (CAP-Gly) domain at their N-terminus (Fig. 8). These domains mediate binding to both microtubules and EB

proteins (161, 162). Globular CAP-Gly domains are structures with a unique hydrophobic cavity encompassing ~ 80 highly conserved amino acid residues. This hydrophobic cavity contains the conserved GKNDG sequence motif and several characteristic glycine residues that are involved in shaping the loop of the globular fold of the CAP-Gly domain (154, 163). Both CLIPs and $p150^{Glued}$ contain flexible central coiled coil domains that mediate dimerization and allow intramolecular folding back of the protein (162). Furthermore, only CLIP-170 contains the C-terminal cargo-binding domain with two tandemly repeated zinc binding motifs and additionally a C-terminal EEY/F sequence with high similarity to that of EB1 and α-tubulin. Structural studies have shown that CLIP-170 can fold back on itself, owing to the intramolecular interaction between the N-terminal CAP-Gly domain and the C-terminal zinc-binding domain, creating a closed autoinhibitory conformation (162). By that mechanism, CLIP-170 can be protected from other interactions at its both ends. CLIP-115 lacks the C-terminal zinc-binding domain and therefore can not be folded into an inactive state. CLIP-170 and CLIP-115 share a high degree of homology, especially in the N-terminal part of the protein (164).

CLIP-170 is the first described and best studied member of the CAP-Gly proteins. The function of CLIP-170 was originally assigned as being a linker between endosomes and microtubules (165) and subsequently was identified as the first +TIP (166). Both CLIP-170 and CLIP-115 bind to microtubule plus ends through the interactions of the CAP-Gly domains with EB1 or EB3 (167, 150). CAP-Gly domains can also bind directly to microtubules via the C-terminal EEY/F motif of α-tubulin. CLIP-170 as well as CLIP-115 stabilize microtubules by preventing catastrophes and promoting rescue events (168, 169). CLIP-170 is additionally involved in the recruitment of the molecular motor dynein to the plus ends (Fig. 10). This recruitment depends on the dynactin complex, since the dynactin large subunit $p150^{Glued}$ binds to the C-terminal zinc-binding domain of CLIP-170 and additionally binds dynein (170). Furthermore, the zinc-binding domain of CLIP-170 also interacts with Lis1, a regulator of dynein function (173). CLIP-170 together with dynein is present at the kinetochores in dividing cells where the complex may play a role in microtubule capturing, since overexpression of the C-terminal part of CLIP-170 displaced the endogeneous protein from kinetochores and caused a delay in prometaphase (171, 172).

In addition to CLIP-170, CLIP-115 and p150^{Glued} there are also other, less known and not that well characterized CAP-Gly proteins. CLIP-related protein of 59 kDa (CLIPR-59) contains two CAP-Gly domains and a palmitoylation membrane-targeting motif at the C-terminus. CLIPR-59 binds to the trans-Golgi network and to the plasma membrane. It is involved in the trafficking from endosome to trans-Golgi and possibly regulates microtubule dynamics near certain membrane domains such as lipid rafts (174).

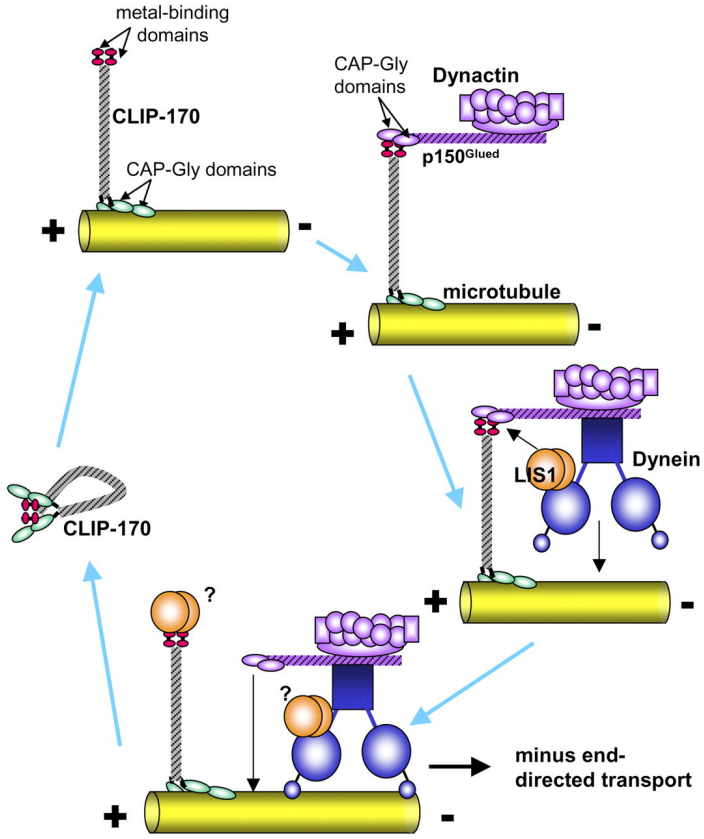

Figure 10. **A model showing the possible interactions between CLIP-170, dynactin, dynein, and LIS1 at the plus end of a growing MT.** Free CLIP-170 can adopt a folded conformation through an intramolecular interaction of its terminal domains. Binding to MTs correlates with the unfolding of CLIP-170, which allows the interaction via the COOH-terminal domain with its binding partners, such as p150^{Glued}, resulting in p150^{Glued}/dynactin recruitment to the MT +end. Dynactin can subsequently recruit cytoplasmic dynein and LIS1. LIS1 might act to release dynactin from the complex with CLIP-170, facilitating microtubule minus end-directed transport. LIS1 may remain associated with dynein or it may form a transient complex with CLIP-170. *(Adapted from Lansbergen et al. 2004; J. Cell Biol.)*

Another member of the CLIP family, CLIP-4 is poorly characterized and consists of three CAP-Gly domains and an ankyrin-repeat-like domains of unknown function

(175). Tubulin folding cofactors TBCB and TBCE are the most evolutionarily conserved CAP-Gly domain-containing proteins. They participate in tubulin dimer biogenesis and turnover, and their CAP-Gly domains are required for stable interactions with microtubules (176).

Also the deubiquitylating tumor-suppressor protein CYLD belongs to the CAP-Gly family of proteins. Through its C-terminal catalytic domain, CYLD hydrolyzes polyubiquitin chains on different proteins and in that way negatively affects NF-κB- and JNK kinase-dependent signaling (177). The role of two other CAP-Gly proteins, CAP350 and KIF13B, remains obscure. CAP350 is a large centrosomal protein with its single CAP-Gly domain mediating interaction with the Golgi network. CAP350 additionally stabilizes microtubules and is required for anchoring microtubules to the centrosomes (178). KIF13B is a kinesin-3 family member and is involved in the transport of the tumor suppressor protein disc large Dlg and PIP3-containing vesicles to microtubule plus ends (179).

2.6.3. Proteins containing basic/Serine-rich sequences

There are several large multidomain microtubule plus end binding proteins containing extensive sequence regions, enriched with basic and serine residues. These regions are predicted to be very flexible and very often mediate interactions with EB proteins and microtubules.

CLASP proteins

CLIP-associating proteins CLASPs are a group of microtubule associated proteins conserved in animals and fungi and were originally identified as interacting partners of CLIPs (180). CLASP1 is ubiquitously expressed in all tissues, whereas CLASP2 shows highest expression level in the brain. Both CLASPs are regulators of microtubule dynamics, bind dynamic microtubule plus ends and stabilize them by rescuing them from depolymerization (181). Domain analysis of CLASPs revealed the presence of several HEAT repeats (see chapter 2.6.4.) and a region which is rich in serine and arginine residues in the middle part of the protein responsible for interactions with EB1 and microtubules (18, Fig. 8). The HEAT repeat is located in the N-terminal domain which is similar to the Dis1/TOG family of microtubule stabilizing proteins. The C-terminal region of both CLASPs is required for the interaction with CLIPs, the Golgi-network and the cell cortex (18). CLASP proteins

play an essential role in cell division. For instance, CLASP1 is an important component of the kinetochore where it regulates spindle microtubule dynamics (182). CLASPs also participate in generating polarized microtubule arrays in interphase cells (180). CLASPs can bind directly to microtubules as well as to CLIP-170 and EB1 (180, 181) and these interactions contribute to the localization of CLASPs at the microtubule plus ends. CLASPs association with microtubules is spatially regulated. In migrating fibroblasts, CLASPs specifically bind to the microtubule plus ends in cortical patches close to the leading edge (180, 184). In epithelial cells, CLASPs bind to the MT +ends in the cell body and they also bind preferentially to microtubules in the lamella, decorating the entire length of the microtubule lattice. The MT +end binding of CLASP in cell body is independent of the microtubule lattice-localization of CLASP in the lamella (183). Glycogen synthase kinase 3β (GSK3β) acting downstream of Rac1 appears to be a key regulator in binding of CLASPs to microtubules (180, 183). GSK3β disrupts the CLASP microtubule association by phosphorylation of CLASPs (180, 183). Recent studies in HeLa cells have revealed that microtubule plus ends can be attached to the cell cortex via CLASPs with the help of LL5β and ELKS in a process that is controlled by phosphatidylinositol-triphosphate PIP3 (56).

APC proteins

Another prominent example of a basic/Serine-rich sequence-containing protein is the adenomatous polyposis coli (APC) tumor suppressor (see chapter 2.3.). APC is a large multidomain protein implicated in colorectal cancer. Due to truncation mutations that delete large region of the C-terminus of APC, deregulation of Wnt signaling and disrupted cell proliferation is evident (185). APC is also involved in microtubule organization. Loss of APC results in defects in chromosome segregation and defects in parallel organization of microtubule arrays (186, 187). The N-terminal part of the molecule contains heptad repeats predicted to form coiled coil domains involved in oligomerization (190, 192). These heptad repeats contain characteristic armadillo repeats, responsible for interactions with many proteins including the regulatory subunit of phosphatase 2a (PP2A), APC-stimulated guanine exchange factor (ASEF) and kinesin linker protein KAP3 (190, 192). The middle part of the APC molecule comprises domain that contains 15/20-residue repeats involved in β-catenin binding. The binding of β-catenin is regulated by phosphorylation and is part

of the WNT signaling pathway (190, 192). The less conserved, C-terminal region of APC contains basic/Serine-rich regions mediating interactions with microtubules, EB1 and the PDZ domain-containing protein Dlg (190, 192). Detailed domain structure of APC is depicted on Figure 8.

APC localizes at clusters of microtubule plus ends that invade cellular protrusions and supports cell migration by local stabilization of microtubules (188). APC association with microtubules, similarly to CLASP, is regulated by GSK3β (188). APC-dependent stabilization of microtubules and promotion of cell migration also depend on EB1 binding to APC and the formation of a common complex with mDia, a downstream effector of Rho (189). Finally, APC has been observed to associate with IQGAP1 at the actin-rich leading edge of the cell, suggesting a role for APC in the cross-talk between actin and the microtubule cytoskeleton (55, see chapter 2.3.).

Other basic/Serine-rich sequences-containing proteins

To the group of the basic/Serine-rich sequences-containing proteins also belongs the broadly expressed microtubule-actin crosslinking factor MACF/ACF7 (see chapter 2.3.). MACF/ACF7 possesses the ability to bind both actin and microtubule filaments (57). This protein contains two calponin homology domains, one plakin domain and several small spectrin domains with basic/Serine rich region (Fig. 8). Another example of the basic/Serine-rich sequences-containing proteins is the stromal interaction molecule 1 (STIM1) which is a microtubule plus end tracker involved in remodeling of the endoplasmic reticulum (ER). STIM1 is a transmembrane protein essential for the store-operated calcium entry, a process of extracellular calcium influx in response to depletion of Ca^{2+} stores in ER. STIM1 is localized predominantly to the ER and when Ca^{2+} is released from the ER, STIM1 is translocated to the ER-plasma membrane junctions actvating Ca^{2+} channels. STIM1 binds directly to EB1 and brings the polymerizing microtubules in contact with the ER network (192). Other proteins containing basic/Serine-rich sequences are melanophilin, neuron navigator-1 and Rho-type guanine nucleotide exchange factor RhoGEF2, but will not be explained in more detail here.

2.6.4. Other microtubule plus end tracking proteins

HEAT- and WD40-repeat-containing proteins

The HEAT- and WD40-repeat-containing +TIPs encompass XMAP215 and Lis1 (Fig. 8). XMAP215 contains tumour-overexpressed gene (TOG) domains at the N-terminal end, involved in microtubule binding, and comprising several HEAT repeats. HEAT repeats are modules containing ~37 – 47 aminoacids, and an array of HEAT repeats forms a rod-like structure that participates in protein-protein interactions (193, 194). XMAP215 is a processive microtubule polymerase which accelerates microtubule growth by tenfold. This process is most probably regulated by reducing the dissociation of incoming tubulin dimers and stabilizing the GTP cap (193, 194).

Lissencephaly-1 (Lis1) proteins contain an N-terminal Lis homology (LISH) domain and a C-terminal WD40 repeat (195). WD40 repeats consist of a 40-amino acid repeat, that forms a characteristic β-propeller structure. WD40 repeats are implicated in G protein mediated signal transduction, transcription regulation and vesicle formation and trafficking. The WD40 domain of Lis1 is required for targeting to CLIP-170 and this interaction also involves recruitment of dynein/dynactin complex. (66, 162, see chapter 2.6.2.). Overexpression studies with dynactin and Lis1 indicate that these two proteins compete for interaction with the CLIP-170 C-terminus (Fig. 10). Lis1 might thus act to release dynactin from the complex with CLIP-170, thereby facilitating minus end directed transport (162).

Microtubule motor proteins

Both plus-end and minus-end directed molecular motors can bind to microtubule plus ends. Theoretically, due to their directed movement, all plus-end directed kinesins could accumulate at the microtubule plus ends. However, at normal expression levels most of them do not show plus-end localization. A prominent example of the plus end tracking kinesins is a member of the microtubule depolymerizing kinesin-13 family – MCAK (see chapter 2.5.1.). Additionally yeast kinesins Tea2, Kip2 and Kar3 as well as *Drosophila melanogaster* KLP10A are reported to bind to microtubule plus ends (152). The accumulation of kinesins and cytoplasmic dyneins at the microtubule plus ends usually relies on their association with other +TIPs (152).

2.6.5. Reciprocal interactions between microtubules and +TIPs at the cell cortex

Although +TIPs are complex multidomain proteins, the interactions between them and microtubule rely on a limited number of protein modules, such as CAP-Gly-, CH-, EBH- domains, C-terminal EEY/F motifs and basic/Serine-rich sequences. The C-terminal aromatic residue of the EEY/F motif, which is present in EB1 is crucial for recruitment and binding of CAP-Gly domains (154). It has been proven that CAP-Gly domain-containing proteins do not bind to microtubules composed of α-tubulin that lacks the C-terminal tyrosine of the EEY/F motif (128). The C-terminal part of EB1, in addition to the EEY/F motif also contains an EBH domain that is crucial for the interactions with basic/Serine-rich sequences, present in APC and CLASPs proteins. Highly conserved residues of the EBH motif form a surface comprising a deep hydrophobic cavity and a polar rim. The hydrophobic cavity within the EBH domains is thought to function as a binding site where the Ile-Pro motif present in basic/Serine-rich domains is anchored (148). This indicates a conserved mode of binding of APC and CLASP to EB1, thereby enabling "hitchhiking" of these proteins on EB1 (18). It is most likely that many other +TIPs, including CLIPs use a similar EB-dependent mechanism to target growing microtubule plus ends. Having two interaction motifs at the C-terminus, EB1 proteins seem to be a master integrator of the +TIP network assembly. As EB1 tracks microtubule plus ends independently of its binding partners, it makes it a common factor in the web of functional interactions between several +TIPs (Fig. 11). Since microtubules in many cell types extend from the cell center to the cell boundary, it is not surprising that the activity of many +TIPs is involved in microtubule-cortical interactions. These interactions involve attachment of microtubule plus ends to actin cytoskeleton and plasma membrane, connection of microtubules with cortical structures and exertion of pulling forces on the microtubule network. Four mechanisms of microtubule-cortical interactions can be distinguished (Fig. 11). First, cytoplasmic dynein together with its regulator dynactin can pull the plus ends of cortically attached microtubules and make them slide along the membrane, thereby contributing to centering the centrosome and positioning the mitotic spindle (197, see chapter 2.3.). Due to its direct binding to dynactin, CLIP-170 can contribute to this dynein function in a process that is regulated by Lis1 (162). A second mechanism of microtubule capture at the cell cortex involves APC proteins,

which stabilize microtubules and attach them to the cell cortex (189, see chapter 2.6.3.). Because APC itself does not interact with the cell cortex, it links microtubules to cortical regions through actin-binding proteins, such as mDia (in complex with EB1) or IQGAP1 (Rac1/Cdc42 effector) (189, 55). Additionally, IQGAP1 can capture microtubules through the interaction with CLIP-170 (199), thereby connecting first two mechanisms. In addition, APC can attach microtubule plus ends to the membrane in an actin-independent mechanism, by binding to the PDZ domain-containing protein Dlg1 that is associated to the membrane via its PDZ domains (200). A third mechanism involves the spektraplakin ACF7, that together with EB1, directly links microtubules to actin (see chapter 2.3.). This interaction is regulated by mDia (57, 149). The fourth mechanism invovles CLASPs that can attach microtubules to the cell cortex through LL5β (see chapter 2.3.) and stabilize them with the help of EB1 (56, 181). All above mentioned mechanisms involve interactions with EB1 and most of them are regulated by the same signaling molecules such as mDia and GSK3β, but whether these pathways can act simultaneously on the same microtubules and whether they compete with each other is still not entirely clear.

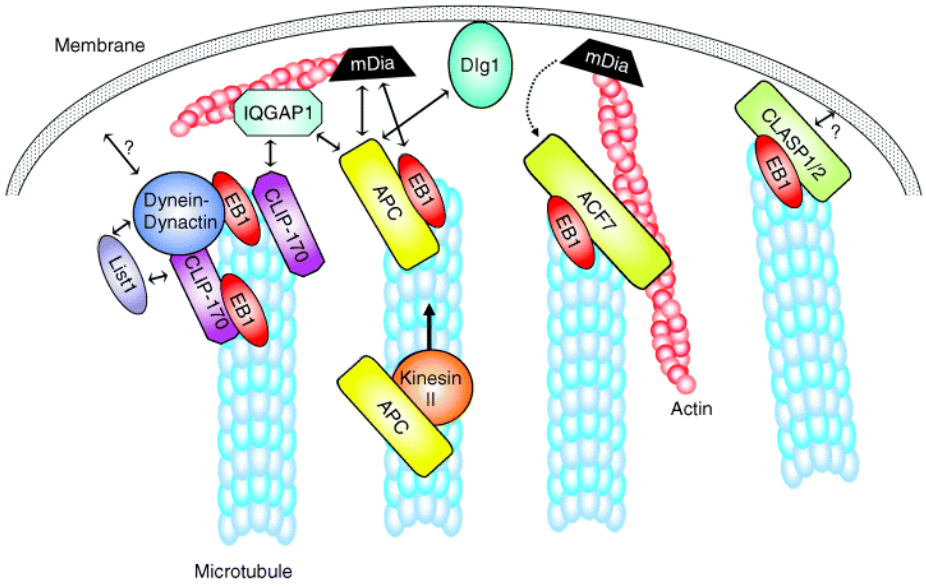

Figure 11. **Cortical interactions of microtubules and +TIPs in mammalian cells.** Schematic drawing of distinct mechanisms of microtubule association to the cell cortex. For details see text. *(Adapted from Lansbergen & Akhmanova 2006; Traffic 7)*

2.7. Role of microtubules in polarity of migrating cells

Cell polarity is essential for the proper function of many cell types. It can be established by the asymmetric distribution of mRNA, proteins, organelles and cell functions. Due to their inherent structural polarity actin and microtubule filaments are well suited to provide the structural basis for cell polarization. During cell migration the microtubule cytoskeleton shows a typically polarized structure. The microtubule minus ends are localized at the centrosome in the cell center and the plus ends contact the actin-rich leading edge and furthermore target focal adhesions at the rear-end of the cell. The first evidence showing that microtubules are involved in regulation of cortical polarity came from experiments, in which fibroblasts were treated with microtubule depolymerizing drugs which resulted in reduced, unpolarized membrane ruffling and lack of directional migration (202). Furthermore, it has been proven that microtubules are important for positioning the leading edge of the cell but not for the migration itself. The mechanism by which microtubules alter cortical polarity it is not well understood, however it has been speculated that the small Rho GTPase Rac1 could contribute to that process. As already mentioned, microtubules can stimulate cortical Rac1 activity and cell migration through IQGAP1 (see chapter 2.3.). It has been described that the expression of dominant negative IQGAP1 lacking the Rac1-binding site leads to a decreased level of active Rac1 and a decreased rate in cell migration. Additionally, knock-down of IQGAP1 results in actin depletion from the leading edge, reduction of lamellipodia formation and finally a decreased migration rate (54, 55, 203). How IQGAP1 stimulates Rac1 to induce polarized cell migration is not truly clear, but one model assumes that small amounts of IQGAP1 are transported by microtubule plus end-bound CLIP-170 to the cortex at the leading edge, where IQGAP1 binds to APC and activates Rac1 (204). Rac1 activity can also be stimulated via microtubule-based delivery of guanine nucleotide exchange factors (GEFs) to the leading edge. One of them, the PAK4 kinase-associated GEF-H1 (see chapter 2.3.) promotes Rac1 activation and thereby lamellipodium formation. In the absence of PAK4 or in the absence of microtubules, GEF-H1 activates Rho and promotes stress fibers formation (39, 205-207). GEF Trio, another one which shows microtubule-dependent localization at the leading edge, induces lamellipodia formation by activating Rac1 (208). Finally, ASEF (see chapter 2.3.) has not been detected on microtubules, however it interacts with APC and is implicated in microtubule-dependent polarized migration (51, 52).

Microtubules may coordinate cell migration not only by delivering GEFs to the sites of actin polymerization but also by targeting and destroying focal adhesions at the rear-end of the cell (see chapter 2.3.). Microtubules that target focal adhesions can disassemble them by a Rho/Rac-depentent pathway that involves FAK and dynamin (a component of endocytosis pathway). Dynamin binds to microtubules, and in this way, is delivered to the focal adhesions where it triggers their dissociation (44, 204, 209). Additionally, microtubule-dependent promotion of Rac1-mediated lamellipodium formation can also have a positive feedback on microtubule stabilization. It is described that Rac1-mediated PAK1 kinase activation results in phosphorylation and inactivation of the potent microtubule destabilizer stathmin, thereby promoting microtubule stabilization (210). Cell polarization requires the formation of a subset of persistently stable microtubules that very often accumulate posttranslational modifications (see chapter 2.5.). GSK3β, which can be locally inactivated and influence microtubule stability at specific cellular locations, appears as an important regulator of microtubule based polarity. Among the many GSK3β targets are proteins involved in microtubule stabilization such as CLASPs and APC. It is known that active Cdc42 at the leading edge leads to PKC-dependent phosphorylation and inactivation of GSK3β, which in turn leads to recruitment of APC to microtubule plus ends and microtubule stabilization (211). Also CLASP-mediated stabilization of peripheral microtubules that likely occurs in the vicinity of focal adhesions, may be regulated by local GSK3β inactivation (183, 212). Another important source of cellular asymmetry can be derived from centrosome positioning between the nucleus and the leading edge, which takes place in many types of migrating cells including macrophages, fibroblasts, endothelial cells, astrocytes and neurons. This process, which also employs subsets of stable microtubules, involves a large variety of signaling factors, such as Cdc42, Par6, PKC and dynein and is nicely reviewed by Rong Li and Gregg G. Gundersen (213).

2.8. Goal of this thesis

The aim of this study was to analyze the localization patterns and behavior of microtubule plus end tracking proteins in tubulin tyrosine ligase-deficient mouse embryonic fibroblasts. The hierarchy of binding of the numerous +TIPs to microtubules and the mutual interactions between them are still poorly understood.

Since many possible interactions between the +TIPs and microtubules are possible and because microtubules undergo multiple posttranslational modifications that are reported to influence MT / +TIPs associations (18, 48, 152), RNA interference has been used to shed more light on the mechanisms and the hierarchy of binding of the +TIPs in cells lacking tyrosinated microtubules. Recently, it has been reported that the localization of CAP-Gly domain-containing proteins is influenced by tubulin tyrosination / detyrosination (125, 128). Therefore, it is of great interest to study these proteins in more detail. Here we show that two closely related CAP-Gly domain-containing +TIPs, CLIP-170 and CLIP-115, were found to be differently affected by the knock-down of EB1, one of the key-players at the growing microtubule plus end, in wild type and *TTL*-knock out cells. Furthermore, GFP-CLIP-115/170 hybrid proteins were employed to get more detailed knowledge about the observed distinct MT binding behavior of the CLIPs.

It is well accepted that all +TIPs are prominent regulators of microtubule dynamics (152). Additionally, also the TTL-cycle is implicated to play a role in the dynamicity of microtubules, as tyrosinated microtubules are known to be more dynamic (119, 120). Therefore, the analysis of the dynamic behavior of microtubules in *TTL* knock-out cells and additionally in *TTL* knock-out cells after down regulation of distinct +TIPs is of particular interest. In this study, different variants of GFP-labeled α-tubulin as well as a new microtubule-binding GFP fusion protein are used to measure microtubule dynamics.

However the cross-talk between microtubules and the actin cytoskeleton is not well studied, the small Rho GTPases are implicated to play a role in this interplay (28, 45, 54). Some +TIPs, such as CLIP-170, EB1 and APC can also participate in the actin/microtubule cross-talk, mainly at the cell periphery (48, Fig. 11, chapter 2.6.5.) Understanding the role of these actin/microtubule-regulating proteins in context of the TTL cycle is of great interest. Therefore analyzing the activity levels of the small GTPases (RhoA, Rac1 and Cdc42) in wild type and TTL-deficient cells may pinpoint a cross section between these two elements of the cytoskeleton. Moreover, the RhoA downstream effector mDia1 is known to interact with some +TIPs such as EB1 and subsequently is involved in microtubules stabilization (33, 189). As *TTL* knock-out cells do contain more stable detyrosinated microtubules (120) it is interesting to examine the expression levels of mDia1 proteins in these cells.

3. Materials and Methods

3.1. Chemicals

All chemicals used in this study were purchased from following companies: Amersham Bioscience, Biorad, Boehringer Mannheim, Cytoskeleton, Fermentas, Finnzymes, Fluka, Invitrogen, Macherey-Nagel, Merck, Milipore, New England Biolabs, Pharmacia, Promega, Qiagen, Roche, Sigma-Aldrich and Stratagene

3.2. Molecular Biology Techniques

3.2.1. Enzymes and reagents for molecular biology

Enzymes were obtained from New England Biolabs, MBI Fermantas or Roche. T4 DNA ligase and alkaline phosphatase were from Roche. Phusion Taq DNA polymerase was from Finnzymes. Oligonucleotydes were from MWG-Biotech. DNA markers were from Eurogentec.

3.2.2. Constructs

All plasmids and constructs used in this work are listed in Table I.

Table I. **List of the plasmids used in this work**

Plasmid	Antibiotic resistance	Source
pcDNA3.1+	Ampicillin	Invitrogen
pcDNA3.1+mCherry-α-tubulin	Ampicillin	Anna Akhmanova, Rotterdam, The Netherlands
pcDNA3.1+mCherry-α-tubulinΔY	Ampicillin	this work
pEGFP-C1	Kanamycin	Clontech
pEGFP-C1-CLIP-115	Kanamycin	Niels Galjart, Rotterdam, The Netherlands
pEGFP-C1-CLIP-170	Kanamycin	Niels Galjart, Rotterdam, The Netherlands
pEGFP-C1-CLIP-170-ΔC	Kanamycin	this work
pEGFP-C1-MBD	Kanamycin	Margit Oelke, HZI

pEGFP-C2	Kanamycin	Clontech
pEGFP-C2-CLIP-115/170-1	Kanamycin	this work
pEGFP-C2-CLIP-115/170-2	Kanamycin	this work
pEGFP-C2-CLIP-115/170-3	Kanamycin	this work
pEGFP-C2-CLIP-115/170-4	Kanamycin	this work
pEGFP-C2-CLIP-115/170-5	Kanamycin	this work
pEGFP-C2-CLIP-115/170-6	Kanamycin	this work
pEGFP-C2-CLIP-115/170-7	Kanamycin	this work
pEGFP-C2-CLIP-115/170-8	Kanamycin	this work
pEGFP-C2-CLIP-115/170-9	Kanamycin	this work
pEGFP-C2-CLIP-115/170-10	Kanamycin	this work
pSuper.neo+GFP	Ampicillin	OligoEngine
pSuper.neo+GFP-EB1A	Ampicillin	this work
pSuper.neo+GFP-EB1C	Ampicillin	this work
pSuper.neo+GFP-EB1/3A	Ampicillin	this work
pSuper.neo+GFP-EB2	Ampicillin	this work
pSuper.neo+GFP-EB3	Ampicillin	this work
pSuper.neo+GFP-CLASP1A	Ampicillin	this work
pSuper.neo+GFP-CLASP1B	Ampicillin	this work
pSuper.neo+GFP-CLASP2A	Ampicillin	this work
pSuper.neo+GFP-CLASP2B	Ampicillin	this work
pSuper.neo+GFP-CLIP-115A	Ampicillin	this work
pSuper.neo+GFP-CLIP-115B	Ampicillin	this work
pSuper.neo+GFP-CLIP-170A	Ampicillin	this work
pSuper.neo+GFP-CLIP-170B	Ampicillin	this work
pGEX-6p3	Ampicillin	Amersham Bioscience
PGEX-6p3-CLIP-170	Ampicillin	Niels Galjart, Rotterdam, The Netherlands
pGEX-6p3-CLIP-115	Ampicillin	Niels Galjart, Rotterdam, The Netherlands
pIRES2-EGFP-TTL sense	Kanamycin	Christian Erck, Marco van Ham, HZI
pIRES2-EGFP-TTL antisense	Kanamycin	Christian Erck, Marco van Ham, HZI

The pEGFP-CLIP170-ΔC construct was generated as follows. pEGFP-CLIP-170 full length construct was digested using BamH1 and XhoI restriction enzymes and the resulting ~ 3700 bp fragment lacking the C-terminal ~500 bps was cloned into the

pEGFP-C1 plasmid that was previously digested with BglII and SalI enzymes. The resulting clones were tested for the presence of the proper inserts using BsrGI and BamHI restriction enzymes.

pEGFP-CLIP170/115 hybrid constructs were generated as follows. The 5'-terminal fragments of CLIP-115 and CLIP-170 were amplified by the PCR using specific primers introducing an EcoRI restriction site at the 5'-terminus. Subsequently, the 5'-terminal PCR products as well as pEGFP-C2 vector were digested with EcoRI and SalI restriction enzymes and ligated. The resulting 5'-terminal intermediate constructs were then digested with SalI and BamHI, into which the respective 3'-terminal SalI/BamHI digested CLIP-170 and CLIP-115 PCR products were cloned. Obtained constructs were verified by sequencing.

The mCherry-α-tubulin-ΔY construct, lacking C-terminal tyrosine on α-tubulin, was generated by performing the deletion PCR with specific primers introducing an EcoRV restriction site on 5'-terminus and an ApaI on 3'-terminus together with deletion of C-terminal tyrosine residue. mCherry-α-tubulin was used as DNA template. The resulting PCR product was subsequently digested with EcoRV and ApaI enzymes and cloned into mCherry-α-tubulin fragment that was digested with EcoRV/ApaI. The generated construct was verified by DNA sequencing.

3.2.3. Primers

Oligonucleotide primers used in this study were synthesized by MWG-Biotech and are listed in Table II.

Table II. **List of the primers used in this work**

Number	Name	Purpose	Sequence 5' to 3'
M55	pRSseq	sequencing	AGGGGAACAGGAGAT
-	PGEX3SQ	sequencing	AAACCTCTGACACATGCAGCTC
-	PGEX5SQ	sequencing	GCCTTTGCAGGGCTGGCAAG
M62	α-tubulin-EcoRV for	cloning	CCTCGATATCGAGCG
M63	α-tubulin-ΔY rev	cloning	GGTGGATCCTTATTATTCCTCTCC
M121	α-tubulin-ΔY-ApaI rev	cloning	GGTGGGCCCTTATTATTCCTCTCC

M73	RatE_2T567seq rev	sequencing	TAGAAGGCACAGTCGAGG
3	Actin for	cloning	GCACTCTTCCAGCCTTCC
4	Actin rev	cloning	AGAAAGGGTGTAACGCAACTAAG
M153	EB1 for	cloning	CCGAAGAAACCTCTC
M154	EB1 rev	cloning	GGTCCAGGCTGCTTA
M155	EB2 for	cloning	TCATCCAGTGGCTCT
M156	EB2 rev	cloning	TGATGAGACGGTTCA
M157	EB3 for	cloning	ATCCTCGAGCTTAAC
M158	EB3 rev	cloning	CTGGCGCCTCCCTCA
M136	mCLIP-115ATGEcoRI	cloning	GGCGAATTCATGCAGAAGCCCAGT
M137	hCLIP-170ATG EcoRI	cloning	CAGAATTCATGAGTATGCTAAAGCC
M161	mCLIP-115rev1	cloning	AGGTCGACGCGGCTGGGCCG
M162	mCLIP-115rev2	cloning	GAGTCGACGAGACAGTGTTGC
M163	mCLIP-115rev3	cloning	CCGTCGACCTCCTCCTGGACC
M164	mCLIP-115rev4	cloning	GCGTCGACGAGTCTATTCTCAGC
M165	mCLIP-115rev5	cloning	TCGTCGACTGGGGAGTGGCG
M166	mCLIP-115 stop rev6	cloning	CCGGATCCTCAGTGTTTGTCC
M167	mCLIP115 for1	cloning	CCGTCGACAGTGGCCTGCTC
M168	mCLIP-115 for2	cloning	ACGTCGACCTCCAGTCAGGC
M169	mCLIP-115 for3	cloning	AGGTCGACCTGGCCGGGCTG
M170	mCLIP-115 for4	cloning	ATGTCGACCAGGCTGCCGAG
M171	mCLIP-115 for5	cloning	ACGTCGACGGGCCCGAGAGAG
M172	hCLIP-170 rev1	cloning	CGGTCGACCCTGCTGCTCACAG
M173	hCLIP-170 rev2	cloning	TTGTCGACTAGCCTTCTTCGG
M174	hCLIP-170 rev3	cloning	TTGTCGACTTCTTTAATAACTTT
M175	hCLIP-170 rev4	cloning	AAGTCGACAATCTGTTTCTCAG
M176	hCLIP-170 rev5	cloning	TGGTCGACACTTGCATTTTCAT
M177	hCLIP-170 stop rev6	cloning	AGGGATCCTCAGAAGGTTTCGTC
M178	hCLIP-170for1	cloning	GCGTCGACCCCAGTCGGACAG
M179	hCLIP-170for2	cloning	GAGTCGACGAGTCCAATAAGC
M180	hCLIP-170for3	cloning	TTGTCGACAAGGAAAACAGTC
M181	hCLIP-170for4	cloning	AAGTCGACAAACATTTAGAGATT
M182	hCLIP-170for5	cloning	ATGTCGACTTTCTGCAAAAAAG
M183	hCLIP-170rev3-2	cloning	AGGTCGACCCTGATGGCTTCCAG
M93	mCLIP-115seq1	sequencing	GTGGAATCCCTCACG

M94	mCLIP-115seq2	sequencing	TCAGGCACCACAGC
M96	mCLIP-115seq4	sequencing	AAGCCATCGAGTTCC
M100	mCLIP-115seq3a	sequencing	TGGCAGACCTCAAGG
M122	hCLIP-170seq1	sequencing	CTCCGATCAGCAACC
M123	hCLIP-170seq2	sequencing	GGAACGGGATCTGG
M124	hCLIP-170seq3	sequencing	TTCCGAAGGTAAATCG
M125	hCLIP-170seq4	sequencing	TGAAGGAGCATTTTGG
M126	hCLIP-170seq5	sequencing	GAAACAAGCCACAACC
M127	hCLIP-170seq6	sequencing	GCAGATGAAGAGAAAGC

3.2.4. Polymerase chain reaction (PCR)

Polymerase chain reactions were performed for cloning the mCherry-α-tubulinΔY and pEGFP-CLIP115/170 constructs and additionally for examining expression levels of EB1, EB2, and EB3 in mouse embryonic fibroblasts (MEFs). The oligonucleotides, which were used as primers are listed in Table II. DNA amplification using PCR is based on repeated cycles of denaturing the template DNA by breaking down the hydrogen bonds at high temperatures, cooling down to anneal the primers and increasing the temperature to optimal conditions of DNA synthesis by a DNA polymerase. The reactions were done using the proofreading DNA polymerase Pfu (*Pyrococcus furiosus*) in a T3 Biometra thermocycler. Reaction temperatures and extension time were adapted to appropriate melting temperature that depends on the primer sequence and on the length of the DNA fragment to be amplified, respectively. A typical PCR program used in this study is given as an example.

PCR mix:

DNA template (~100ng)	1 µl
5' primer (10 pmol)	5 µl
3' primer (10 pmol)	5 µl
dNTPs 20 pmol/nucelotide	2 µl
5x PCR HF buffer	10 µl
DNA polymerase (2-3U/µl)	0.5 µl
H_2O sterile	27 µl

Program:

98ºC 120 s	
98ºC 30 s	
50ºC 30 s	35 cycles
72ºC 90 s	
72ºC 10 min	
4ºC ∞	

3.2.5. DNA sequencing

DNA sequencing was performed by MWG-Biotech AG (Ebersberg, Germany) or GATC company (Konstanz, Germany). Primers used for sequencing are listed in Table II. For constructs sequenced by GATC company, sequencing reactions were performed according to BigDye Kit (Applied Biosystems) protocol:

PCR mix:		**Program:**	
DNA	0.5 µg	95ºC 5 min	
Primer 3.2 pmol	0.15 µl	95ºC 15 s	25 cycles
5x sequencing buffer	1 µl	50ºC 15 s	
BigDye reagent	2 µl	62ºC 4 min	
H_2O sterile	up to 10 µl	72ºC 10 min	
		4ºC ∞	

3.2.6. DNA digestion and purification

Restriction enzyme digestions were performed using the following protocol:

DNA	2 µl (~0.5 - 2 µg)
Restriction enzymes	0.2 µl each (10U/ µl)
enzyme buffer 2x	2 µl
H_2O sterile	up to 10 µl

Reaction mixtures were incubated for 1h at 37ºC. Different enzymes required different digestion buffers that were provided by the producer. In case of a preparative digest, the amounts of the enzymes, buffer and water were appropriately increased. Resulting DNA fragments were column purified or separated using agarose gel electrophoresis, extracted from agarose gel and then column purified by using the PCR clean-up and gel extraction kit (Macherey-Nagel) according to manufacturer's protocol. Briefly, DNA fragments excised from agarose gels were dissolved in double amount of NT buffer (200 µl NT buffer / 100 mg agarose) at 50ºC. PCR products were diluted in double amount of NT buffer (200 µl NT buffer / 100 µl DNA). The DNA was then loaded on the column and centrifuged for 1 minute at 11000 x g. The column was washed with 600 µl NT3 washing buffer by centrifugation for 1 minute at 11000 x g. The supernatant was discarded and the column was dried by

centrifugation for 2 minutes at 11000 x g. The DNA was eluted from the column by adding 15 – 50 µl elution buffer NE or sterile H_2O and spinning down for 1 minute at 11000 x g.

3.2.7. DNA ligation

The ligation of DNA inserts into vector DNA was carried out using T4 DNA ligase from Roche according to a standard protocol as described below:

Vector DNA	50-400 ng
Insert DNA	1:1, 1:2, 1:3, 1:5 molar ratio of vector/insert DNA
10x ligation buffer	2 µl
T4 DNA ligase	1 µl
H_2O sterile	up to 20 µl

Reaction mixtures were incubated 12 – 16 hours at room temperature and subsequently used for transformation (as described in chapter 3.2.8.).

3.2.8. Generation of competent *E.coli*

In order to achieve highly efficient transformation, competent *Escherichia coli* bacteria were generated as follows: bacteria were plated on a LB-plate without antibiotics and cultured overnight at 37ºC. Fifty ml of LB-medium was inoculated with 1 colony and incubated at 37ºC while shaking, until OD550 reached 0.8 – 1.0. After that, bacteria were spun down for 10 minutes at 4000 rpm, the resulting pellet was resuspended in 1 ml of cold 0.1 M $CaCl_2$ and an additional 4 ml 0.1 M $CaCl_2$ was added. Bacteria were then spun down for 10 minutes at 4000 rpm at 4ºC and the pellet was resuspended in 5 ml cold 0.1 M $CaCl_2$. After that, bacteria were put on ice-cold water for 25 – 30 minutes, spun down for 10 minutes at 4000 rpm and finally the pellet was resuspended in 500 µl 0.1 M $CaCl_2$ containing 14% glycerol. Bacteria were alliquoted in 25 µl portions and immediately frozen in liquid nitrogen. Competent bacteria were stored at -70ºC.

3.2.9. Transformation of *E.coli*

Transformation is based on the DNA take-up by bacteria and is performed in order to amplify DNA in bacteria. To do this, 80 µl 0.1 M $CaCl_2$ was added to the ligation mix (described in chapter 3.2.7.) and the mixture was put on ice for 15 minutes. During that time competent bacteria cells (see chapter 3.2.8.) were thawed and left on ice for 10 minutes. Five µl of bacteria were added to the mix and mixed gently by pipetting. The resulting mixture was put on ice for 10 minutes. A so-called heatshock was applied for 90 seconds at 42ºC and the bacteria were put on ice for an additional 90 seconds. Then, 800 µl of LB-medium without antibiotics was added and the mixture was incubated at 37ºC while shaking. Bacteria were spun down for 4 minutes at 3500 rpm and the pellet was plated on LB-plates containing the appropriate antibiotics. The plates were incubated overnight at 37ºC.

3.2.10. Plasmid isolation from *E.coli*

Plasmid DNA preparations were performed in small amounts (Mini-Prep) for the screening of bacterial clones and in higher amounts (Midi-Prep) to get high yield of pure plasmid for cloning, transfections and transformations. Purification procedures were performed according to the manufacturer's protocol using Nucleobond plasmid purification kits (Macherey & Nagel). Bacterial cultures for mini-preparations were incubated overnight at 37ºC while shaking in 2 ml LB medium with the addition of the right antibiotics. Bacteria were then spun down for 30 seconds at 11000 x g and the pellet was resuspended in 250 µl of resuspension buffer A1. A volume of 250 µl of lysis buffer A2 was added and after 5 minutes incubation at room temperature the lysis was ceased by the addition of 300 µl neutralization buffer A3. The mixture was then centrifuged for 10 minutes at 11000 x g at room temperature and the supernatant was loaded on a column followed by centrifugation for 1 minute at 11000 x g. Bound DNA was washed with to 50ºC pre-warmed 500 µl of washing buffer AW by spinning down the column for 1 minute at 11000 x g. The column was washed again with 600 µl of ethanol-based A4 washing buffer and after discarding the flow-through the column was centrifuged again for 2 minutes at 11000 x g to completely remove ethanol. A volume of 50 µl sterile H_2O was applied to the column and DNA was eluted by centrifugation for 1 minute at 11000 x g. DNA purity was tested by agarose gel electrophoresis and DNA was stored at -20ºC.

Bacterial cultures for midi-preparations were inoculated in 100 ml of LB medium with antibiotics and incubated overnight 37ºC while shaking. Bacteria were centrifuged at 6000 x g for 15 minutes at 4ºC and the pellet was resuspended in 4 ml ice-cold resuspension buffer S1. Bacteria were then lysed by the addition of 4 ml lysis buffer S2 and after 5 minutes incubation at room temperature the lysis was neutralized by adding 4 ml neutralization buffer S3. The mixture was centrifuged at 12000 x g for 30 minutes at 4ºC and the cleared lysate was loaded on a column which was equilibrated with 2.5 ml buffer N2. After DNA binding, the column was washed with 10 ml washing buffer N3. Plasmid DNA was then eluted from the column by the addition of 5 ml elution buffer N5 and precipitated in 3.5 ml isopropanol. After centrifugation at 19000 x g for 30 minutes at 4ºC the pellet was washed with 2 ml of 70% ethanol and centrifuged at 19000 x g for 10 minutes at room temperature. Ethanol was carefully removed and the DNA pellet was dried at room temperature and finally dissolved in an appropriate volume of sterile H_2O. The plasmid integrity was confirmed by agarose gel electrophoresis and stored at -20ºC for further use.

3.2.11. Agarose gel electrophoresis

For DNA separation 1% and 2% agarose gels were used. 1% or 2% (w/v) agarose in Tris-Acetate-EDTA-buffer (TAE)-buffer (2M Tris base pH 7.5, 1M Sodium acetate, 50 mM EDTA) was dissolved by boiling in a microwave oven, cooled down to approximately 50ºC, poured into a chamber and allowed for polymerization. Before polymerization, an appropriate amount of the DNA intercalating agent ethidium bromide (2 µl / 50 ml of gel) was added to the gel thereby allowing visualization of DNA in UV light. The solid agarose was then transferred to a gel chamber filled with TAE-buffer. DNA samples were mixed with 5x DNA loading buffer (15 % (v/v) Ficoll, 50 mM EDTA pH 8, 0,5 % (v/v) SDS, 2 % (v/v) 50x TAE buffer, 0,05 % (w/v) Bromophenol blue, 0,05 % (w/v) Xylencyanol) and loaded into the gel. Smart-ladder (200 bp – 10000 bp DNA marker Eurogentec) was loaded as a DNA standard and the DNA was separated using 70-100 V current for 30 – 60 minutes. Subsequently, gels were exposed to UV light and DNA patterns were documented by photoimaging (Intas UV-Systeme).

3.2.12. DNA quantification

DNA quantification was performed using the Nanodrop device (Peqlab). Quantification is based on the fact that the photometric absorption of DNA in solution has a maximum at a wavelength of 260 nm. Blank measurements were done with the appropriate elution buffer, e.g. elution buffer or water, and DNA concentrations were measured by applying ~1 µl of DNA solution onto the sensor of the Nanodrop device.

3.3. Bacterial Culture

3.3.1. Media and additives

- LB medium: bacto-crypton 10 g/L
  bacto-yeast extract 5 g/L
  NaCl 10 g/L

- SOB medium: bacto-crypton 20 g/L
  bacto-yeast extract 5 g/L
  NaCl 0.6 g/L
  KCl 0.19 g/L
- SOC medium: SOB medium
  $MgCl_2$ 10 mM
  $MgSO_4$ 10 mM
  Glucose 2 mM

- LB plates : agar in LB medium 0.4 % (w/v)
- Antibiotics: ampicillin 100 µg/ml
  kanamycin 34 µg/ml

3.3.2. Bacterial strains

E.coli strain TG2 (Stratagene) was used for cloning and plasmid amplification.
E.coli strain BL21 (Stratagene) was used for GST-tagged protein expression.
Bacterial cultures were incubated overnight at 37ºC under 180 rpm agitation.

3.4. Cell Culture, Transfections and Treatments

3.4.1. Media, reagents and plasticware

Cell culture media and additives were from Gibco, Invitrogen, PAA and Sigma-Aldrich. Plasticware were obtained from Nunc, Corning and Falcon. Most commonly used media are listed below.

- DMEM/F10 medium for MEFs:
  1 volume of DMEM was mixed with 1 volume of F10
  DMEM (Dulbecco's modified Eagle's medium) high glucose (4,5 g/L)
  F10 (Nutrient Mixture – Ham)

FCS lot 047K3395	10% (v/v)
Glutamine	2 mM
Pecnicillin/Streptomycin	50 U/ml

- DMEM medium for B16 cells:
  DMEM (Dulbecco's modified Eagle's medium) high glucose (4,5 g/L)

FCS lot PAA clone	10% (v/v)
Glutamine	2 mM
Pecnicillin/Streptomycin	50 U/ml

- PBS (pH 7.4):

NaCl	137 mM
KCl	2.7 mM
$Na_2HPO_4 \cdot H_2O$	10 mM

- Trypsin-EDTA

Trypsin	0.05 %
EDTA	0.53 mM

3.4.2. Cell lines

Multiple wild-type and TTL-deficient MEFs were derived from mouse embryos and used in the different experiments. The numbers of the used cell lines are listed in the

figure legends. Cells were cultivated at 37 ºC, 5% CO_2 and 85% humidity. Cell lines used in this study are listed in Table III.

Table III. **List of cells used in this work**

Name	Organism	Type	Source
MEFs WT	*Mus musculus*	TTL(+/+) embryonic fibroblasts	Erck et al 2005
MEFs KO	*Mus musculus*	TTL(-/-) embryonic fibroblasts	Erck et al 2005
B16-F1	*Mus musculus*	Skin melanoma cells	ATTC (CRL-6323)

3.4.3. Transfections

Transfections of mammalian cells were performed in order to ensure transient expression the DNA construct. MEFs and B16 cells were transiently transfected using Fugene 6 (Roche) at 50% - 80% confluency according to manufacturer's protocol. Briefly, for 6 well plate, 90 µl Optimem was mixed with 12 µl Fugene 6 and 1 – 2 µg DNA, and incubated for 30 minutes at room temperature. The mixture was then added dropwise to the cells and cells were cultured for 24 hours. The medium was changed and cells were incubated for suitable time depending on the subsequent experiments. For transfections that were not performed in 6 well plates, the mixtures were scaled according to the protocol.

3.4.4. AlF_4 treatment

Aluminum fluoride treatment was performed to study microtubule organization in conditions where all GTPases were (unspecifically) activated. Semiconfluent cells, seeded on coverslips were incubated for 20 – 30 minutes at 37ºC and 5% CO_2 in a mixture of 30 µl 1M NaF and 5 µl 100 mM $AlCl_2$ in 1 ml DMEM/F10. After that, AlF_4 solution was removed and cells were washed once with PBS. Cells were subsequently fixed according to the protocol described in chapter 3.6.1.

3.4.5. Taxol Treatment

Taxol treatment was performed to stabilize microtubules and to study localization of microtubule associated proteins. Cells were treated with 10 µM Taxol (Paclitaxel, Sigma) premixed with medium containing 10% FCS. Medium from cells cultured in a 6 well plate was removed and 0.5 ml of the Taxol-containing medium was added per well. Cells were then incubated at 37ºC and 5% CO_2 for 30 to 120 minutes. After that,

Taxol was removed and cells were washed with PBS and fixed according to the protocol described in chapter 3.6.1.

3.4.6. Wound healing experiments

Wound healing experiments were performed to induce directional migration of cells and study the localization of microtubule associated proteins. For wound healing experiments cells were seeded on 12 mm coverslips in 24 well plates. Cells were washed with PBS and serum-starved overnight. Starved cells were then scratched using a yellow tip and the medium was changed to DMEM/F10 with 10% FCS. Cells were allowed migrating into the wound for 8 – 16 hours until the wound was about to close. Cells were then fixed and subjected to immunofluorescence staining, as described in chapter 3.6.1.

3.4.7. RNA interference

Introduction of double-stranded RNA has proven to be a powerful tool to suppress gene expression through a process known as RNA interference. The pSUPER RNAi system used in this study provides a mammalian expression vector that directs intracellular synthesis of short interfering RNA (siRNA)-like transcripts, which interact with mRNA leading to the specific knock-down of the gene of interest. The pSuper.neo+GFP vector is used together with a pair of oligonucleotides that contain a unique 19-nucleotide sequence derived from the mRNA transcript of the gene targeted for suppression. The expressions of GFP proteins allow the identification of transfected cells. Constructs containing the specific interfering sequences were generated using standard techniques. For that, forward and reverse oligonucleotides were annealed and cloned into the pSuper.neo+GFP vector using BglII and HindIII restriction enzymes. This resulted in the localization of the forward oligonucleotide at the correct position downstream of the H1 promoter TATA box to generate the desired siRNA duplex. The resulting transcript applies an intramolecular conformation forming a 19–base pair stem-loop structure, that is quickly cleaved in the cell to produce a functional double-stranded RNA (dsRNA). Constructs were generated to specifically knock-down +TIPs and the used oligonucleotides are listed in Table IV. The newly generated pSuper.neo+GFP constructs were verified by sequence analysis and transfected into MEFs. 3 – 4 days after transfection, when

protein knock-down has occurred, cells were fixed and subjected to immunofluorescence using specific antibodies detecting +TIPs.

Table IV. **List of the sense sequences used for RNAi oligonucleotide synthesis**

Number	Sequence 5' to 3'	Target	Source
M1/2	TCTGACAAAGATAGAACAG	EB1A	Komarova *et al.,* 2005
M3/4	TTGCCTTGAAGAAAGTGAA	EB1B	Komarova *et al.,* 2005
M89/90	CAGACAAGGTCAAGAAACT	EB1C	Straube *et .al.,* 2007
M91/92	TGGACATGCTCTTCCCTGG	EB1/3A	Straube *et .al.,* 2007
M5/6	GATGAATGTTGATAAGGTA	EB2	Komarova *et al.,* 2005
M7/8	CTATGATGGAAAGGATTAC	EB3	Komarova *et al.,* 2005
M9/10	GGAGAAGCAGCAGCACATT	CLIP170A	Lansbergen *et al.,* 2004
M11/12	TGAAGATGTCAGGAGATAA	CLIP170B	Lansbergen *et al.,* 2004
M14/15	GGCACAGCATGAGCAGTAT	CLIP115A	Lansbergen *et al.,* 2004
M16/17	CTGGAAATCCAAGCTGGAC	CLIP115B	Lansbergen *et al.,* 2004
M18/19	GCCATTATGCCAACTATCT	CLASP1A	Mimori-Kiyosue *et al.,* 2005
M20/21	GGATGATTTACAAGACTGG	CLASP1B	Mimori-Kiyosue *et al.,* 2005
M22/23	GTTCAGAAAGCCCTTGAT	CLASP2A	Mimori-Kiyosue *et al.,* 2005
M24/25	GCACTCATTATGACTCCAT	CLASP2B	Mimori-Kiyosue *et al.,* 2005

M1/2 corresponds to the pair of sense and antisense oligonucleotides, M1 and M2 that were subsequently annealed and cloned into the pSuper.neo+GFP.

3.5. Biochemical Methods

3.5.1. Cell lysis and protein extraction

Cells cultured and treated as described in chapter 4 were washed twice with icecold 1x PBS and then lysed by adding 150 µl lysis buffer per 100 mm dish. Then, cells were scraped from the dish using cell scraper followed by 10 minutes boiling at 95ºC. Lysates were stored at -20ºC. The recipe for the lysis buffer is given below:

Lysis buffer	
Tris pH 7.5	25 mM
EDTA	1mM
EGTA	1mM
SDS	1%

3.5.2. Protein quantification

Protein concentrations were determined using Micro BC Assay (Uptima) and is based on the Biuret reaction using bicinchoninic acid. The BC assay is a colorimetric assay, which involves the reduction of Cu^{2+} ions to Cu^{+} ions by peptidic bonds present in proteins. Added bicinchoninic acid chelates Cu^{+} ions to form purple colored complexes, of which the optical absorbance is measured at 562 nm. Measured absorbance is proportional to the protein concentration in a linear range between 20 – 2000 µg/ml. Protein concentration was calculated using references obtained from BSA standard protein ranging between 1 – 100 µg/ml (1, 2.5, 5, 15, 25, 40, 70, 100 µg/ml). For the assay, the reagents were diluted in a ratio of A : B : C = 25 : 25 : 1. Protein samples were diluted 1 : 100, 1 : 200 or 1 : 1000 in water in a final volume 100 µl. Duplicates of each sample were supplemented with 100 µl of the pre-mixed reagent in a 96 well plate. Water was used as a blanc reference. The mixtures were incubated at 37ºC for 30 minutes. Then, the absorbance was measured at OD 562 nm using an UV spectrophotometer (Tecan). Data analysis was performed using Microsoft Excel 2000 (version 9.0.8948 SP-3).

3.5.3. Sodiumdodecylsulphate-polyacrylamide gel electrophoresis (SDS-PAGE)

Sodiumdodecylsulphate-polyacrylamide gel electrophoresis (SDS-PAGE) was performed according to Laemmli (Laemmli, 1970). SDS-PAGE were run in minigel-chambers (Biometra) with 1 mm spacers. Five % acrylamide stacking gels and separation gels of 6%, 7.5%, 8.5% or 10% acrylamide were prepared as given in Table V. Protein samples were mixed with 4x loading buffer and boiled for 5 minutes at 95ºC before they were loaded onto the gel. Proteins were separated for about 1h at 80 – 120 V. Prestained protein-ladder (Fermantas) was used as molecular marker. The buffers recipes used in SDS-PAGE are listed below.

SDS running buffer:

SDS	0,1 % (w/v)
Glycine	192 mM
Tris base	25 mM

SDS sample buffer (4x):

SDS	3,4 % (w/v)
Tris HCl, pH 6,8	25 mM
Glycerin	2,4 % (v/v)

Table V. **Mixes for polyacrylamide gels**

	Stacking gel [µl]	**Separation gel [µl]**			
	5%	**6%**	**7.5%**	**8.5%**	**10%**
H_2O	1405	3675	3853	3653	2772
1.5 M Tris HCl pH 8.8	-	1750	1500	1500	1758
0.5 M Tris HCL pH 6.8	625	-	-	-	-
30 % Acrylamide	425	1400	1500	1700	2331
10 % SDS	25	70	70	70	70
TEMED	2.5	7	7	7	7
10% APS	25	70	70	70	70

Mixes are for 1 gel

3.5.4. Coomassie-blue-staining

SDS gels or PVDF membranes after Western blot analysis (see chapter 3.5.4.), were stained with coomassie (Westermeier 1997) for 30-60 min. After that, nonspecific background was reduced by applying consecutive washing steps using destaining solution (10% acetic acid, 40% methanol).

3.5.5. Western blot

After protein separation on SDS-PAGE gels, as described in chapter 3.5.3., proteins were transfered onto PVDF membranes (Millipore) using semi-dry blot chambers (Pegasus). Protein transfer was performed in SDS blotting buffer (see below) at a constant current 150 mA for 90 – 150 minutes. Membranes were then blocked for 60 minutes in 10% FCS in TBS-T or in 2% BSA in TBS-T. Membranes were then incubated with primary antibodies diluted in blocking solution for 60 minutes at room temperature or at 4ºC overnight. After that, the membranes were washed three times with three washing solutions (TBS-T, TBS-T/0.5 M NaCl, TBS-T/0.5 % Triton) for 10 minutes each washing step. Then membranes were incubated with secondary

antibodies diluted in blocking solution for 60 minutes at room temperature. Membranes were washed again as described above and developed by applying Lumilight chemiluminescence substrate (Roche) for 2 minutes to the membranes followed by exposure to a film (Amersham Hyperfilm). Antibodies used for Western blot analysis are listed in Table VI.

Table VI. **List of primary antibodies used for Western blot analysis in this work**

Description	Protein	Type	Dilution	Source
TUB2.1	β-tubulin	mouse	1:2000	Sigma Aldrich
α3A2	α-tubulin	mouse	1:50000	Biotem, France
YL1/2	Tyr-tubulin	rat	supernatant	Wehland *et.al.*, 1983
20C6	Tyr-tubulin	mouse	1:5000	Wehland and Weber, 1987
ID5	Glu-tubulin	mouse	supernatant	Wehland and Weber, 1987
L3	Glu-tubulin	rabbit	1:5000	Paturle-Lafanechere *et.al.*, 1994
37B5D2	Δ2-Glu-tubulin	rat	1:1000	SySy
6-11B-1	acetylated-tubulin	mouse	1:2500	Sigma-Aldrich
H5-8	GFP	rabbit	1:1000	HZI
27F5	GFP	mouse	1:1000	HZI
αDSred	mCherry	rabbit	1:2500	Hans Faix, MH Hannover
clone5	EB1	mouse	1:2500	BD Transduction Laboratories
11B11	EB1	mouse	1:2500	Absea
clone7	EB3	mouse	1:2500	BD Transduction Laboratories
15H11	EBpan	mouse	1:2500	Absea
αDrf1	mDia1	rabbit	1:2000	Hans Faix, MH Hannover
αDrf3	mDia2	rabbit	1:1000	Hans Faix, MH Hannover
p140	mDia1	mouse	1:2000	BD Transduction Laboratories
p150	p150Glued	mouse	1:2000	BD Transduction Laboratories

Table VII. **List of secondary antibodies used for Western blot analysis in this work**

Name	Description	Dilution	Coupled to	Source
A4c	Goat anti-mouse IgG (H+L)	1:5000	HRP	Dianova
B4c	Goat anti-rabbit IgG (H+L)	1:5000	HRP	Dianova
C4c	Goat anti-rat IgG (H+L)	1:5000	HRP	Dianova

List of buffers used for Western blot analysis:

TBS:

Tris-Base pH 7,6	20 mM
NaCl	137 mM

TBS-T:

Tween 20 in TBS	0,1 % (v/v)

Bloting buffer:

Tris	50mM
Glycine	39 mM
SDS	0.037 (w/v)
Methanol	20% (v/v)

3.5.6. Purification of recombinant proteins from E. coli

Expression of recombinant proteins was performed using *E. Coli*, BL 21 strains. pGEX-CLIP115 and pGEX-CLIP170 constructs (provided by Marco van Ham and Niels Galjart, Rotterdam, The Netherlands) containing the C-terminal parts of CLIP-115 and CLIP-170 respectively fused to GST, were expressed, GST-fusion proteins were purified and subsequently used for immunization of rabbits. First, the constructs were transformed into *E.coli* according to the protocol described in chapter 3.2.9. Expression of recombinant proteins was then carried out according to standard protocols. For that, 7.5 ml of LB medium containing ampicillin was inoculated with a single colony and incubated overnight at 37ºC while shaking. The culture was then expanded to 800 ml in antibiotic-containing LB medium and incubated for another 3 – 5 hours at 37ºC until OD600 reached 0.4. Protein expression was then induced by adding 0.1 mM IPTG to the culture and incubation at 37ºC was continued for 4 hours. After that, bacteria were centrifuged at 6000 x g for 15 min at 4ºC. Supernatant was discarded and harvested bacteria were then washed with 40 ml ice-cold 1x PBS. After centrifugation bacteria were resuspended in 64 ml 0.5% Triton X100 in 1 x PBS and subjected to two rounds of freeze/thawing. Then, bacteria were lysed by sonication, applying 3 pulses of 30 s each. The bacterial suspension was centrifuged at 12000 x g for 10 min at 4ºC and the supernatant was used for further isolation. Glutathione

Sepharose Beads 4B (GE Healthcare) were prepared as follows: 0.5 ml 75% slurry of Glutathione Sepharose Beads 4B was loaded onto a provided column and beads were washed with 200 ml ice-cold 1 x PBS. Bacterial supernatant was added to the beads supplemented with protease inhibitors (1 tablet, Roche) followed by incubation for 2 hours or overnight at 4ºC on a rotary wheel to allow protein binding. Beads were then washed with 200 ml 1 x PBS. Proteins were eluted from the beads by addition of 1 ml elution buffer (50 mM Tris-HCl, 10 mM reduced glutathione, pH 8.0). Expression and purity of the proteins was confirmed by SDS-PAGE using samples from each purification step. Protein yield was assessed by SDS-PAGE using BSA standards ranging from 0.02 mg/ml to 1 mg/ml.

3.5.7. G-LISA assays

G-LISA assays were performed to measure the levels of active RhoA, Rac1 and Cdc42 in mouse embryonic fibrobasts. Experiments were carried out using commercially available G-LISA kits (Cytoskeleton) according to manufacturer's protocol. In brief, 60-80 % confluent cells were lysed with lysis buffer and snapped frozen in liquid nitrogen. After thawing the samples, protein concentrations of the samples were equalized after protein concentration determination. Protein concentration determination was done using The Precision Red Advanced Protein Assay Reagent (Cytoskeleton). For that, 300 µl reagent was added to 10 µl of cell lysate in a 96-well plate. The mixture was incubated for 1 minute at room temperature and absorbance at 600 nm was measured in a microplate spectrophotometer (Tecan). Absorbance was then multiplied by 3.75 to obtain the protein concentration in mg/ml. Lysis buffer was used as a blanc reference. The protein lysates were subsequently applied on provided G-LISA plates containing Rho GTPase-GTP-binding proteins coupled to the wells and incubated for 15 – 30 minutes at 4ºC under agitation at 400 rpm. Only active GTP-bound Rho GTPases bind to the wells while inactive GDP-bound Rho GTPases do not. After incubation, plates were washed twice with washing buffer and were treated with antigen presenting buffer for exactly 2 minutes at room temperature. After three wash steps with washing buffer, the bound active Rho GTPase was detected with Rho GTPase specific antibodies, under agitation (400 rpm) for 30 – 45 minutes at room temperature. The plate was again washed three times and incubated with secondary HRP conjugated antibody for 30 – 45 minutes at room

temperature while shaking (400 rpm). After three wash steps the plate was incubated with HRP detection reagent for 5 – 15 minutes at 37ºC followed by addition of HRP Stop buffer to cease the reaction. The absorbance at 490 nm wavelength was measured using a microplate spectrophotometer (Tecan). The levels of active Rho GTPases obtained from wild type and TTL-deficient cell lysates were compared. Active RhoGTPase proteins provided by the kit were used as positive controls, and lysis buffer was used as a negative control.

3.6. Microscopy

3.6.1. Immunofluorescence staining

Immunofluorescence stainings were performed to visualize protein localization within fixed cells by using specific antibodies. Cells seeded and cultured on 12 mm coverslips were fixed according to a protocol adapted for +TIP detection. First, cells were washed once with 1 x PBS and fixed at -20ºC for 10 – 15 minutes in ice-cold methanol containing 1 mM EGTA. Coverslips were then transferred without rinsing to 4% formaldehyde in 1 x PBS and fixed for 15 – 20 minutes at room temperature. After that cells were washed with 1 x PBS and permeabilized for 10 minutes in 1 x PBS/0.15% Triton X-100. Cells were then blocked for 60 minutes in 1 x PBS/1% BSA/0.05% Tween20. Then, fixed cells were incubated with the first antibody diluted in blocking solution for 60 minutes at room temperature or overnight at 4ºC. Cells were washed three times for 10 minutes in 1 x PBS/0.05% and incubated for 60 minutes at room temperature with the second antibody diluted in blocking solution. Again, cells were washed three times for 10 minutes in 1 x PBS/0.05% and then subsequently for 10 seconds in 1 x PBS, for 1 – 2 minutes in 70 % ethanol and for 1 minute in 100% ethanol to dehydrate. Coverslips were then airdried, mounted in Mowiol (2.4 g mowiol, 6 g 87% glycerol, 0.2 ml 200mM Tris pH 8.5, 6 ml H_2O) containing Anti-bleach (25 mg/ml n-propyl-gallate in 87% glycerol) and stored at 4ºC in the dark. Depending on the used antibodies, the standard protocol could be adapted. Primary and secondary antibodies used in this work are listed in Table VIII and IX, respectively.

Table VIII. **List of primary antibodies used for immunofluorescence in this work**

Description	Protein	Type	Dilution	Source
TUB2.1	β-tubulin	mouse	1:300	Sigma Aldrich
α3A2	α-tubulin	mouse	1:50000	Biotem, France
YL1/2	Tyr-tubulin	rat	supernatant	Wehland *et.al.*, 1983
20C6	Tyr-tubulin	mouse	1:1000	Wehland and Weber, 1987
ID5	Glu-tubulin	mouse	supernatant	Wehland and Weber, 1987
6-11B-1	acetylated-tubulin	mouse	1:200	Sigma-Aldrich
H110	Fascin	rabbit	1:50	Santa Cruz
55k2	Fascin	mouse	1:50	Santa Cruz
#2238	CLIP-115	rabbit	1:250	Hoogenraad, *et.al.,* 2000
#2163	CLIP-115	rabbit	1:1000	HZI
#2360	CLIP-170	rabbit	1:250	Coquelle *et al.,* 2002
#2358	CLASP2	rabbit	1:300	Akhmanova *et.al.,* 2001
H5-8	GFP	rabbit	1:500	HZI
270F3	GFP	mouse	1:1700	SySy
clone5	EB1	mouse	1:2500	BD Transduction Laboratories
11B11	EB1	mouse	1:200	Absea
clone7	EB3	mouse	1:200	BD Transduction Laboratories
15H11	EBpan	mouse	1:200	Absea
β-catenin	β-catenin	rabbit	1:50	Theresia Stradal
p150	$p150^{Glued}$	mouse	1:200	BD Transduction Laboratories

Cells were observed on an Axiovert 100TV (Zeiss) microscope with inverted optics, equipped with phase contrast and epifluorescence with appropriate filters for green, red or blue emission. Objective lenses 63x NA 1.4 and 100x NA 1.4 plan-apochromatic were used. Images were acquired with a back-illuminated, cooled charge-coupled-device (CCD) camera (The Photometrics® CoolSNAP*HQ2,* Roper Scientific®, Inc.). Images were stored as 8- bit and 16-bit digital images and analyzed using Adobe Photoshop 9.0 software.

Table IX. **List of secondary antibodies used for immunofluorescence in this work**

Name	Description	Dilution	Coupled to	Source
A12c	Goat anti-mouse IgG (H+L)	1:200	Alexa Fluor 488	Dianova
A13c	Goat anti-mouse IgG (H+L)	1:200	Alexa Fluor 594	Dianova
A16c	Goat anti-mouse IgG (H+L)	1:100	Alexa Fluor 350	Dianova
B12c	Goat anti-rabbit IgG (H+L)	1:400	Alexa Fluor 488	Dianova
B13c	Goat anti-rabbit IgG (H+L)	1:500	Alexa Fluor 594	Dianova
B16c	Goat anti-rabbit IgG (H+L)	1:200	Alexa Fluor 350	Dianova
C12c	Goat anti-rat IgG (H+L)	1:200	Alexa Fluor 488	Dianova
C13c	Goat anti-rat IgG (H+L)	1:200	Alexa Fluor 594	Dianova
C16c	Goat anti-rat IgG (H+L)	1:100	Alexa Fluor 350	Dianova

3.6.2. Quantification of the length of microtubule plus-ends

The length of microtubule plus-ends was quantified using ImageJ (version 1.32j) software by drawing lines along microtubules plus-ends and subsequently measuring their length using the option "measure" in panel "analyze". The generated data files were imported and analyzed using Microsoft Excel 2000 (version 9.0.8948 SP-3) and SigmaPlot (version 8).

3.6.3. Live cell imaging and analyzing microtubule dynamics

For live cell imaging cells were seeded on 15 mm coverslips and transiently transfected with the mCherry-α-tubulin and MBD-GFP constructs (as described in chapter 4). Cells were imaged in an open chamber (Warner Instruments, Reading, UK) with a heater controller (model TC-324B) at 37°C using an Axiovert 100TV (Zeiss) inverted microscope equipped with EPI fluorescence lamp, electronically controlled shutters, filters and cooled CCD camera (see chapter 3.6.1.) controlled by MetaMorph software. Images were recorded at 2 seconds time interval using a 100x NA 1.4 plan-apochromatic objective lens. Cell culture medium was used and during live cell imaging the medium was exchanged every 30 minutes. Images were saved as "stack files" and analyzed using MetaMorph software. Movie sequences were subjected to a "low pass" filter in order to firmly expose microtubules and to reduce the background noise. Microtubule dynamics was analyzed by tracking microtubule

plus-ends of approximately 50 microtubules using MetaMorph "track points" function. Obtained data points were additionally analyzed in Microsoft Excel 2000 (version 9.0.8948 SP-3). Growth and shortening rates were calculated as the instantaneous velocities for each pair of consecutive image frames and then the average speed of growing or shrinking microtubules was calculated. Transition events from pause to shortening (or growth) were only classified as catastrophes (or rescues) if growth (or shortening) preceded pause. The catastrophe (or rescue) frequency was defined as number of catastrophe (or rescue) events in single frame divided by the time microtubules spent growing (or shortening).

4. Results

4.1. Influence of tubulin tyrosination on the localization of +TIPs

4.1.1. Subcellular localization of microtubule plus end tracking proteins

Subcellular localization of the most common +TIPs was analyzed in wild type and TTL-deficient mouse embryonic fibroblasts (MEFs). For that, cells were fixed and immunostained with antibodies directed against EB1, CLIP-170, CLIP115 and CLASP2. As shown in Figure 12A and B, EB1 revealed a normal comet-like localization at the microtubule plus end in both cell types, forming "comets" at the end of (growing) microtubules. It has been described that CAP-Gly domain-containing proteins (like CLIP-170) bind specifically to tyrosinated microtubules and do not bind to microtubules that have the C-teminal tyrosine residue on α-tubulin removed as the result of tubulin detyrosination (128). Surprisingly and in contrast to published data, in our set-up CLIP-170 is localized at MT + ends both in TTL+/+ and TTL-/- MEFs independently of the tubulin tyrosination (Fig. 12C and D). Also, the MT plus end localization of CLIP-115 was affirmed regardless to the tyrosination status of microtubule (Fig. 12E and F), which is also in contrast to the published data. Additionally, as it was already shown in the PhD thesis of Andreas Fischer, a notable difference in the length of CLIP-115 decorated MT +ends between TTL+/+ and TTL-/- MEFs was observed. This issue will be elaborated in detail in the further sections of this work. Finally, CLASP2 displays a slight plus end localization on microtubules and furthermore, perinuclear localization as well as microtubule lattice decoration in the lamella of migrating cells were obvious (Fig. 12G and H).

4.1.2. Generation of +TIP-specific RNAi knock-down vectors

The discovery of RNA interference and the development of several knock-down systems based on this widely abundant biological mechanism by which double-stranded RNA (dsRNA) induces gene silencing by targeting complementary mRNA for degradation, have revolutionized the way of studying gene function in living cells. The commercially available pSuper.neo+GFP vector bearing the green fluorescent protein (GFP)-coding cassette (Fig. 13), which allows selection of transfected cells, turned out to be a useful tool for knock-down of genes of interest. In this study this

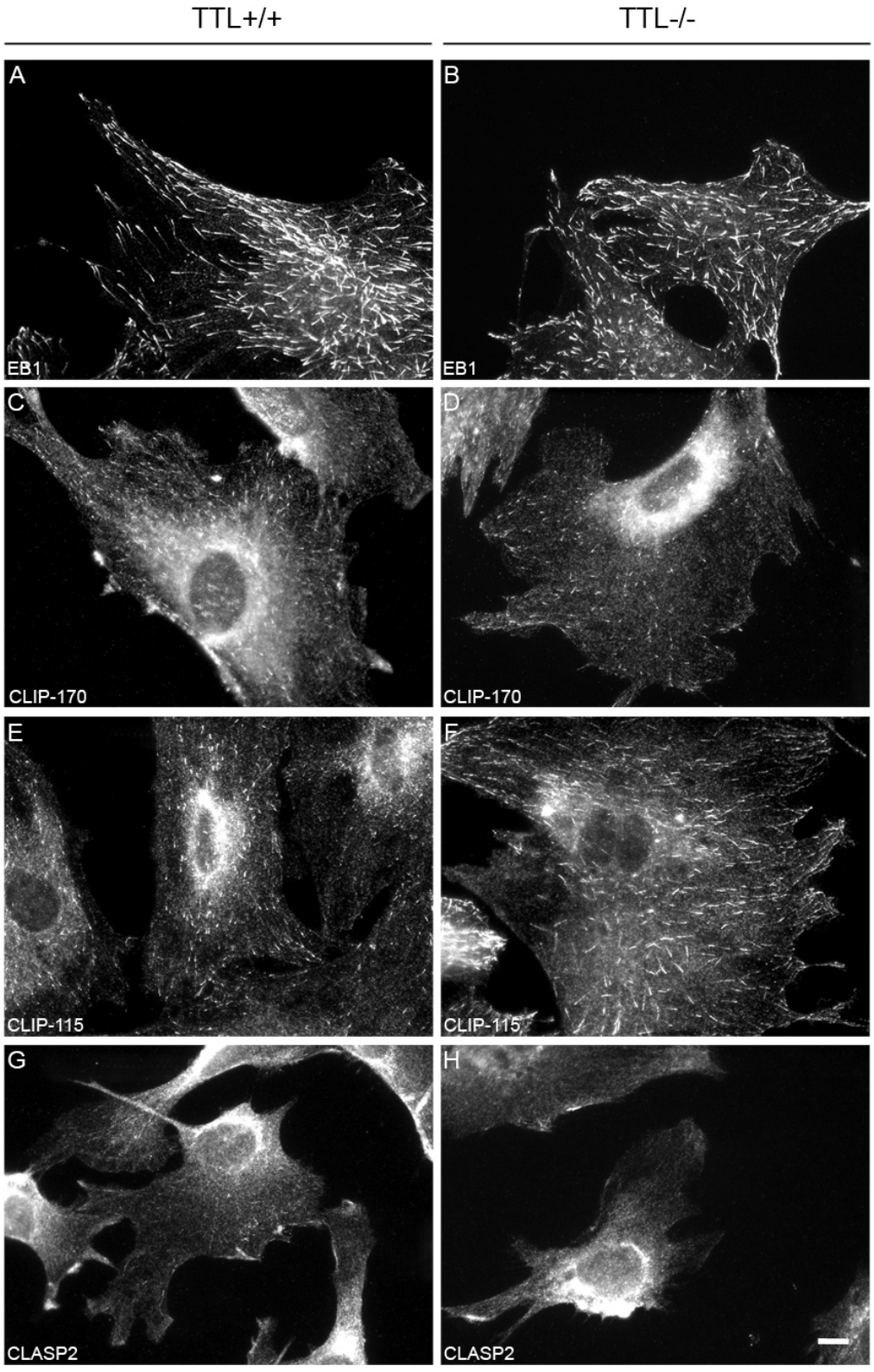

Figure 12. **Localization of +TIPs in TTL+/+ and TTL-/- MEFs.** Cells were fixed and immunostained using antibodies directed against EB1 (A, B), CLIP-170 (C, D), CLIP-115 (E, F) and CLASP2 (G, H). Clearly microtubule plus end localization was observed. Note the

difference in CLIP-115 microtubule plus end decoration between wild type and TTL-deficient cells. Multiple TTL+/+ and TTL-/- cell lines were used. Scale bar – 10 µm.

vector is used for investigating the +TIPs localization patterns in the context of the TTL cycle in mouse embryonic fibroblasts (MEFs). Specific oligonucleotide sequences designed to target mRNA of distinc +TIPs were cloned into pSuper.neo+GFP vector. For all of the +TIPs studied in this work, two separate constructs with different oligosequences were used to ensure high specificity of the knock-down. Oligonucleotide sequences that have already been published (146, 150, 162, 181) were used (see chapter 3.4.7.). After construct generation and sequence verification, functionality of the contructs was tested in B16 mouse melanoma cells. In all experiments the empty pSuper.neo+GFP plasmid was used as a negative control.

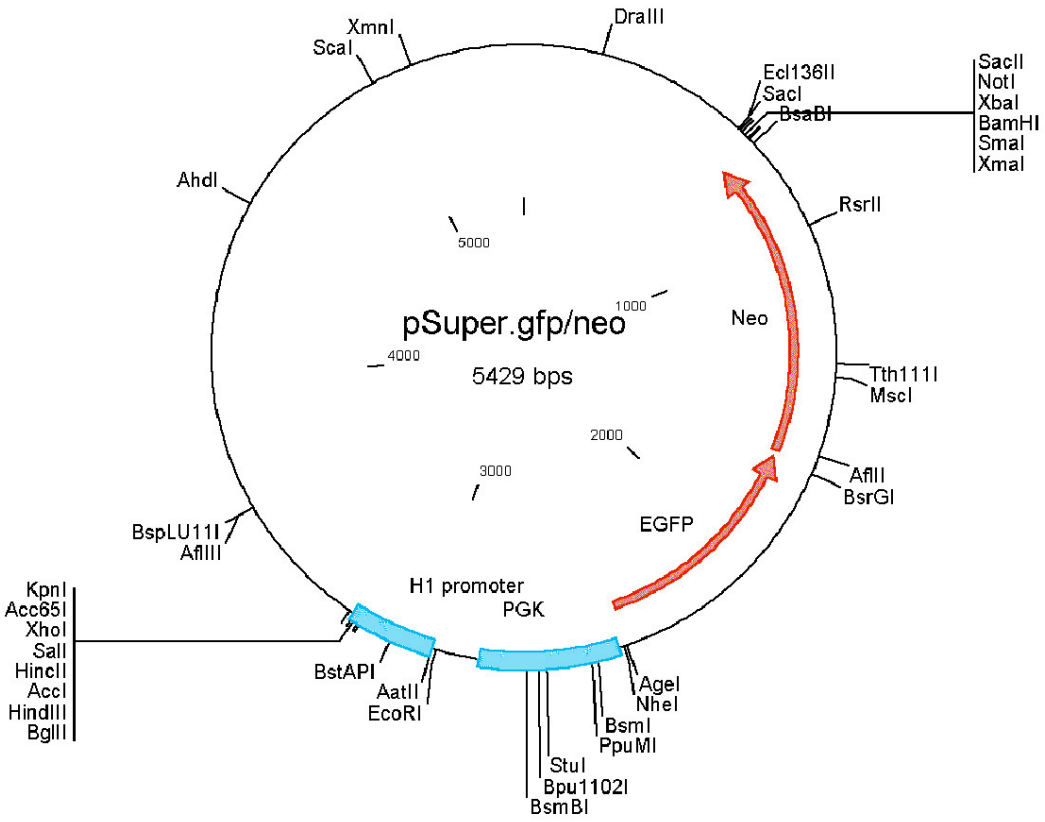

Figure 13. **Schematic representation of pSuper.neo+GFP RNAi.** Vector was used to clone the oligonucleotides for specific silencing of microtubule plus end binding proteins. For cloning the BglIII and HindIII restriction sites were used. *(Adapted from pSUPER RNAi system manual – OligoEngine 2003)*

Three to four days after transfection, cells were fixed and immunostained using specific antibodies detecting several +TIPs. All cloned RNAi contructs turned out to be functionally correct. The reduction of gene expression reached high level approximately 70 – 90%, which was visualized by immunofluorescence microscopy. The RNAi vectors were then used for transfection into wild type and TTL-deficient MEFs. Subsequently, localization of several +TIPs on microtbubule plus ends was compared using immunofluorescence microscopy. The results obtained by these RNAi experiments are described in the next chapters.

4.1.3. CLIP-170 knock-down in MEFs

CLIP-170 is the first discovered and one of the most studied plus end tracking proteins and is known to interact with many other +TIPs, like EB1, CLIP-115, CLASPs and Lis1 (18, 162). CLIP-170 can bind directly to MT +ends or through interactions with EB proteins (150, 152). Therefore, we analyzed how knock-down of CLIP-170 in MEFs might influence the binding of the other +TIPs in the context of tubulin tyrosination. 60 – 80 % confluent wild type and TTL-deficient MEFs were transfected with both CLIP-170 RNAi constructs and cells were fixed after 3 – 4 days. Transfected EGFP-expressing cells were selected and analyzed by immunofluorescence microscopy using antibodies detecting CLIP-170 as well as CLIP-115, EB1 and CLASP2. In transfected TTL+/+ and TTL-/- MEFs CLIP-170 was clearly no longer visible at MT +ends (Fig. 14B and 15B). In GFP-expressing cells, i.e. CLIP-170 knock-down, CLIP-115 proteins remained bound to the MT +ends in TTL+/+ and TTL-/- cells (Fig. 14D and 15D). Also, the localization of EB1 proteins on microtubules in both TTL+/+ and TTL-/- MEFs after CLIP-170 knock-down was unaffected (Fig. 14F and 15F). Finally, no changes in the localization of CLASP2 were noticed in CLIP-170 depleted TTL+/+ and TTL-/- MEFs (not shown).

4.1.4. CLIP-115 knock-down in MEFs

CLIP-115 belongs to the CAP-Gly domain-containing family of plus end tracking proteins and shows a high sequence homology to CLIP-170. CLIP-115 lacks the C-terminal zinc binding domain that is present in CLIP-170 (18). Since CLIP-115 interacts with CLIP-170, EB1 and CLASPs (18), we decided to analyze the localization of +TIPs in TTL wild type and *TTL* knock-out cells that were depleted from CLIP-115. For that, 60 – 80% confluent wild type and TTL-deficient MEFs

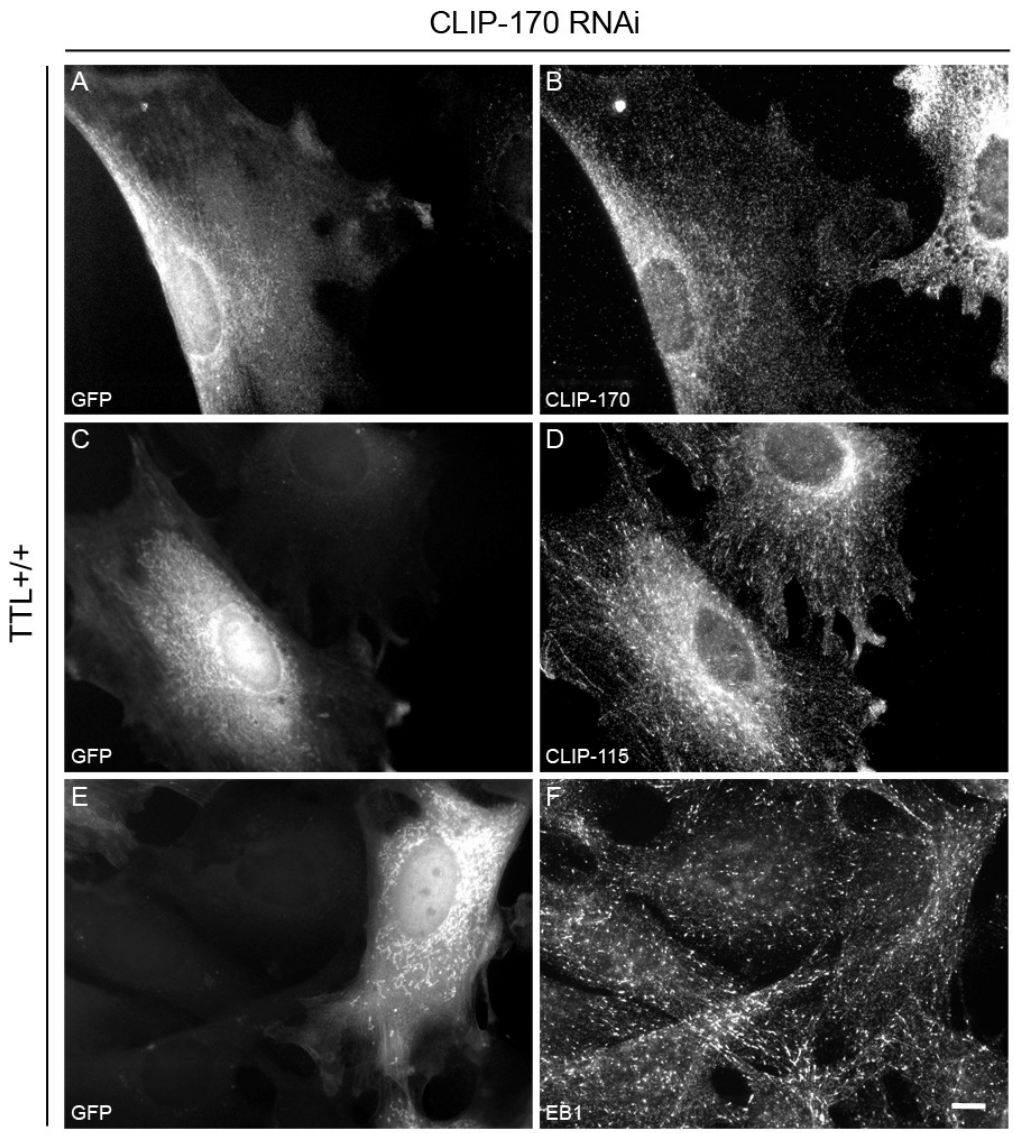

Figure 14. **CLIP-170 knock-down in TTL+/+ MEFs.** TTL+/+ cells (#67) were transfected with a CLIP-170 RNAi construct, fixed and immunostained using GFP (A,C,E) CLIP-170 (B), CLIP-115 (D) and EB1 (F) antibodies. GFP expressing cells clearly showed dislocalization of CLIP-170 (B), however this did not influence the localization of CLIP-115 (D) and EB1 (F). Scale bar – 10 μm.

were transfected with both CLIP-115 RNAi constructs and cells were fixed after 3 – 4 days. Cells were then immunostained using antibodies detecting CLIP-115 as well as CLIP-170, EB1 and CLASP2 to check their subcellular localization by immunofluorescence microscopy.

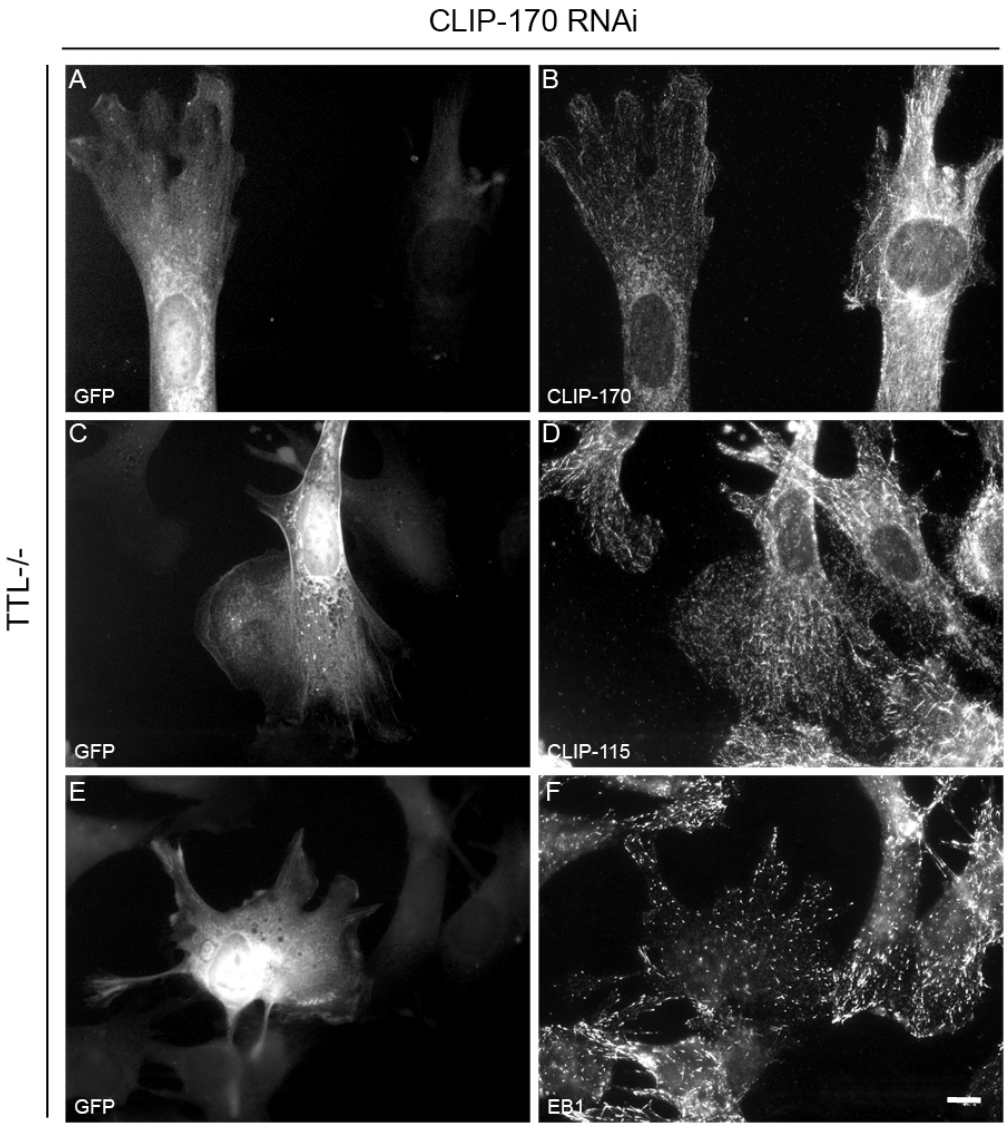

Figure 15. **CLIP-170 knock-down in TTL-/- MEFs.** TTL-/- cells (#59) were transfected with a CLIP-170 RNAi construct, fixed and immunostained using GFP (A,C,E) CLIP-170 (B), CLIP-115 (D) and EB1 (F) antibodies. As for wild type cells (Figure 14), GFP expressing cells clearly showed dislocalization of CLIP-170 (B), however this did not influence the localization of CLIP-115 (D) and EB1 (F). Scale bar – 10 μm.

In general, CLIP-115 depletion did not result in dislocalization of any of the other +TIPs tested, this observation is seen in both TTL+/+ and TTL-/- MEFs (Fig. 16B,D,F and 17B,D,F). These results are similar to the results found in CLIP-170 knock-down experiments. Thus, EB1, CLIP-170 and CLASP2 localization at MT+ ends is not affected by both CLIP-170 and CLIP-115 knock-down in wild type and TTL-deficient cells.

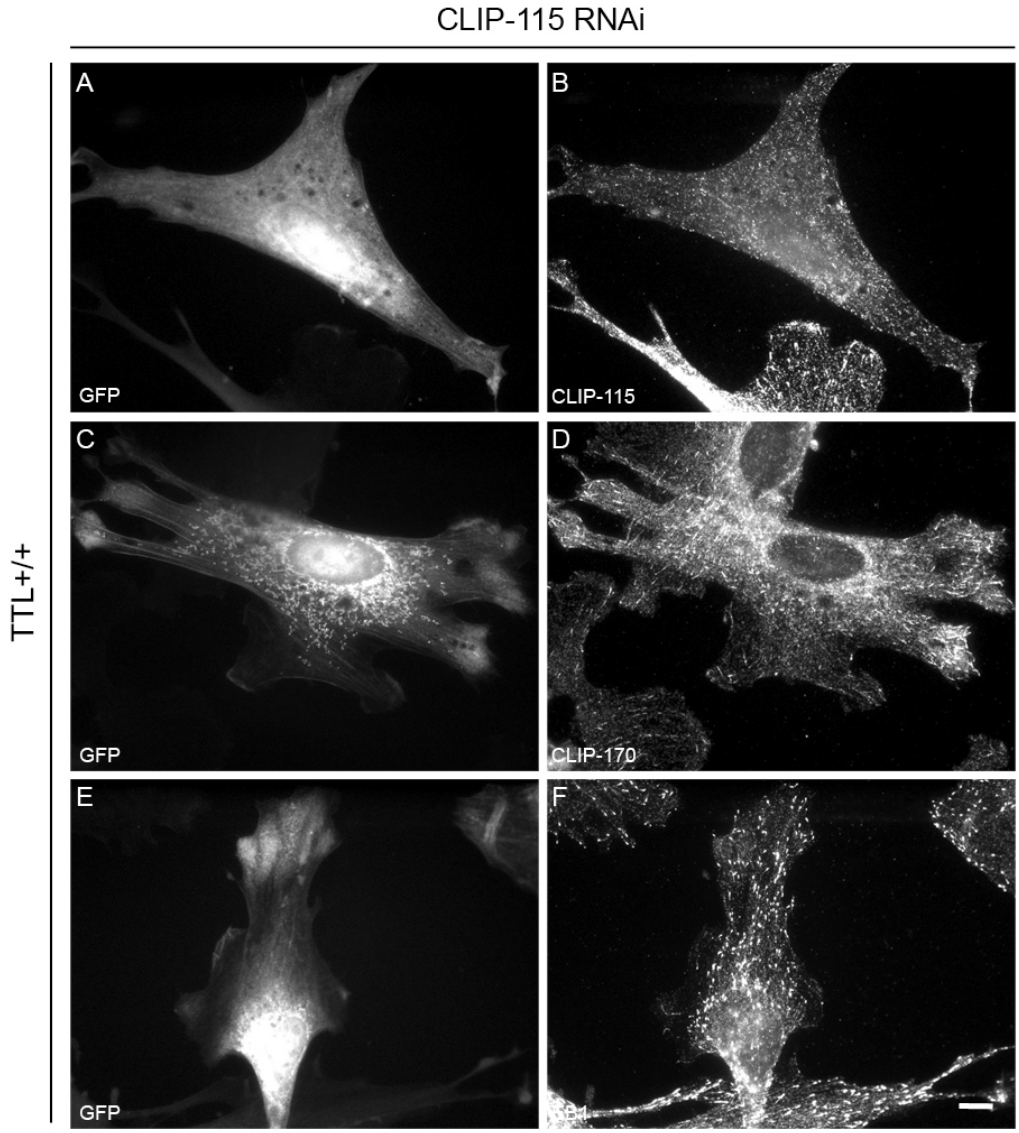

Figure 16. **CLIP-115 knock-down in TTL+/+ MEFs.** TTL+/+ cells (#67) were transfected with a CLIP-115 RNAi construct, fixed and immunostained using GFP (A,C,E) CLIP-115 (B), CLIP-170 (D) and EB1 (F) antibodies. GFP expressing cells clearly showed dislocalization of CLIP-115 (B), however this did not influence the localization of CLIP-170 (D) and EB1 (F). Scale bar – 10 μm.

4.1.5. CLASP2 knock-down in MEFs

CLASP2 is a member of the basic/Serine-rich sequences-containing protein family and was initially identified as a CLIP-170 interacting protein (18, 180). CLASP2 can bind directly to microtubules and additionally can interact with EB1, CLIP-115 and CLIP-170 (18, 181). Since CLASP proteins are also prominent regulators of microtubule dynamics (181), we tested how tyrosination / detyrosination of

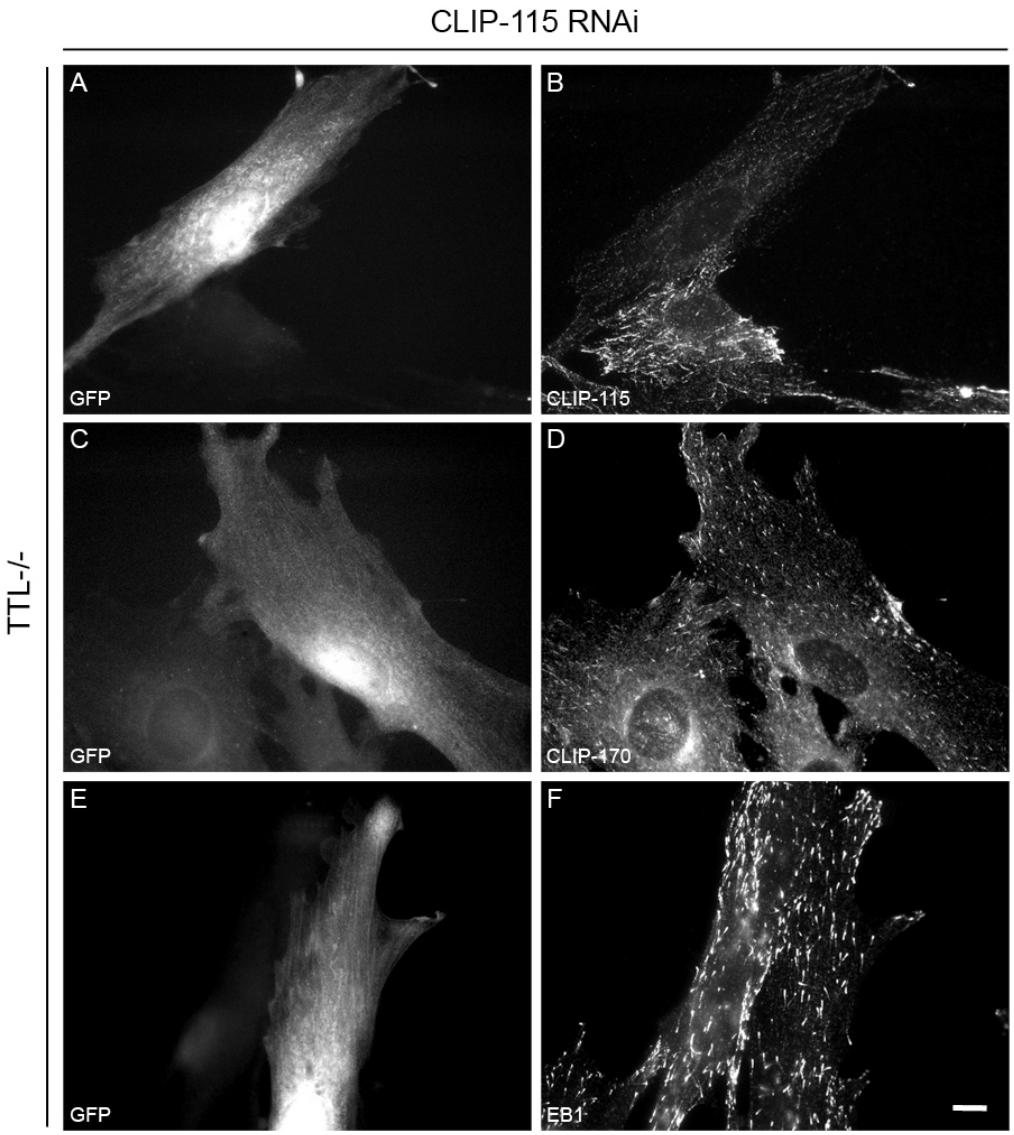

Figure 17. **CLIP-115 knock-down in TTL-/- MEFs.** TTL-/- cells (#59) were transfected with a CLIP-115 RNAi construct, fixed and immunostained using GFP (A,C,E) CLIP-115 (B), CLIP-170 (D) and EB1 (F) antibodies. As for wild type cells (Figure 16), GFP expressing cells clearly showed dislocalization of CLIP-115 (B), however this did not influence the localization of CLIP-170 (D) and EB1 (F). Scale bar – 10 μm.

microtubules would affect the binding of +TIPs to microtubules after CLASP2 depletion. Since immunostaining of CLASP2 requires a different fixation protocol as for the other +TIPs, it was not possible to obtain double labeling of CLASP2 together with CLIPs or EB1. Therefore, the GFP-expressing and thus CLASP2-depleted MEFs were selected and analyzed for CLIPs and EB1 localization. As shown in Figure

18B,D,F and 19B,D,F, CLASP2 RNAi treatment, did not affect EB1 as well as CLIP-170 and CLIP-115 localization on the MT +ends in both TTL+/+ or TTL-/- MEFs.

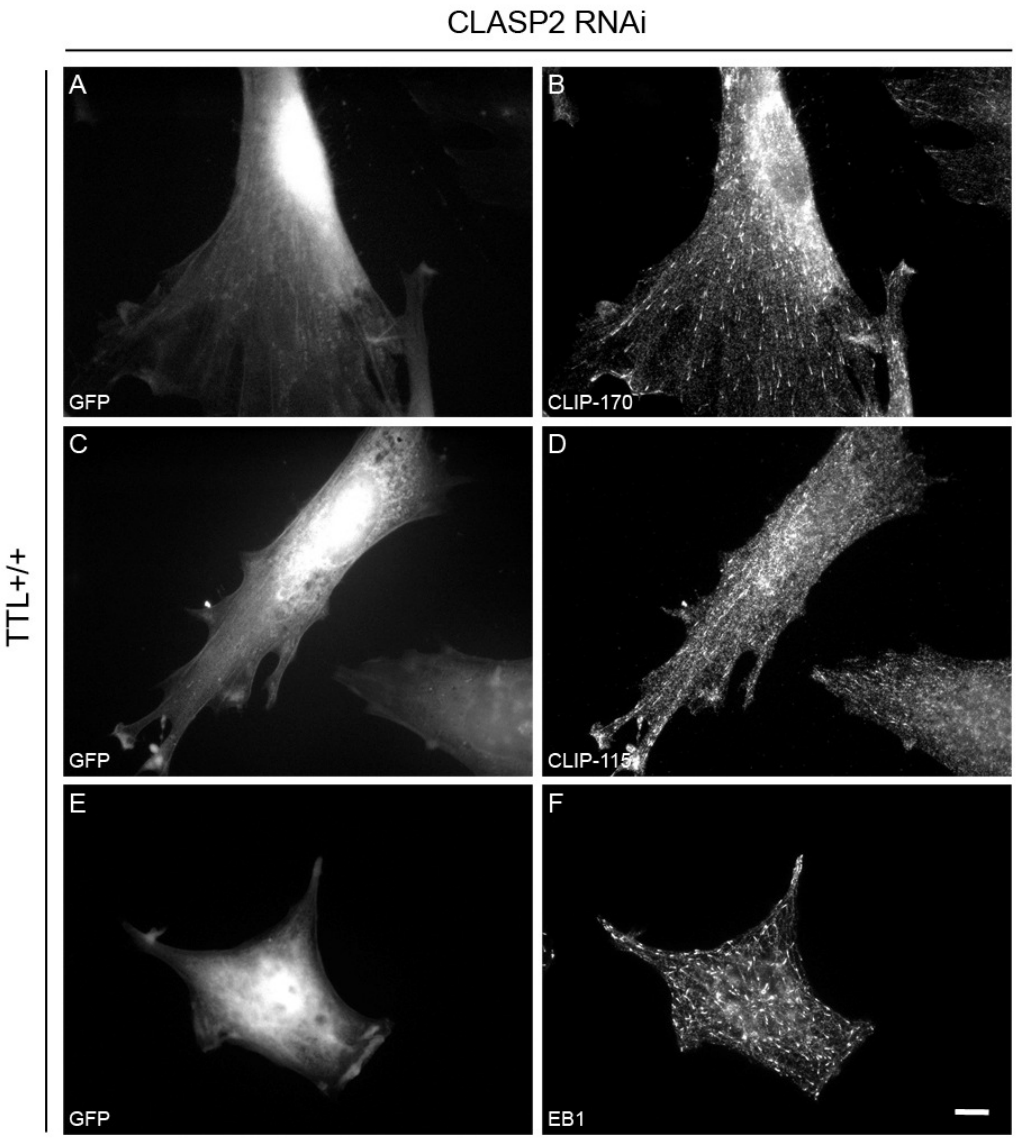

Figure 18. **CLASP2 knock-down in TTL+/+ MEFs.** TTL+/+ cells (#67) were transfected with a CLASP2 RNAi construct, fixed and immunostained using GFP (A,C,E) CLIP-170 (B), CLIP-115 (D) and EB1 (F) antibodies. CLASP2 knock-down did not influence the localization of CLIP-170 (B), CLIP-115 (D), and EB1 (F). Scale bar – 10 μm.

4.1.6. EB knock-down in TTL+/+ and TTL-/- MEFs

The EB family of microtubule plus end tracking proteins is comprised of the three closely related members EB1, EB2 and EB3. EB proteins are known to display microtubule plus end binding behavior independent of the presence of any other

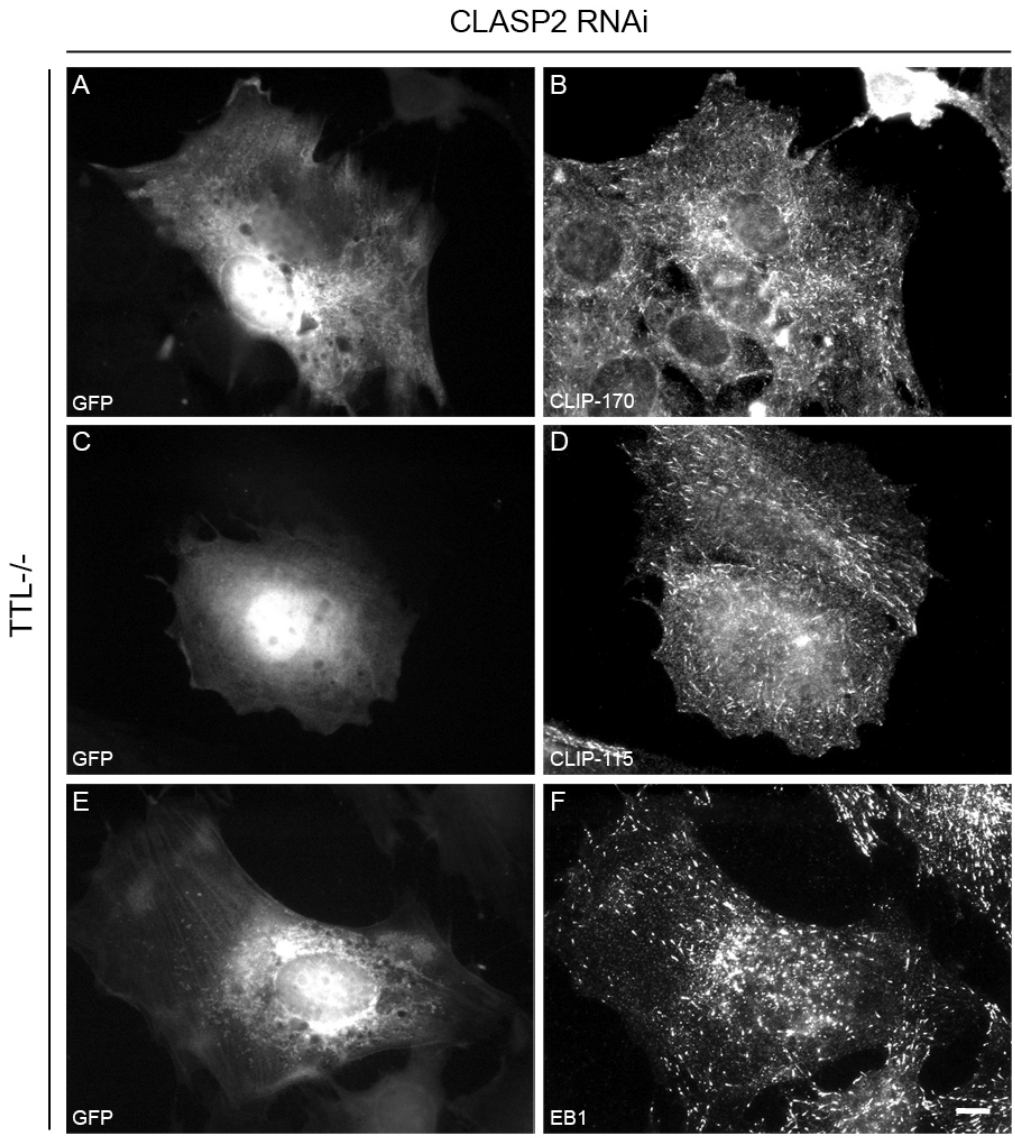

Figure 19. **CLASP2 knock-down in TTL-/- MEFs.** TTL-/- cells (#59) were transfected with a CLASP2 RNAi construct, fixed and immunostained using GFP (A,C,E) CLIP-170 (B), CLIP-115 (D) and EB1 (F) antibodies. As for wild type cells (Figure 18), CLASP2 knock-down did not influence the localization of CLIP-170 (B), CLIP-115 (D) and EB1 (F). Scale bar – 10 μm.

+TIPs (150, 152). Moreover, EBs can interact with and recruit many other +TIPs to the microtubule plus ends by a mechanism known as "hitchhiking" (150, 152). EBs are also regulators of microtubule dynamics acting as potent stabilizer of growing microtubules (145). Because EB proteins seem to be the spider in the web at the MT +end, we decided to analyze the influence of EB protein depletion on the localization of other +TIPs. We have focused on the CLIP family of +TIPs. Moreover, the effects were analyzed in the background of TTL deficiency. As all three EB proteins can be

differentially expressed and can fulfill distinct functions in different cell types, first, the expression pattern of EB1, EB2 and EB3 were tested in mouse embryonic fibroblasts.

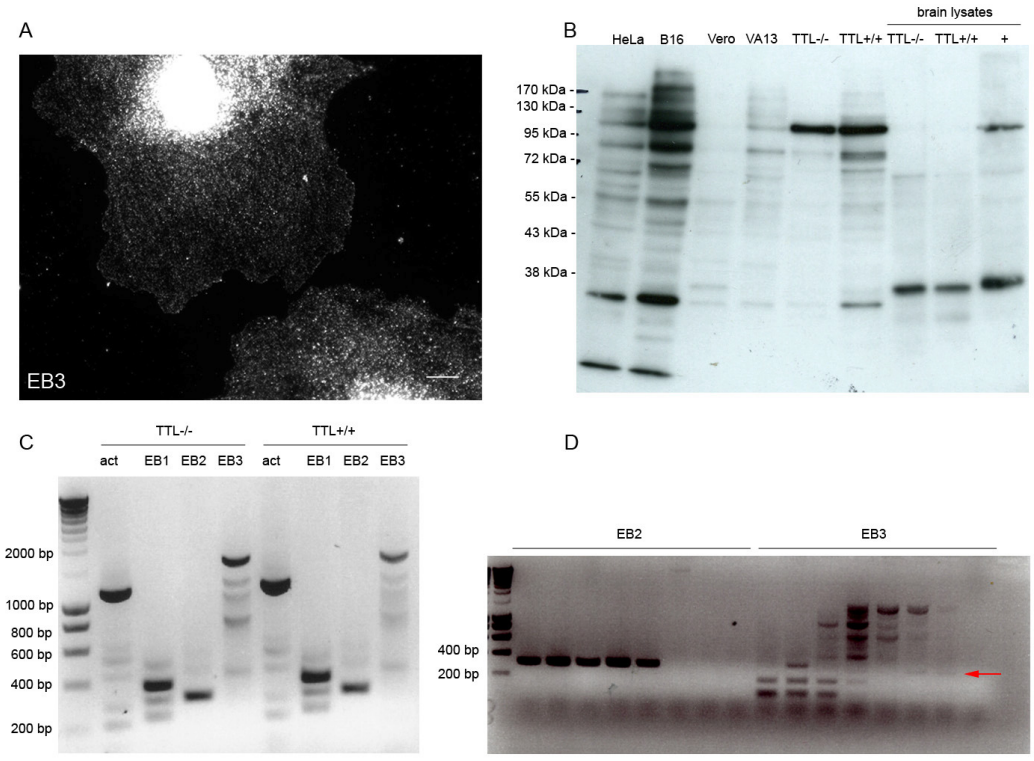

Figure 20. **EB expression in MEFs.** A) Immunofluorescence staining of TTL-/- MEFs using anti-EB3 antibodies. Cells were fixed and immunostained using an anti-EB3 monoclonal antibody. No clear EB3 localization at the MT +ends was observed. Scale bar – 10 µm. B) Western blot analysis using an EB3 monoclonal antibody. Cell lysates from different cell types were used and are listed above the image. Last three lanes show brain lysates from TTL +/+, TTL-/- mice and a "+" - positive brain lysate control. EB3 protein corresponds to ~38 kDa band. Obviously, no EB3 protein could be found in MEFs C) RT-PCR. cDNA from TTL+/+ and TTL-/- MEFs was isolated and analyzed by RT-PCR using specific primers for EB1, EB2, and EB3, and for actin as a positive control. PCR products of ~400 bp and ~350 bp correspond to EB1 and EB2 respectively. EB3 mRNA could not be detected in TTL +/+ and TTL-/- MEFs. D) Gradient PCR. cDNA from TTL+/+ and TTL-/- MEFs was isolated and analyzed by RT-PCR using specific primers for EB2 and EB3. A range of 30°C annealing temperature (from 42.8 to 67.2°C) was applied and PCR products were analyzed on an agarose gel. EB3 mRNA transcripts could only be detected as a faint band in the lanes marked with a red arrow.

By using EB1-specific primers in RT-PCR analysis, we found EB1 to be expressed in MEFs. No remarkable difference concerning mRNA levels between wild type and TTL-deficient MEFs was observed (Fig. 20C). Next, also EB2-specific mRNA was shown to be present in MEFs (Fig. 20C), however, using immunofluorescent microscopy, no specific EB2 localization could be observed (not shown). Finally, also

immunostaining using EB3-specific antibodies revealed no clear localization at microtubule plus ends (Fig. 20A) which is in contrast to published data (145, 150). To check these findings, Western blot analysis and RT-PCR were performed. Using total brain protein lysates obtained from the BD Biosciences as a positive control, wild type embryonic brain and *TTL* knockout brain it was clearly shown that EB3 protein is present as a ~38 kDa band in these lysates (Fig. 20C, lanes: brain lysates). In the same experiment obviously no EB3 protein is present in lysates derived from wild type and TTL-deficient MEFs (Fig. 20C, lanes: TTL+/+ and TTL-/-). Finally, although a very faint band was detected, RT-PCR analysis did not reveal the presence of EB3 specific mRNAs in MEFs (Fig. 20C and D). In conclusion, the fibroblasts used in this study do mainly express EB1. Both EB2 and EB3 turned out to be not detected at all, or at a very low level respectively.

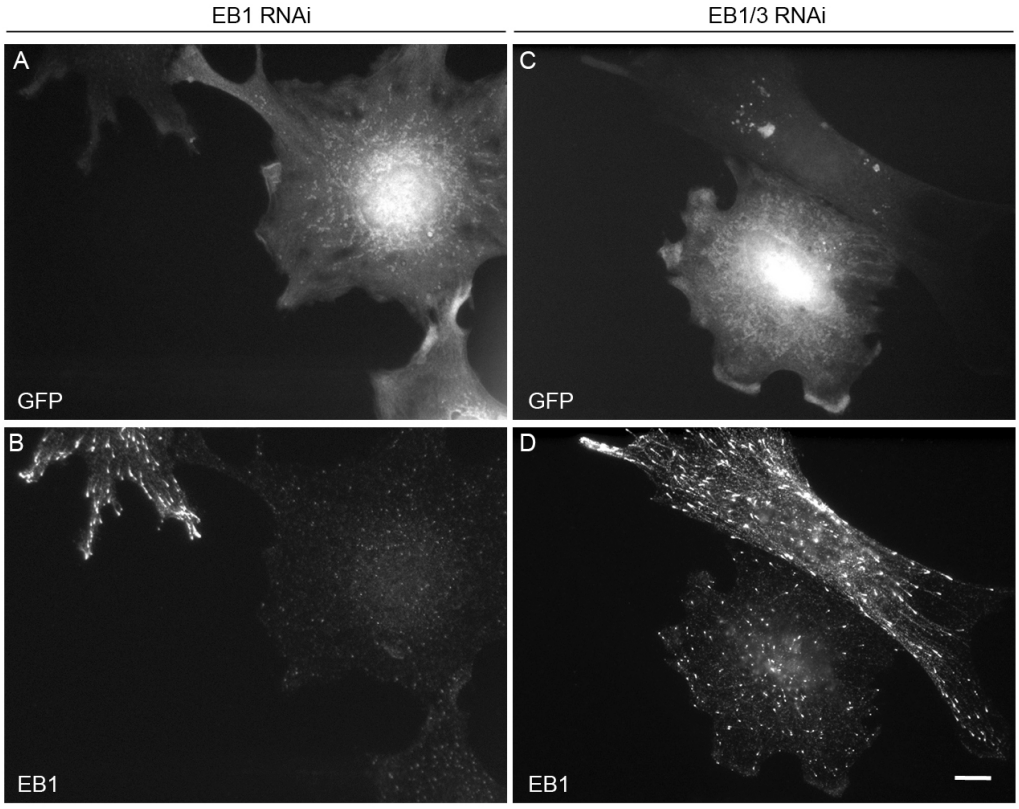

Figure 21. **Knock-down of EB proteins in MEFs.** TTL+/+ cells (#67) were transfected with EB1 or EB1/3 RNAi constructs, fixed and immunostained using GFP (A, C) and EB1 (B, D) antibodies. EB1-downregulated, GFP expressing cells show a clear reduction in EB1 expression (B), whereas EB1/EB3-downregulated, GFP expressing cells still show clear EB1 localization at microtubule plus ends (D). Scale bar – 10 μm.

To study the influence of EB proteins on the localization of the other +TIPs in the background of TTL-deficiency, RNAi knock-down was used to remove EB1 from MT +ends. Two sets of RNAi constructs, specific for EB1 and EB1/3, were used that supposed to result in the knock-down of EB1 and both EB1 and EB3 respectively. Because EB2 seems not to be present in our cell system, this protein was not further analyzed in this work. As described before, wild type and TTL-deficient MEFs were transfected with the different RNAi constructs. Cells were fixed after 3 – 4 days and immunostained using EB1-specific antibodies. EB1 RNAi construct-transfected cells were identified by the presence of GFP and in these cells, the amount of EB1 was reduced and dislocalized from MT +ends (Fig. 21A and B). In cells transfected with the constructs that should lead to EB1/EB3 double knock-down, EB1 was still present in the cells and still showed localization at the MT +ends, indicative for non-specific knock-down (Fig. 21C and D). For that reason the EB1/3 RNAi constructs were no longer used in this work.

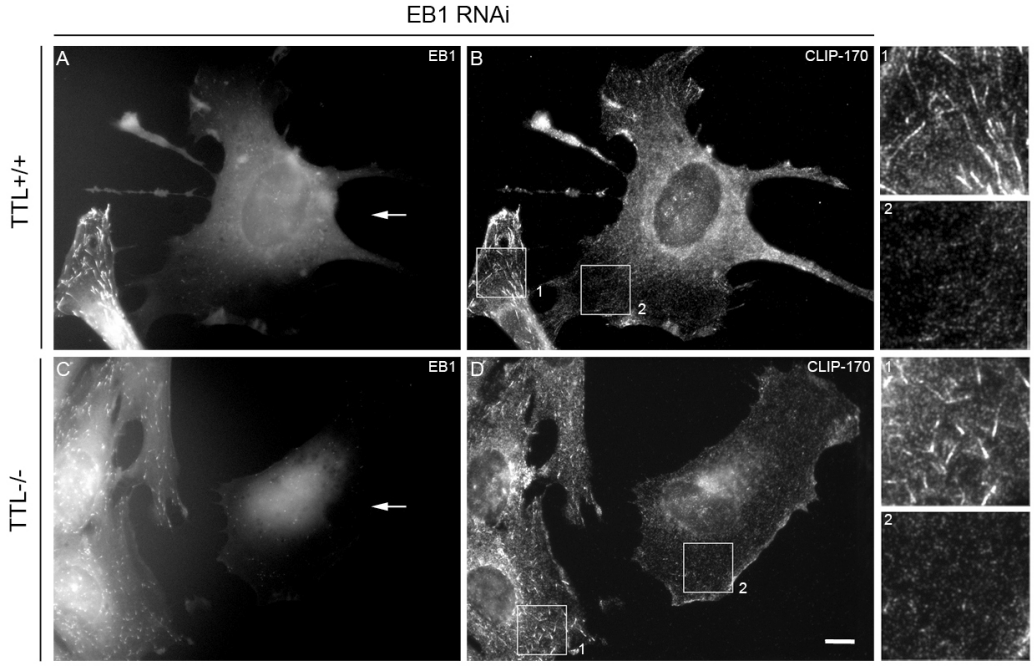

Figure 22. **EB1 knock-down influences CLIP-170 localization in TTL+/+ and TTL-/- MEFs.** TTL+/+ (#67) and TLL-/- (#59) MEFs were transfected with an EB1 RNAi construct, fixed and immunostained using EB1 (A, C) and CLIP-170 (B, D) antibodies. Transfected cells are marked by white arrows. EB1 knock-down leads to CLIP-170 dislocalization from MT +ends in both TTL+/+ and TTL-/- cells. The boxed regions are magnified and shown as insets 1 and 2 at the right. Scale bar – 10 μm.

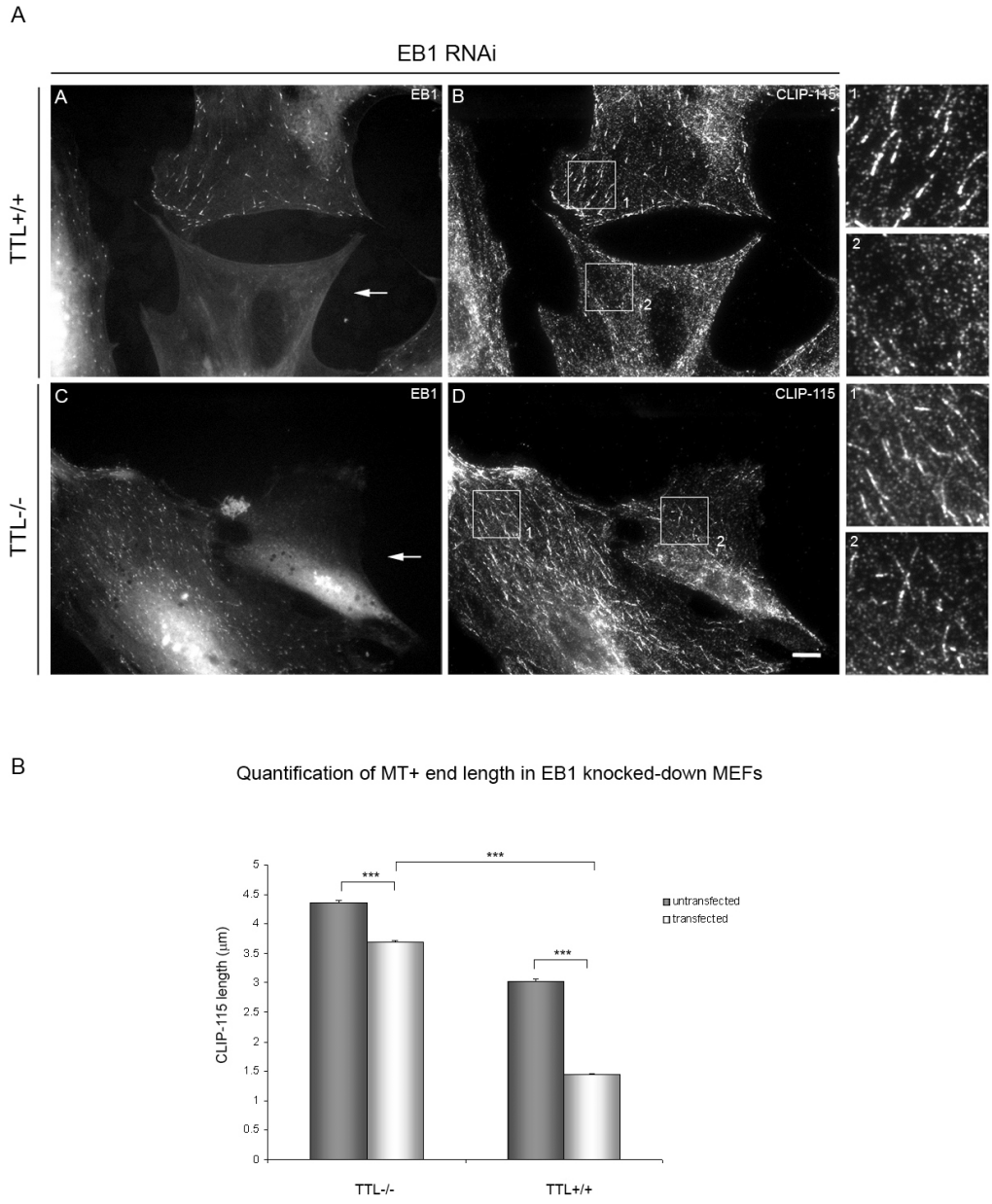

Figure 23. **EB1 knock-down influences CLIP-115 localization in TTL+/+ and TTL-/- MEFs.** A) TTL+/+ (#34) and TTL-/- (#33) MEFs were transfected with an EB1 RNAi construct, fixed and immunostained using EB1 (A, C) and CLIP-115 (B, D) antibodies. Transfected cells are marked by white arrows. Note: EB1 knock-down leads to CLIP-115 dislocalization from MT +ends only in TTL+/+ cells and not in TTL-/- cells. The boxed regions are magnified and shown as insets 1 and 2 at the right. Scale bar – 10 µm. B) Quantification of MT +ends length. CLIP-115 decorated MT +ends (<500 per condition) of cells treated as in A were measured. CLIP-115 comet length is significantly higher in TTL-/- cells. Statistical significance was assessed using *student T test*, *** - significant for p < 0,001. Bars on the chart show standard error of the mean (SEM).

As the EB1 knock-down turned out to be effective, the localization of CLIP proteins in EB1-depleted TTL+/+ and TTL-/- MEFs was analyzed. Again, transfected cells

could be recognized by EGFP fluorescence. In both TTL+/+ and TTL-/- cells, CLIP-170 was removed from microtubule plus ends upon EB1 knock-down (Fig. 22B and D), which is in line with published data (150).

Next, CLIP-115 localization in EB1 depleted MEFs was analyzed. As seen for CLIP-170, also CLIP-115 proteins were dislocalized from the MT +ends in TTL wild type cells after EB1 knock-down (Fig. 23B, panel A). In contrast, in TTL-deficient cells CLIP-115 remained present on the microtubule plus ends after EB1 knock-down (Fig. 23D, panel A). Quantification revealed significant differences in the length of CLIP-115 positive plus ends between TTL+/+ and TTL-/- MEFs. As it was already shown in the thesis of Andreas Fischer, in nontransfected cells, CLIP-115-decorated MT +ends were longer in TTL -/- MEFs compared to wild type cells (Fig. 12F). The length of CLIP-115 comets at microtubule plus ends in EB1-depleted TTL+/+ MEFs, that sometimes were still detectable, was much shorter then those in EB1-depleted TTL-/- MEFs (Fig. 23, panel B). Also the CLIP-115-decorated plus ends in EB1-depleted wild type cells were significantly shorter as the CLIP-115 plus ends in nontransfected wild type cells (Fig. 23, panel B). The same was observed in TTL-/- MEFs, Also here the CLIP-115-MT plus end length was significantly shorter in EB1-depleted cell compared to non-depleted cells. Furthermore, this difference was much smaller than that observed in TTL wild type MEFs (Fig. 23, panel B). Finally, the localization of CLASP2 was not affected by the knock down of EB1 in either wild type or TTL-deficient cells (not shown).

4.1.7. Reconstitution of TTL in EB1-depleted TTL-/- MEFs

Because a difference in binding behavior was observed for CLIP-115 in TTL+/+ and TTL-/- MEFs after EB1 knock-down, it was interesting to check whether it is possible to restore the CLIP-115 binding phenotype observed in TTL+/+ MEFs by re-introduction of TTL protein in TTL-deficient cells. For that purpose, TTL rescue experiments were performed in TTL-/- MEFs together with EB1 knock-down. The TTL-/- MEFs were co-transfected with the EB1 RNAi construct and the pIRES2-EGFP-TTL construct to simultaneously downregulate EB1 and overexpress TTL. After 3 – 4 days, cells were fixed and immunostained using antibodies directed against EB1, CLIP-115 and tyrosinated-tubulin. GFP expressing cells were selected and analyzed with respect to EB1, tyrosinated-tubulin and CLIP-115.

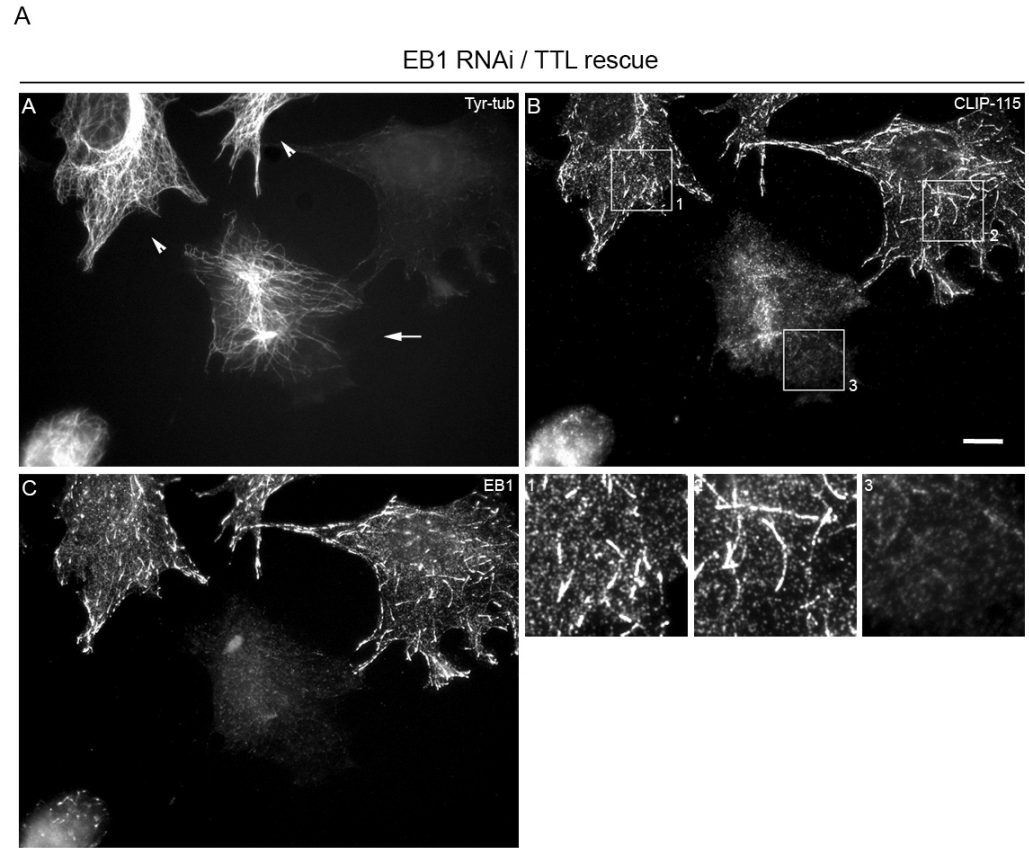

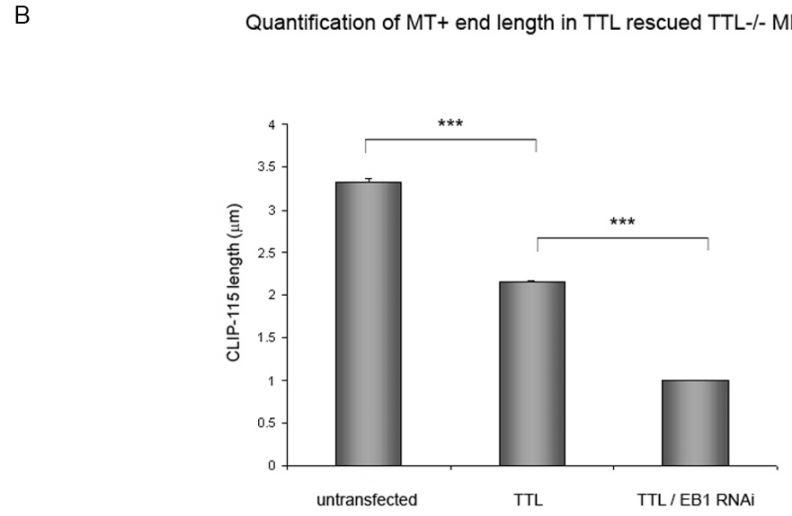

Figure 24. **TTL rescue experiments.** A) TTL-/- MEFs (#111) were cotransfected using EB1 RNAi and pIRES2-EGFP-TTL constructs, fixed and immunostained using tyrosinated-tubulin Y1/2 (A), CLIP-115 (B) and EB1 (C) antibodies. An EB1 downregulated and TTL overexpressing cell is marked by white arrow. Cells only overexpressing TTL are marked by white arrowheads. EB1 knock-down together with TTL rescue leads to CLIP-115 dislocalization from MT +ends in TTL-/- cells. The boxed regions are magnified and shown as

insets 1 to 3. Scale bar – 10 μm. B) Quantification of MT +ends length. CLIP-115 decorated MT +ends (<500 per condition) of cells treated as in A were measured. CLIP-115 comet length is significantly lower in EB1 downregulated rescued TTL-/- cells. Statistical significance was assessed using *student T test*, *** - significant for p < 0,001. Bars on the chart show standard error of the mean (SEM).

In EB1-depleted (Fig. 24C, panel A), TTL-rescued TTL-/- MEFs (Fig. 24A, panel A), e.g. cells that lack EB1 but do contain tyrosinated tubulin, CLIP-115 protein is removed from microtubule plus ends (Fig. 24A,B,C arrow, panel A). This is in line with observations in TTL+/+ MEFs. In TTL-/- cells that only re-express TTL and were not subjected to EB1 knock-down, CLIP-115 was still present on microtubule plus ends (Fig. 24A,B,C arrowheads, panel A). Non-transfected TTL-/- MEFs still have EB1 and CLIP-115 at the MT plus ends. Again, in these cells, CLIP-115-decorated plus ends were longer than those observed in TTL rescued cells which was assessed by microtubule plus end length quantification (Fig. 24, panel B). In some cases, CLIP-115 was still present at the microtubule plus ends of TTL-deficient cells that were reconstituted with TTL and were EB1-depleted. These reminiscent CLIP-115 structures were most probably due to non-complete knock-down in these cells. We were thus able to restore the differences in CLIP-115 comet length at microtubules in TTL-deficient cells by reconstitution of TTL.

4.1.8. Influence of the zinc-binding domain on CLIP-170 localization

CLIP-170 and CLIP-115 share a high similarity in amino acid sequences and only the absence of the C-terminal zinc-binding domain in CLIP-115 is the most remarkable difference between those two proteins (18). The zinc-binding domain of CLIP-170 interacts with its N-terminal CAP-Gly domain and thereby initiating a closed autoinhibited conformation that both ends of the protein are no longer accessible for the interactions with other proteins or organelles (18). Since a distinct localization of CLIP-115 on MT +ends was observed in TTL+/+ and TTL-/- MEFs, it was reasoned to test if this is simply due to the lack of zinc-binding domain in CLIP-115. To address this question a CLIP-170 construct that lacks the C-terminal zinc-binding domain was generated as a N-terminal GFP fusion protein. The pEGFP-CLIP170-ΔC construct was amplified and its expression was verified using Western blot analysis on transfected B16 cell lysates (not shown). Subsequently, the generated construct was used to transfect TTL+/+ and TTL-/- MEFs to analyze its subcellular distribution. Transfected cells were fixed and immunostained with antibodies against

GFP and CLIP-170. EGFP-CLIP170-ΔC as well as EGFP-CLIP-170-full length (used as a positive control) both localized to MT +ends. Obviously the MT plus ends

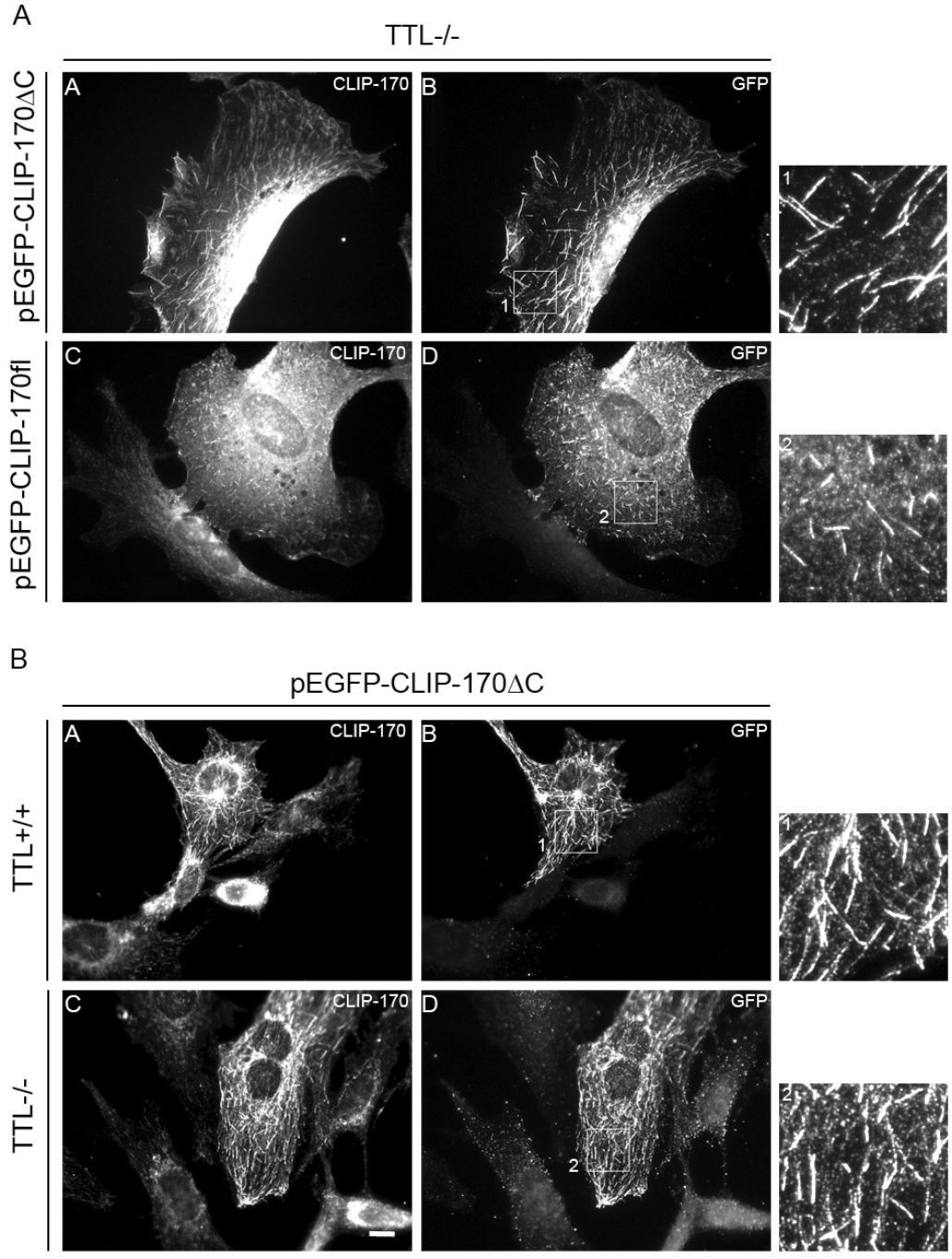

Figure 25. **EGFP-CLIP-170-ΔC localization in TTL+/+ and TTL-/- MEFs.** A) TTL-/- (#91) MEFs were transfected with EGFP-CLIP-170-ΔC or EGFP-CLIP-170-fl constructs, fixed and immunostained with CLIP-170 (A, C) and GFP (B, D) antibodies. The boxed regions are magniefied and shown as insets 1 and 2 at the right. EGFP-CLIP-170-ΔC binds stronger to MT +ends than EGFP-CLIP-170-full length. B) TTL+/+ (#110) and TTL-/- (#111) cells were transfected with EGFP-CLIP-170-ΔC, fixed and immunostained for CLIP-170 (A, C) and GFP (B, D). The boxed regions are magnified and shown as insets 1 and 2 at the right. No

difference in EGFP-CLIP-170-ΔC localization between TTL+/+ and TTL-/- MEFs could be observed. Scale bar – 10 μm.

decorated with EGFP-CLIP170-ΔC were longer (Fig. 25A, B, panel A) than those of EGFP-CLIP170-full length decorated MT plus ends (Fig. 25C, D, panel A). However, no difference in MT +ends length was observed when EGFP-CLIP170-ΔC was overexpressed in either wild type (Fig. 25A, B, panel B) or TTL-deficient MEFs (Fig. 25C, D, panel B).

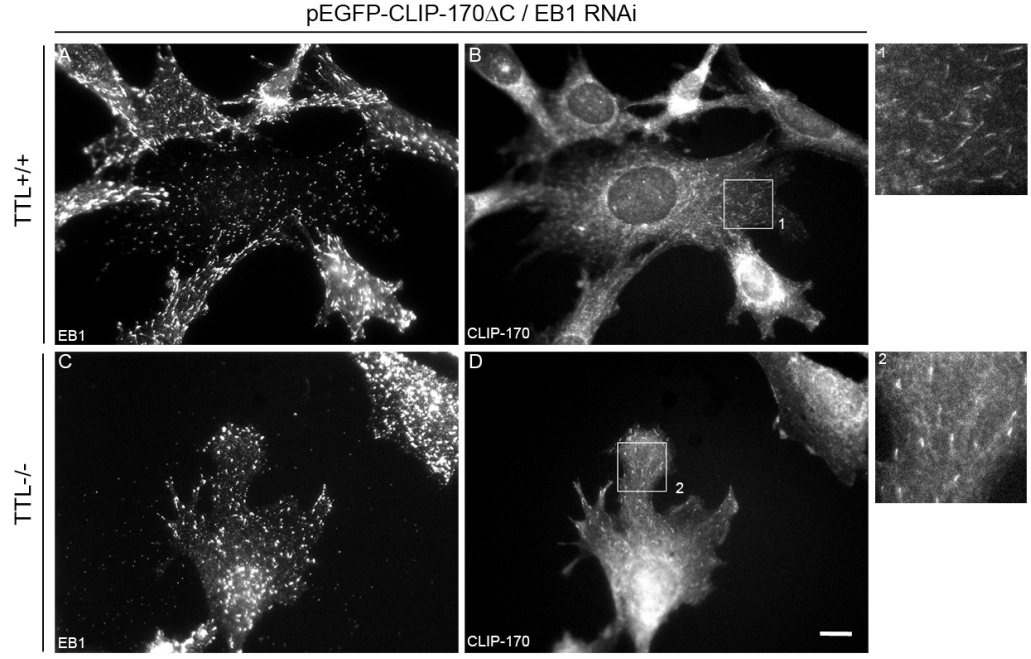

Figure 26. **EGFP-CLIP-170-ΔC localization in TTL+/+ and TTL-/- MEFs after EB1 knock-down.** TTL+/+ (#110) and TTL-/- (#111) MEFs were cotransfected with EB1 RNAi and EGFP-CLIP-170-ΔC constructs, fixed and immunostained with EB1 (A, C) and CLIP-170 (B, D) antibodies. Transfected cells can be distinguished by the reduced EB1 plus end localization. The boxed regions are magniefied and shown as insets 1 and 2 at the right. No difference in localization of EGFP-CLIP-170-ΔC could be observed in EB1-depleted TTL+/+ and TTL-/- cells. Scale bar – 10 μm.

As shown above (chapter 4.1.6.), EB1 knock-down influenced the localization of CLIP-115 in different ways in TTL+/+ and TTL-/- cells. Therefore, the localization of EGFP-CLIP170-ΔC in EB1 downregulated cells was tested. TTL+/+ and TTL-/- MEFs were co-transfected with the EB1 RNAi and EGFP-CLIP170-ΔC constructs. After 3 – 4 days, cells were fixed and immunostained using EB1- and CLIP-170-

specific antibodies. In EB1-depleted TTL+/+ and TTL-/- MEFs, EGFP-CLIP170-ΔC was removed from MT +plus ends equally. Only very short CLIP-170 "comets" were obvious in both cell lines (Fig. 26B and D). In summary, EGFP-CLIP170-ΔC protein showed the same microtubule plus end binding pattern in both TTL+/+ and TTL-/- MEFs that was not influenced by EB1-knock down, implicating that CLIP-170 lacking the zinc-binding domain does not phenocopy CLIP-115 in this experimental set-up.

4.1.9. EGFP-CLIP-115/170 hybrid proteins as a tool to study MT +end binding behavior of CLIPs

Because no differences were observed in the localization of C-terminal-deleted EGFP-CLIP-170 in TTL+/+ and TTL-/- MEFs, the difference in CLIP-115 binding pattern could not be simply accounted for the absence of the zinc-binding domain in this protein. To find out more about which part of CLIP-115 specifies the distinct localization of this protein to MT +ends, several GFP fusion constructs were generated comprising different parts of CLIP-170 and CLIP-115 in different combinations. Constructs were designed using homology blocks that were selected by sequence alignment of both proteins (Fig. 27). Constructs 1 – 5 contain N-terminally GPF fused CLIP-115 fragments followed by CLIP-170 parts. In contrast, constructs 6 – 10 comprise N-terminal GFP fused to CLIP-170 parts followed by CLIP-115 parts. The newly generated constructs were tested by transfecting B16 cells followed by Western blot analysis of the cell lysates. The resulting bands corresponded to the molecular masses of the hybrid proteins (not shown), indicating that all constructs were properly expressed. Subsequently, these constructs were transfected into TTL+/+ and TTL-/- MEFs in order to analyze MT +end localization of the fusion proteins. Cells were fixed and immunostained with anti-GFP antibodies one day after transfection. Additionally cells were stained for tyrosinated tubulin to select TTL-/- cells without any tyrosinated tubulin. All ten EGFP-CLIP-115/170 hybrid proteins showed microtubule plus end localization. Cells that express high levels of these proteins revealed localization of these proteins along the entire microtubule lattice (not shown). Therefore, only cells with low expression levels of the fusion proteins were analyzed. Hybrid proteins 1 – 4 showed typical binding to microtubule plus ends in both TTL+/+ and TTL-/- MEFs (Fig. 28A – H). However, for the proteins 3 and 4

a slightly lower association with the plus ends was observed only in TTL+/+ MEFs (Fig. 28E and G). Fusion protein 5 showed a remarkable difference in binding to MT between TTL+/+ and TTL-/- MEFs. Whereas in TTL-/- cells this protein was typically localized to the MT +ends, in TTL+/+ cells only weak plus end binding was noticed and in many cells a complete removal of this protein from MT +ends was observed (Fig. 28I and J). Additionally, hybrid proteins 1 – 5 displayed remarkable perinuclear localization in both TTL+/+ and TTL-/- MEFs (Fig. 28A – J). The hybrid proteins 6 – 10, that lack the C-terminal zinc-binding domain, showed stronger MT +end binding resulting in longer "comets" (Fig. 28K – T). However, no differences in comet length were observed between the different proteins in both TTL+/+ and TTL-/- MEFs. Only hybrid protein 8 revealed a slight weaker binding to MT +ends in both wild type and TTL-deficient MEFs (Fig. 28O and P). Furthermore, the proteins 6 – 10 showed no obvious perinuclear localization, in contrast to the proteins 1 – 5.

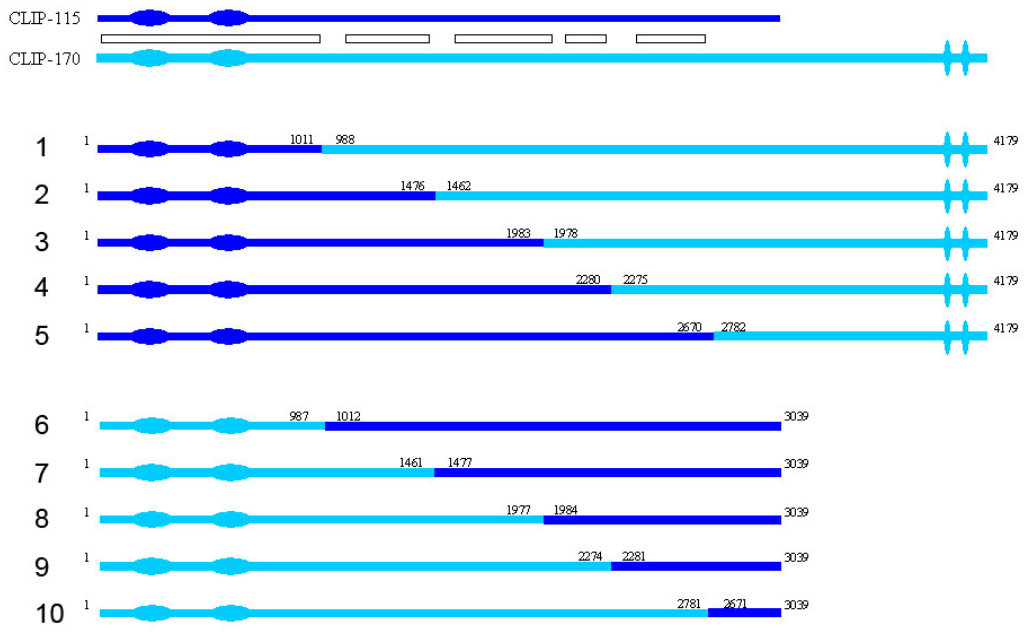

Figure 27. **Schematic representation of EGFP-CLIP115/170 hybrid constructs.** Schematic view of CLIP-115 (dark blue) CLIP-170 (light blue). Empty rectangles correspond to regions that are highly homologous between CLIP-115 and CLIP-170. Shown hybrids are numbered 1 to 10. Small numbers correspond to the respective base pairs in the cDNA. *(Drawing by Marco van Ham)*

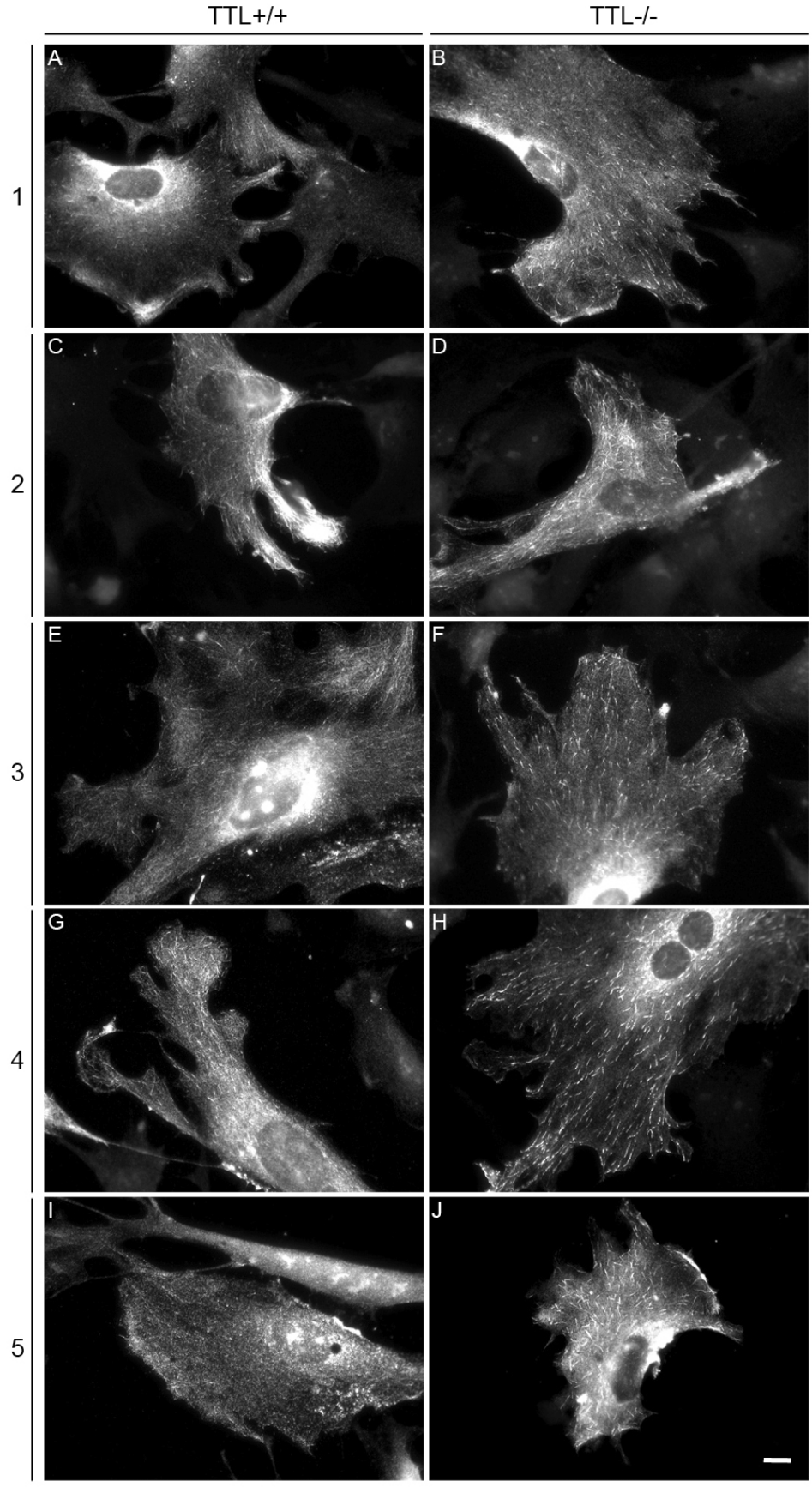
TTL+/+
TTL-/-
1
2
3
4
5
A
B
C
D
E
F
G
H
I
J

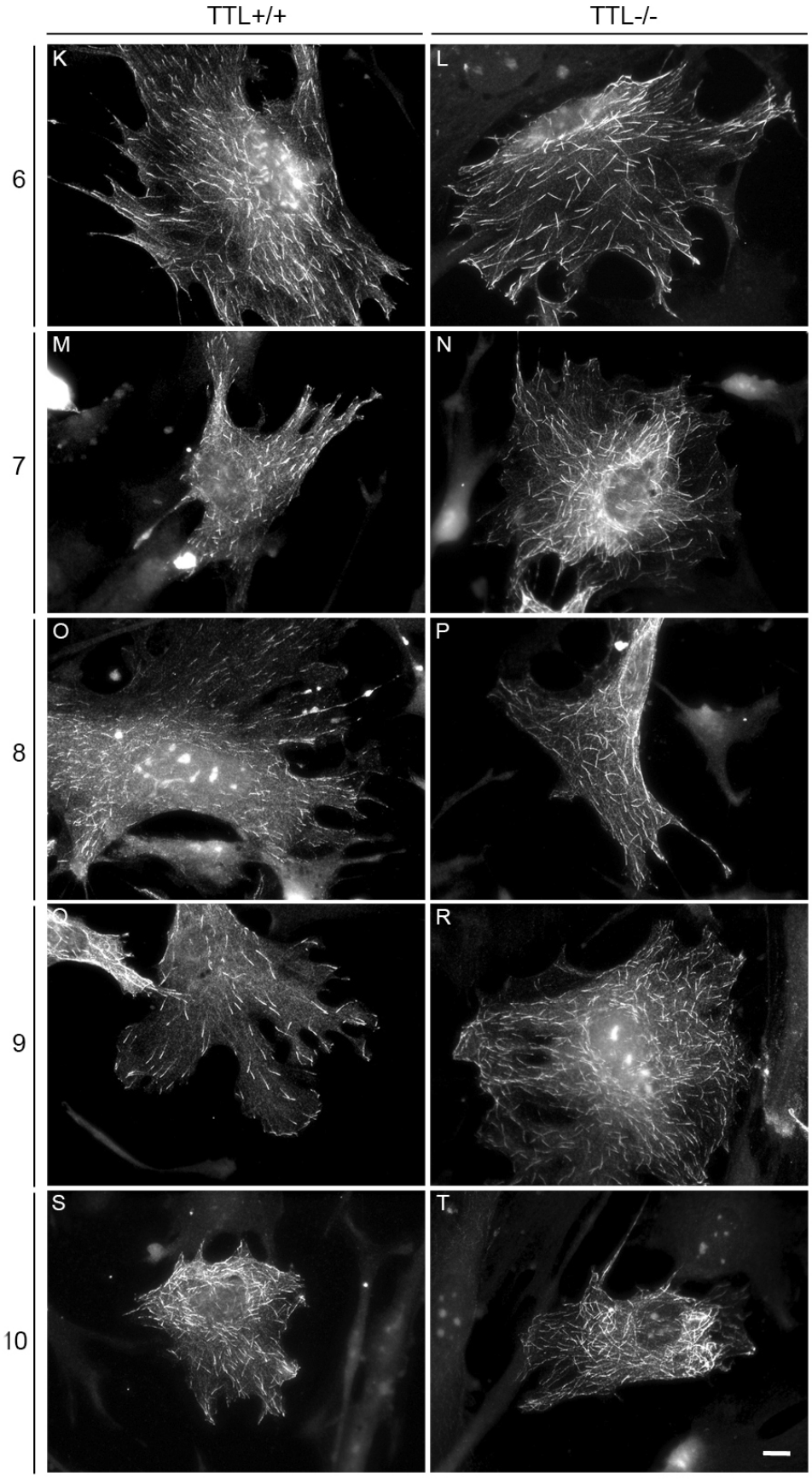
TTL+/+
TTL-/-
6
7
8
9
10
K
L
M
N
O
P
Q
R
S
T

Figure 28. **Localization of EGFP-CLIP115/170 hybrids in TTL+/+ and TTL-/- MEFs.** TTL+/+ (#189) and TTL-/- (#173) MEFs were transfected with the EGFP-CLIP115/170 hybrid constructs, fixed and immunostained with GFP antibodies. Numbers 1 – 10 correspond to the numbers as shown in Figure 27. For details see text. Scale bar – 10 μm.

4.2. Microtubule dynamics

4.2.1. mCherry-α-tubulin as a tool to study MT dynamics instability

Tyrosinated and detyrosinated populations of microtubules can have different dynamic properties. Tyrosinated microtubules display a more dynamic behavior, whereas detyrosinated microtubules appear to be more stable (119 – 121). Since TTL deletion results in accumulation of detyrosinated tubulin and the reduction of tyrosinated tubulin in cells, it is tempting to analyze MT dynamics in TTL wild type and TTL-deficient MEFs. To measure these parameters mCherry-α-tubulin constructs were employed, enabling visualization of dynamic microtubules in live cells using EPI microscope-based live cell imaging techniques. Since mCherry-α-tubulin is tyrosinated and the lack of tyrosinated tubulin is a hallmark of TTL-/- cells, we decided to use also a detyrosinated version of mCherry-α-tubulin in TTL-/- cells. The newly generated mCherry-α-tubulin-ΔY construct was amplified and used for transfection of TTL-/- MEFs. First, microtubule-incorporating properties of mCherry-α-tubulin proteins were tested. TTL+/+ and TTL-/- MEFs were transfected and fixed 1 day after transfection. Cells were subsequently immunostained with anti-DSred antibody recognizing mCherry. Both mCherry-α-tubulin and mCherry-α-tubulin-ΔY proteins were properly incorporated into the microtubule in TTL+/+ and TTL-/- cells (Fig. 29, panel A), indicating that the fusion proteins are fully functional. To measure the parameters of microtubule dynamics, cells seeded on coverslips were transfected and subjected to live cell imaging one day later. As mCherry-α-tubulin constructs fully reproduce MT dynamics, it was possible to analyze growing as well as pausing and shrinking microtubules. The plus ends of microtubules were tracked and the distance that microtubules traveled over time was measured. In that way, it was possible to draw history plots showing typical dynamic behavior of a single microtubule, comprised of the phases of growing, pausing and shrinking (Fig. 29, panel B).

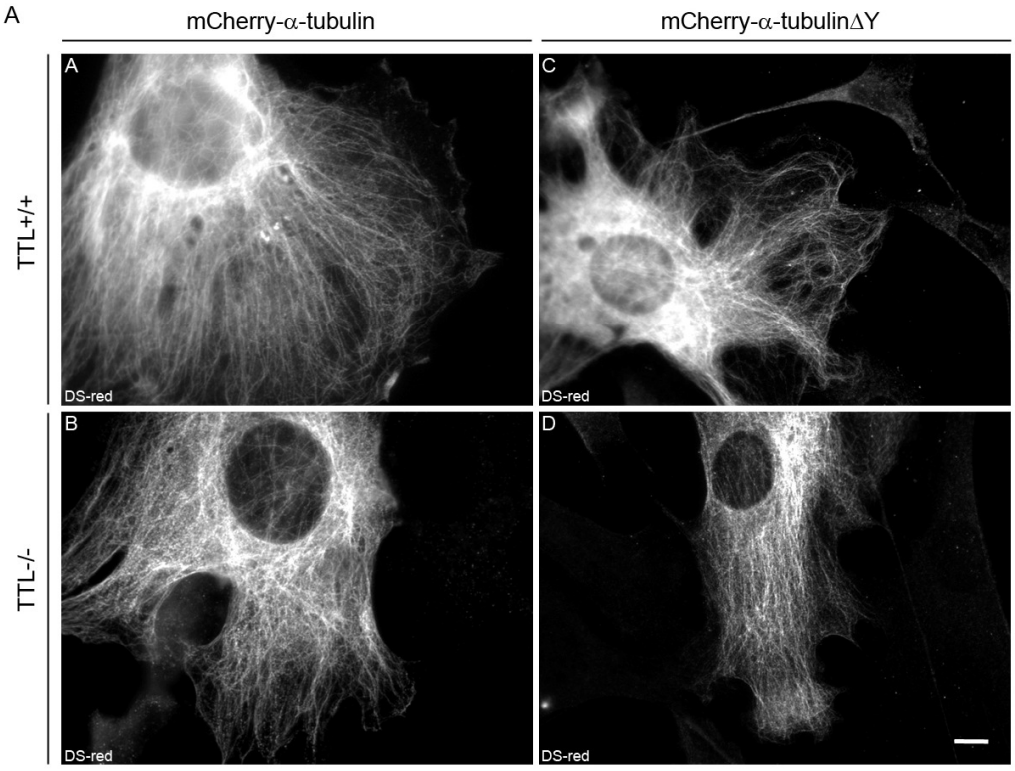

Figure 29. **mCherry-α-tubulin analysis in TTL+/+ and TTL-/- MEFs.** A) TTL+/+ (#67) and #107) and TTL-/- (#59 and #111) MEFs were transfected with mCherry-α-tubulin (A, B) or mCherry-α-tubulin-ΔY (C, D) constructs, fixed and immunostained with anti-DSred antibodies. Both mCherry-α-tubulin and mCherry-α-tubulin-ΔY assemble into microtubules. Scale bar – 10 µm. B) Microtubule history plot. TTL+/+ cells were transfected with a mCherry-α-tubulin construct and microtubule dynamics were analyzed by live-cell imaging. Images were made every two seconds and the distance a microtubule plus end has traveled (µm) is plotted against time (s). The history plot shown here is representative for made movies showing phases or growth, shrinkage and pause.

Parameters for microtubule dynamics including: growth rate, shortening rate, catastrophe and rescue frequency as well as the times microtubules spent growing, pausing and shrinking were analyzed.

Table X. **Microtubule dynamics**

MEFs	**TTL-/-**		**TTL+/+**	**TTL-/-**	**TTL+/+**	**TTL-/-**	**TTL+/+**
Construct	mCherry-tubΔY	mCherry-tub		mCherry-tub/ EB1RNAi		MBD-GFP	
Growth rate							
Mean (μm/min)	5.1 ± 3.6	6.4 ± 6.0	7.6 ± 5.8	5.8 ± 4.3	4.6 ± 3.0	4.4 ± 2.9	3.6 ± 2.3
Median (μm/min)	3.9 (n = 1271)	4.4 (n = 1146)	6.1 (n = 1720)	4.4 (n = 1486)	3.9 (n = 1277)	3.9 (n = 1245)	2.8 (n = 1256)
Shortening rate							
Mean (μm/min)	14.4 ± 13.2	12.0 ± 11.5	25.6 ± 20.7	13.7 ± 13.4	11.5 ± 10.3	8.0 ± 6,5	7.9 ± 6.0
Median (μm/min)	11.3 (n = 400)	7.8 (n = 697)	19.3 (n = 228)	9.2 (n = 528)	7.6 (n = 370)	6.2 (n = 652)	6.2 (n = 619)
Catastrophe frequency (s^{-1})	0.285 (n = 283)	0.232 (n = 325)	0.294 (n = 126)	0.096 (n = 102)	0.372 (n = 275)	0.152 (n = 201)	0.124 (n = 153)
Rescue frequency (s^{-1})	0.055 (n = 140)	0.106 (n = 244)	0.036 (n = 125)	0.040 (n = 119)	0.037 (n = 94)	0.072 (n = 180)	0.100 (n = 269)
Time spent:							
Growing (%)	33.6	31.5	57.3	35.6	23.1	25.1	27.3
Pausing (%)	55.9	49.4	35.6	51.8	70.2	61.7	59.3
Shortening (%)	10.6	19.1	7.1	12.8	6.7	13.2	13.4
Total time observed (min)	124	125	99	138	183	155	152
Number of cells, microtubules	9, 60	4, 50	5, 51	3, 45	2, 45	2, 50	2, 50

TTL+/+ (#34 and #132) and TTL-/- (#33 and #133) MEFs were used for analysis. n, total number of events observed. ± indicates standard deviation (SD).

In total, approximately 50 microtubules from distinct cells were analyzed per experiment. In TTL+/+ and TTL-/- cells transfected with mCherry-α-tubulin only slight differences in microtubule growth rates were observed, as the growth speed in TTL+/+ MEFs was slightly higher (Table X). A two-fold decrease in microtubule

shortening rate was observed in TTL-/- MEFs compared to TTL+/+ cells. No obvious differences in catastrophe frequency between the two cell lines were observed. However, rescue frequencies turned out to be increased in TTL-/- cells. Furthermore, microtubules in TTL-/- MEFs spent more time pausing and shrinking, and less time growing than TTL+/+ cells. TTL-/- cells overexpressing mCherry-α-tubulin-ΔY had slightly decreased MT growth rates and increased shortening rates compared to TTL-deficient cells overexpressing mCherry-α-tubulin. Catastrophe frequencies were comparable in both mCherry-α-tubulin and mCherry-α-tubulin-ΔYexpressing TTL-deficient cells, however, in contrast, rescue frequencies were decreased in TTL-/- MEFs transfected with mCherry-α-tubulin-ΔY compared to mCherry-α-tubulin-transfected TTL-/- MEFs. Microtubules in mCherry-α-tubulin-ΔY-transfected TTL-/- MEFs spent even more time pausing and less time shortening than microtubules in mCherry-α-tubulin-transfected TTL-/- MEFs.

4.2.2. Influence of EB1 on microtubule dynamics

As described in chapter 4.1.1. and 4.1.6., CLIP-115 showed different localization in TTL-deficient MEFs compared to wild type MEFs. Moreover, EB1 downregulation affected CLIP-115 localization differently in wild type and TTL-/- MEFs. Since CLIP-115 might be a potent MT dynamic regulator acting as a rescue factor, it was of most interest to test how EB1 knock-down influences MT dynamics. To test this, TTL+/+ and TTL-/- cells were cotransfected with the EB1 RNAi construct together with mCherry-α-tubulin. 3 – 4 days after transfection cells were subjected to live cell imaging and subsequently MT instability parameters were analyzed. Only cells expressing both GFP and mCherry were selected to be analyzed. It turned out that in both TTL+/+ and TTL-/- EB1-depleted MEFs, the MT growth rate was slightly decreased than in the respective EB1-undepleted cells (Table X). A more than two-fold decrease in shortening rate was observed in EB1-depleted TTL+/+ cells when compared to undepleted TTL+/+ MEFs. The MT shrinking rate of EB1-depleted and EB1-undepleted TTL-/- MEFs remained similar. EB1 knock-down did not affect rescue and catastrophe frequencies in TTL+/+ cells expressing mCherry-α-tubulin but caused a significant decrease in catastrophe and rescue frequencies in TTL-/- cells. The times that microtubules spent growing, pausing and shrinking were not obviously changed in TTL-/- cells upon EB1 knock-down. In contrast, a significant increase in

pausing time and decrease in growing time was observed in EB1-depleted wild type MEFs compared to EB1-undepleted MEFs.

4.2.3. Measuring microtubule dynamics using a MBD-GFP construct

The use of mCherry-α-tubulin can disturb the balance in total amount of tubulin in the cell and that might have a negative impact on the validity of measured microtubule dynamic parameters. To overcome this limitation, a different approach to study MT dynamics was carried out. The MAP4-derived microtubule binding domain (MBD) was used as a GFP fusion protein to study MT dynamics thereby avoiding any effect due to differences in intracellular tubulin levels.

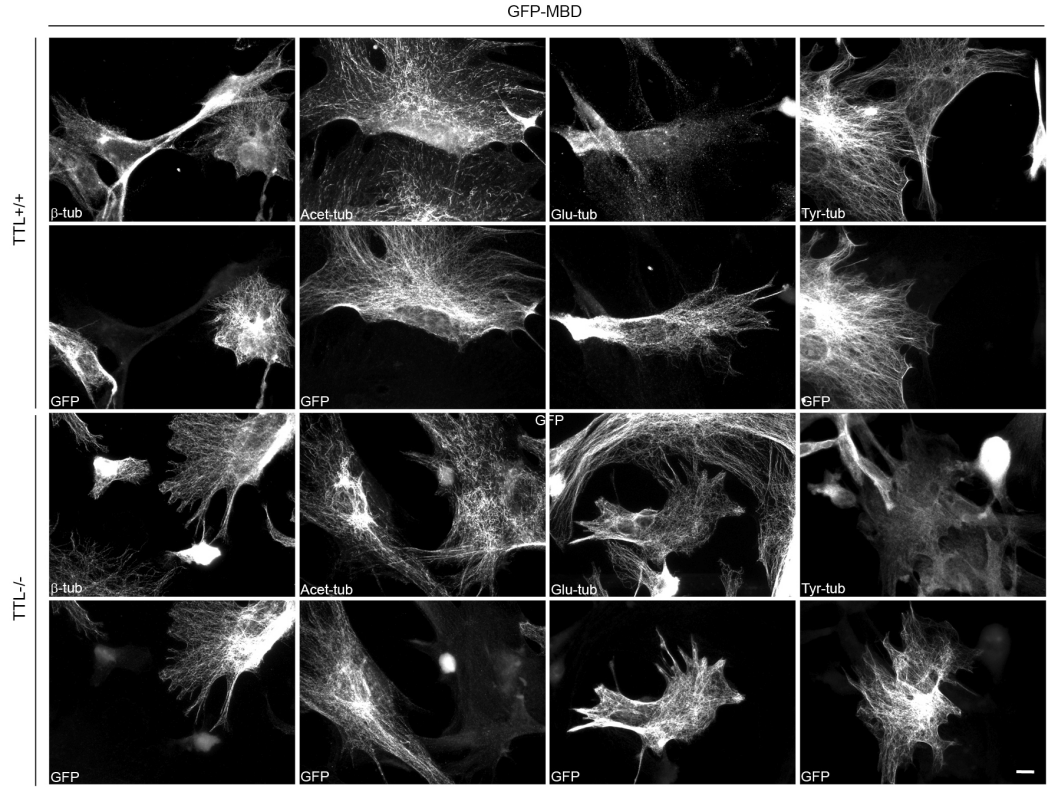

Figure 30. **Localization of MBD-GFP in TTL+/+ and TTL-/- MEFs.** TTL+/+ (#132) and TTL-/- (#133) MEFs were transfected with the MBD-GFP construct, fixed and immunostained using GFP, β-tubulin, tyrosinated-tubulin (YL1/2), acetylated-tubulin (6-11B-1), and glutamylated-tubulin (1D5) antibodies. Clearly, the MBD-GFP fusion protein does localize to microtubules and does not influence the MT-organization and the level of tubulin pools. Scale bar – 10 μm.

In order to check if the MBD-GFP protein is not influencing the different tubulin populations, TTL+/+ and TTL-/- MEFs were transfected and subsequently subjected

to immunofluorescence or Western blot analysis. The MBD-GFP protein localized to the entire microtubule and did not affect levels of acetylated-, glutamylated-, tyrosinated-tubulin nor β-tubulin levels in TTL+/+ and TTL-/- MEFs, as observed in microscopic analysis (Fig. 30). Also in Western blot analysis, no differences in the amount of tyrosinated-, glutamylated-, Δ2- and β-tubulin levels in either TTL+/+ or TTL-/- MEFs was observed (Fig. 31).

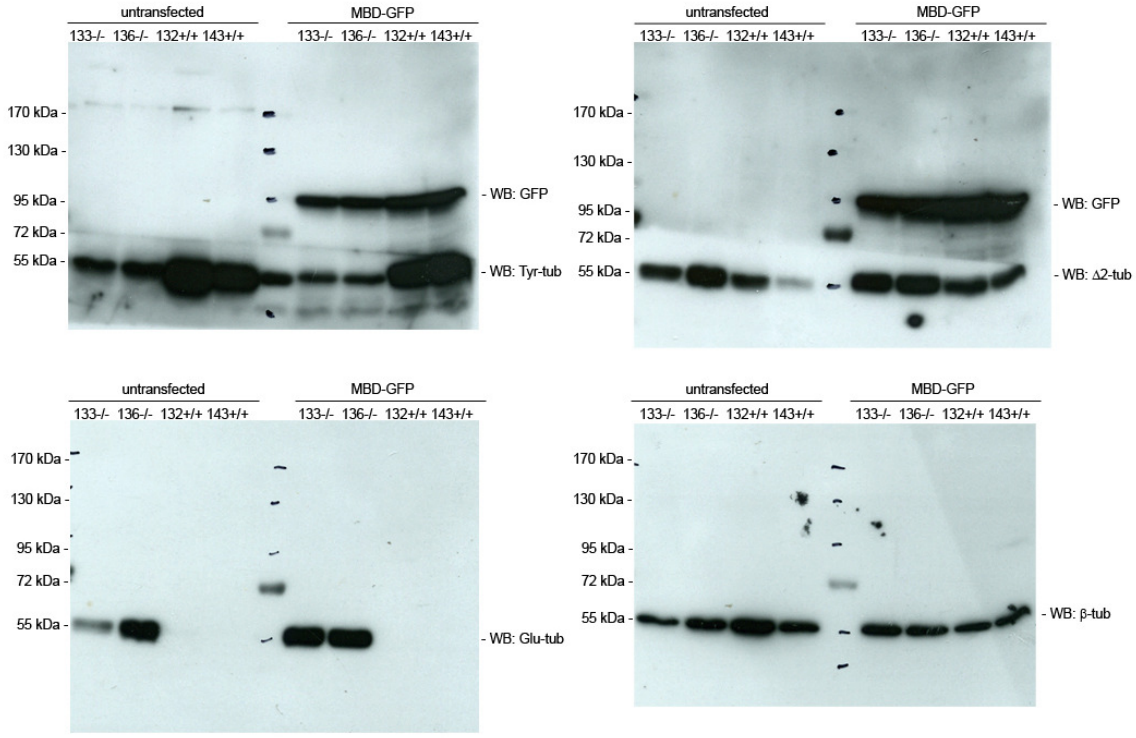

Figure 31. **The influence of MBD-GFP expression on tublin modifications.** TTL+/+ (#132 and #143) and TTL-/- (#133 and #136) MEFs were transfected with the MBD-GFP construct, lysed and subjected for Western blot analysis using GFP, β-tubulin, tyrosinated-tubulin (YL1/2), Δ2-tubulin (37B5D2) and glutamylated-tubulin (1D5) antibodies. Lysates from untransfected cells were used as negative controls. Obviously, MBD-GFP expression has no impact on the levels of posttranslationally modified tubulins in both TTL+/+ and TTL-/- cells. The MBD-GFP protein is recognized as a ~95 kDa band. The tubulins show a band at 55 kDa.

These results led us to anticipate that the MBD-GFP fusion protein would be a new tool to measure microtubule dynamics. To test that, the MBD-GFP construct was transfected into TTL+/+ or TTL-/- MEFs and cells were subjected to live cell imaging after 24 hours to measure the parameters of microtubule dynamics. In general, the MBD-GFP fusion protein led to a reduction of the growth and shortening rate of

microtubules in both TTL+/+ and TTL-/- cells compared to mCherry-α-tubulin-transfected cells. Additionally, the catastrophe frequencies were decreased in MBD-GFP transfected TTL+/+ and TTL-/- MEFs compared to cells expressing mCherry-α-tubulin. Furthermore, the rescue frequencies were increased in TTL-/- cells and slightly decreased in TTL+/+ cells transfected with MBD-GFP compared to cells overexpressing mCherry-α-tubulin. Both in wild type and TTL-deficient MBD-GFP expressing cells, a remarkable increase in time microtubules spent pausing was noticed and furthermore a decrease in growing time was observed compared to cells transfected with mCherry-α-tubulin. Slight changes in the time microtubule spent shortening were also observed in both TTL+/+ and TTL-/- MEFs expressing MBD-GFP, when compared to cells that express mCherry-α-tubulin. These results indicate that the MBD-GFP fusion protein unfortunately can not be used as a valuable tool for measuring MT dynamics in our cell system.

4.3. Cross-talk between MTs and the actin cytoskeleton

4.3.1. Aluminium fluoride (AlF_4) treatment of MEFs

Since it has been shown that microtubules can be coupled to and grow along actin filaments (21), the microtubule network may be influenced by the actin cytoskeleton. It has also been described that detyrosinated and tyrosinated tubulin populations have different dynamic features, as detyrosinated microtubules are usually more stable and tyrosinated microtubules show a more dynamic behavior (119 – 121). There is evidence that proteins, like small Rho GTPases that are involved in the regulation of the actin cytoskeleton could also play a role in the stabilization of microtubules (29, 33, 189). Small Rho GTPases belong to the family of GTPases that encompass a large group of enzymes which bind GTP and undergo conformational changes as GTP is hydrolysed to GDP. They are involved in many critical biological processes and play an important role in signal transduction, protein biosynthesis, cell migration and differentiation. In order to test the influence of small Rho GTPases on the microtubule cytoskeleton in TTL+/+ and TTL-/- MEFs, cells were subjected to AlF_4 treatment, which results in non-specific activation of GTPases leading to the promotion of extensive lamellipodial protrusions. AlF_4 treated cells were fixed and stained with antibodies against tubulin and several +TIPs, such as EB1, CLIP-170

and CLIP-115, to observe possible changes in microtubule organization and localization of +TIPs. The efficiency of the AlF_4 was judged by actin-phalloidin staining (not shown). Clearly, after AlF_4 treatment microtubules displayed a curly appearance and that these curly microtubule structures were decorated with EB1, CLIP-170 and CLIP-115 proteins. Obviously, EB1, CLIP-170 and CLIP-115 were associated along the entire length of microtubules (Fig. 32). This phenotype was not only observed for tyrosinated microtubules (e.g. in wild type cells) but also for detyrosinated microtubules and occurred in both TTL+/+ as well as in TTL-/- cell lines. Concluding, unspecific activation of the GTPases resulted in the TTL-independent response leading to drastic changes in microtubule phenotype.

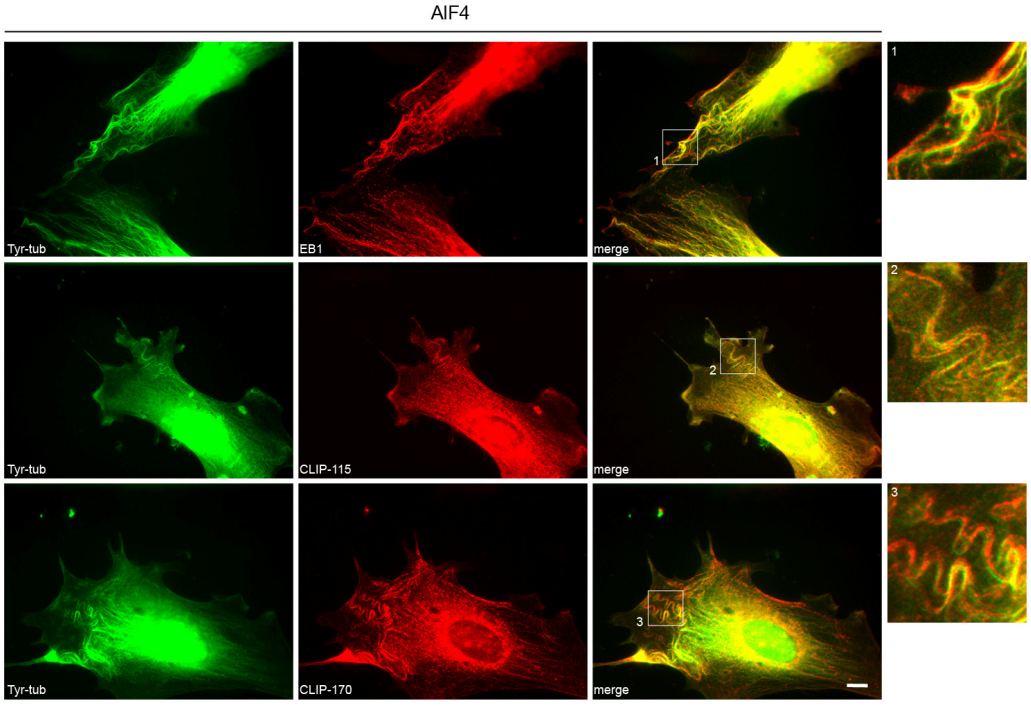

Figure 32. **AlF_4 treatment in MEFs.** TTL+/+ (#34) MEFs were treated with AlF_4, fixed and immunostained with CLIP-115, CLIP-170 tyrosinated-tubulin (20C6) and EB1 antibodies. AlF_4 treatment clearly leads to changes in the microtubule shape and to decoration of the entire microtubules with the analyzed +TIPs. The boxed regions are magnified and shown as insets 1 to 3 at the right. Scale bar – 10 µm.

4.3.2. mDia1 expression levels in MEFs

The establishment of microtubule stability can involve a RhoA-dependent pathway where mDia1 can act downstream of RhoA (29, 33, 189). Since TTL-/- and TTL+/+ cells contain microtubule populations conferring different stability levels, the levels

of protein expression and activity of components of the Rho-dependent microtubule stabilization pathway were analyzed in both cell types. Having specific mDia1 and mDia2 antibodies available, it was possible to test the expression levels of these proteins by Western blot analysis using cell lysates obtained from TTL+/+ and TTL-/- MEFs. Obviously, mDia2 proteins were found to be not expressed in MEFs (not shown). In contrast, mDia1 is being expressed in both wild type and TTL-deficient MEFs. However, an obvious variation in mDia1 expression level was detected and no correlation between mDia1 expression level and the presence of the TTL was observed (Fig. 33).

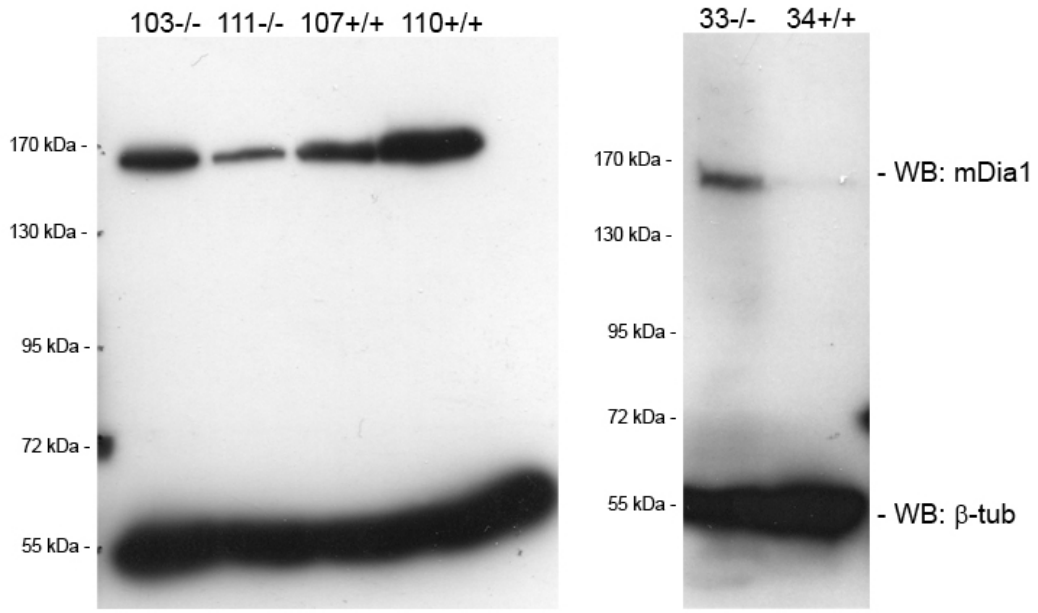

Figure 33. **mDia1 expression levels in TTL+/+ and TTL-/- MEFs.** TTL+/+ (#34, #107 and #110) and TTL-/- (#33, #103 and #111) MEFs were lysed and subjected for Western blot analysis using mDia1 antibodies. β-tubulin antibodies were used as a loading control. Obviously, mDia1 is expressed at different levels in MEFs (i.e. independently of TTL genotype). mDia1 protein is recognized as a ~140 kDa band. β-tubulin shows a band at 55 kDa.

4.3.3. Small Rho GTPase levels in MEFs

Since a diverse expression level of mDia1 was observed in TTL+/+ and TTL-/- MEFs, it was tempting to test the levels the upstream RhoA regulator. Additionally, mDia1 can also mediate MT stabilization and the formation of actin stress fibers (28, 29). Furthermore, it is published that Rac1 activity is enhanced in TTL-deficient neuronal cells (214). Cdc42, another small GTPase, is involved in many microtubule

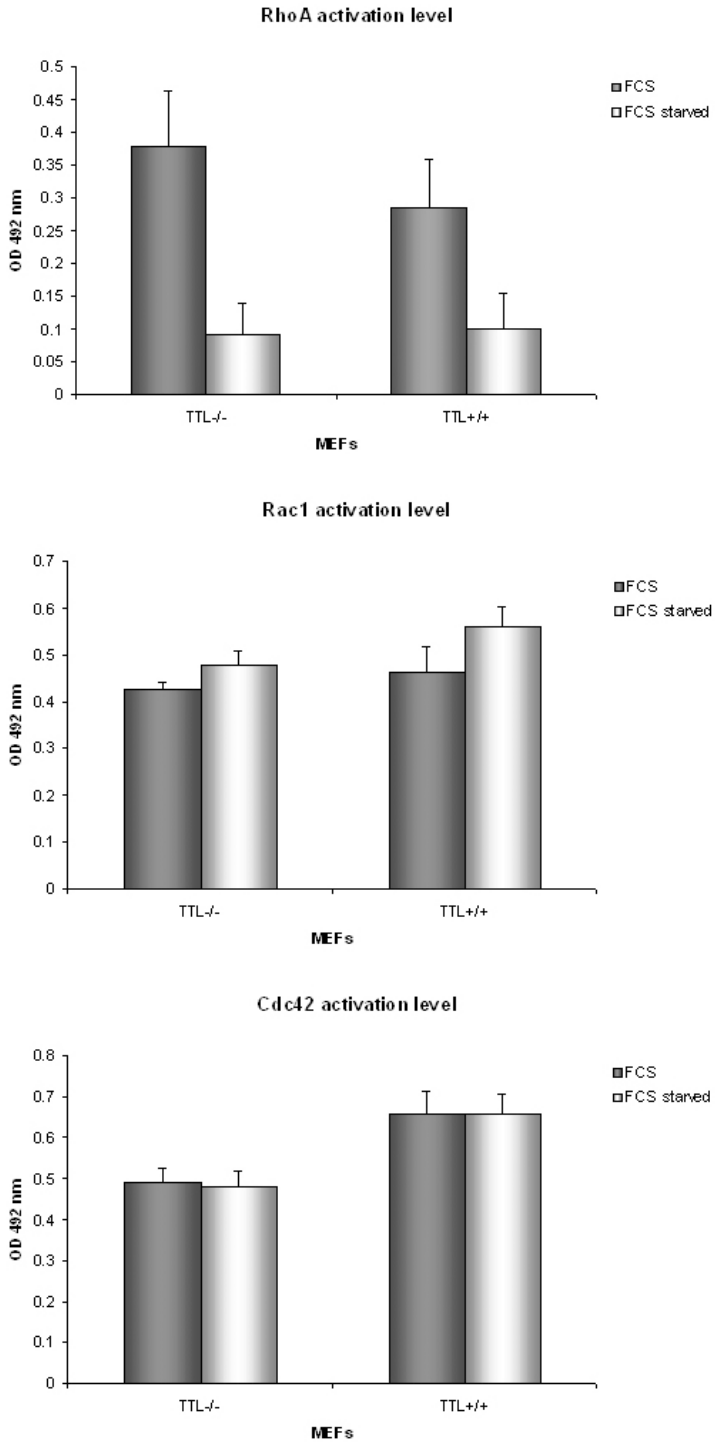

Figure 34. **Levels of activated small Rho GTPases in TTL+/+ and TTL-/- MEFs.** TTL+/+ and TTL-/- MEFs were lysed and subjected to G-lisa assays to analyze RhoA, Rac1 and Cdc42 activity as described in chapter 3.5.7. The pooled results from several experiments on multiple TTL+/+ and TTL-/- MEF cell lines are shown. Error bars indicate standard deviation (SD).

based processes, such as MTOC reorientation (45) and mediates the formation of a common complex with Rac1, APC, CLIP-170 and actin (54). Moreover, Cdc42 plays a role in MT stabilization by triggering the recruitment of APC to microtubule plus ends via GSK3β inactivation (211). Together these observations connect Rho GTPases activity to microtubules. Therefore, activity assays of the small Rho GTPases were performed on cell lysates derived from TTL-/- and TTL+/+ MEFs (see chapter 3.5.7.). In all experiments, control conditions were included, in which serum-starved cells were supposed to show basal decreased Rho GTPase activaton level.

As shown in Figure 34, upper panel, RhoA levels are increased in TTL-/- cells compared to TTL+/+ cells, however a big variation between several tested cell lines was observed. Rac1 activity levels showed a slight tendency towards increased activity in TTL+/+ MEFs (Fig. 34, middle panel), which is in contrast to data obtained in TTL-deficient neurons (214). Finally, Cdc42 also showed a slight tendency to be more activated in TTL+/+ cells (Fig. 34, lower panel). In both Rac1 and Cdc42 activation assay experiments serum starvation did not result in decreased levels of active GTPases which may be indicative for incorrect handling of the cells. Additionally, as seen for RhoA activation assays, a relative large variation between several tested cell lines was observed in the Rac1 and Cdc42 activity experiments.

5. Discussion

Microtubules are one of the three components of cytoskeleton and are critical for cell division, intracellular transport, cell motility and polarization. Tyrosination and detyrosination of α-tubulin has a vital role in neuronal organization during embryonic development. As one of the microtubule posttranslational modifications, it can also have an influence on the localization of microtubule associated proteins. Microtubule plus end-tracking proteins (+TIPs) fulfill important functions, such as regulating microtubule dynamics by acting as anti-catastrophe factor. They also contribute to microtubule stabilization and play a role in positioning of the mitotic spindle during cell division. They are not only present in mammalian cells but also in lower eukaryotes, such as fungi and yeast. In this work multiple attempts have been made to address the subcellular distribution and the cellular roles of +TIPs with regard to the tubulin tyrosination / detyrosination cycle. RNAi approaches were used to study the localization of several +TIPs at microtubules. Using this strategy, our aim was to enlighten the hierarchy of binding of +TIPs to microtubules, and in addition it should reveal modes of interaction within the multiprotein complex situated at the microtubule plus end. Moreover, some of the prominent +TIPs, such as EB1 and CLIP-170, share the same EEY/F motif at the very C-terminus, which corresponds to the same motif at the C-terminus of α-tubulin. This can create many potential direct as well as indirect interactions between these proteins. How the entire protein complex at the microtubule plus end is intertwined still challanges to debate and this study contributes to the clarification of some issues within the microtubule field.

5.1. RNAi knock-down of +TIPs in the context of TTL deficiency

Obviously, CLIP-170 knock-down does not influence the localization of EB1, CLIP-115 and CLASP2 in TTL+/+ and TTL-/- cells (Fig. 14 and 15). CLIP-170 is known to interact via its C-terminal zinc-binding domain to the CAP-Gly domains from CLIP-115 (18). This interaction, however, is apparently not predominant and therefore the majority of CLIP-115 proteins is probably bound to the MT +ends via EB1 and not through CLIP-170. CLIP-170 does not influence binding of EB1 to MT +ends, which is in line with our expectations, since CLIP-170 is known to hitchhike on EB1 and not other way around (150). A small portion of EB1 protein could still bind to the C-

terminus of CLIP-170. This interaction, however, could not have been detected, as depletion of CLIP-170 by RNAi did not result in any visible EB1 removal from MT +ends in TTL+/+ and TTL-/- MEFs. Although CLASP2 initially was identified as a CLIP-associating protein (180), no visible change in localization of CLASP2 upon CLIP-170 down-regulation in TTL+/+ and TTL-/- MEFs was observed. CLASP2 is known to bind not only through CLIP-170 to microtubules but also can bind microtubules directly, i.e. independent from other +TIPs. This direct binding is not only restricted to the MT +ends but can also occur on the entire length of the microtubule lattice (183). The direct association between CLASP2 and microtubules could explain the here observed CLASP2 localization at the microtubule plus ends after CLIP-170 knock-down.

Like for CLIP-170, also for CLIP-115 no influence on the localization of other +TIPs, such as CLIP-170, EB1 and CLASP2 has been observed in both TTL+/+ and TTL-/- cells (Fig. 16 and 17). CLIP-115, which is a close homolog of CLIP-170 only lacking the C-terminal zinc-binding domain, is known to interact directly and, via an EB1-dependent mechanism, indirectly to microtubules (164). As CLIP-170 can not interact with the C-terminus of CLIP-115, this could explain why knock-down of CLIP-115 does not affect MT +end localization of CLIP-170. CLIP-115 knock-down also did not disturb the localization of EB1 on MT+ ends in our MEFs. These observations could be explained by the fact that CLIP-115, similar to CLIP-170, can hitchhike on EB1 but not vice versa. And additionally, since CLIP-115 is lacking the C-terminal zinc-binding domain, EB1 is not able to interact with CLIP-115 as described for CLIP-170. Also CLASP2 localization is not affected by CLIP-115 knock-down which could be explained in the same line as for CLIP-170 knock-down, i.e. due to the different modes of CLASP2 binding to microtubules.

Finally, CLASP2 knock-down in TTL+/+ and TTL-/- cells did not affect the binding of CLIP-170, CLIP-115 and EB1 on MT +end (Fig. 18 and 19). Although CLASP2 is known to bind to CLIPs (180), it does not influence the microtubule plus end localization of these proteins, most probably because the majority of the CLIPs bind to microtubules via EB1 (150). Even if there is a modest CLASP2-dependent MT +end binding of CLIPs, it would most probably be masked by an EB1-dependent binding of CLIPs. Also EB1 localization at the microtubule plus end is not affected in

CLASP2 depleted MEFs, although CLASP2 is known to interact with EB1 (181). Most probably the vast majority of the EB1 molecules bind directly to MT +ends without any assistance of other +TIPs like for instance CLASP2. As in case of CLIP-170, a small portion of EB1 might still possibly bind to microtubules via CLASP2. This interaction however, could not be detected by immunofluorescence staining, as CLASP2 knock-down did not result in a visible removal of EB1 from MT +ends in both TTL wild type and TTL-deficient cells.

In none of the aforementioned knock-down experiments the lack of TTL influenced the observed subcellular localization of the tested +TIPs. This may be surprising since it is published that in mouse embryonic fibroblasts, the CAP-Gly domain-containing proteins, such as CLIP-170 and CLIP-115, are removed from MT+ ends in TTL-deficient cells (128). In our experiments, we were not able repeat this phenotype, probably due to differences in the MEF cell systems used.

The role of EB proteins, that are master regulators at the microtubule plus end (48), in the localization of the +TIPs was investigated in the background of TTL deficiency. We first tested which EB isoforms are expressed in our cell system. EB1, EB2 and EB3 expression and intracellular localization was tested in TTL+/+ and TTL-/- MEFs. Although EB2 is expressed in mammalian cells (215), by using immunofluorescent analysis we could not show EB2 in our MEFs (not shown). However, the presence of EB2 mRNA was detected by RT-PCR (Fig. 20C and D). EB2 is a not very well studied member of the EB family. EB2 is known to be expressed in chinese hamster ovary CHO-K1 cells (145, 150) as well as in HT0180 and SW480 tumor cells (215) and so far, there has been no evidence that this protein is not expressed in MEFs. As expected, EB1 expression could be verified by RT-PCR as well as immunofluorescent assays in our wild type and TTL-deficient cells (Fig. 20C and 21). Surprisingly, EB3 protein, which resembles EB1 function as a catastrophe-suppressor factor (145), was found not to be expressed in our MEFs. EB3 expression could not be confirmed either by immunofluoresence (Fig. 20A) nor by Western blot analysis (Fig. 20B). RT-PCR analysis though revealed the presence of EB3 transcripts on a very low level (Fig. 20D), indicative for a low EB3 expression level in MEFs. This could explain the lack of a clear EB3 localization pattern obtained by immunostaining and the lack of EB3 in Western blot analysis. Recently it

has been shown that EB3 is involved in muscle differentiation, where it is required for myoblast elongation and fusion. Furthermore, EB3 is required for the regulation of microtubule dynamics at the cell cortex in a murine myoblast cell line C2C12 (146). These results directed us to focus on the effects of EB1 knock-down on the localization of the other +TIPs in our further experiments.
EB1 knock-down efficiency was tested using EB1 and EB1/3 RNAi constructs. The EB1 RNAi construct turned out to work efficiently leading to an almost complete EB1 dislocalization from the microtubule plus ends. In contrast, the EB1/3 RNAi construct, which was supposed to down-regulate both EB1 and EB3 proteins, resulted only in partial reduction of EB1 expression and MT +end localization in MEFs. The reason for this is unclear but it could be explained by a possible lower efficiency of the RNAi mechanism when two different mRNAs need to be targeted. As only the EB1 RNAi construct was fully functional in EB1 depletion in our mouse embryonic fibroblasts, this construct was used in further experiments.

CLIP-170 proteins were removed from MT +ends in both EB1-depleted wild type and TTL-deficient cells (Fig. 22 and 35). This finding is consistent with already published data, which showed that coordinated knock-down of EB1 and EB3 in CHO-K1 leads to the dissociation of CLIP-170 from MT +ends (150). As EB3 was found not to be expressed in our cell system (see above), it is not possible to judge whether EB3 knock-down also impairs CLIP-170 plus end localization in our system. The tyrosination / detyrosination status of tubulin did not have any influence on the localization of CLIP-170 upon EB1 knock-down. Since we also did not observe any differences in MT +end localization of CLIP-170 in untransfected wild type and TTL-deficient MEFs, one can conclude that in both cell lines virtually all CLIP-170 molecules are hitchhiking on microtubule bound EB1.

The difference observed in removal of CLIP-115 proteins from MT +ends in TTL+/+ and TTL-/- cells after EB1 depletion is a hallmark in this work (Fig. 23 and 35). Although CLIP-115 is less studied, it is definitely important for cellular functioning as shown by the loss of function of this protein in the hereditary Williams Syndrome, specifically in the neurological symptoms of mental retardation in this disease (216 – 218). The difference in binding of CLIP-115 to MT +ends is obvious in untransfected TTL+/+ and TTL-/- MEFs. The CLIP-115 decorated microtubule plus ends in TTL-/-

MEFs were longer then those in wild type cells. This observation is in disagreement with published data. Peris et al. claimed removal of CLIP-115 and other CAP-Gly domain-containing proteins from MT +ends in Tyr-negative TTL-/- MEFs (128). The reason for increased binding of CLIP-115 to detyrosinated microtubules in our experiments is not clear. Since the interactions between CAP-gly domain-containing proteins and the EEY/F C-terminal motif of α-tubulin have been extensively studied even at the atomic level (154), the lack of the C-teminal tyrosine residue of α-tubulin in TTL-/- cells therefore should rather lead to the inability of microtubule association by CAP-Gly domain-containing proteins like CLIP-115. However, recent biochemical studies show that CLIP-170 binds to both α- and β-tubulin and that this binding is not only limited to the acidic C-terminal tail of tubulin. Enzymatic removal of both α- and β-tubulin C-terminal tails resulted in a still significant affinity of CLIP-170 to MTs, indicating that CLIP-170 does have binding sites at microtubules in addition to the α-tubulin C-terminus (226). The increased binding of CLIP-115 in TTL-/- cells, thus, can not simply be explained by tubulin detyrosination. There are some indications that posttranslational modifications of CLIP-115 could cause the differences in MT +end binding of CLIP-115. It has already been described that efficient binding of CLIP-115 to microtubules is sensitive to phosphorylation and is not mediated by the microtubule binding region alone but additionally requires the presence of the basic/Serine-rich stretch (219). Andreas Fischer in his PhD thesis showed that CLIP-115 is less phosphorylated in TTL-/- cells and that this phosphorylation could regulate the binding of CLIP-115 to MT +ends, however, future experiments are required to confirm this hypothesis.

CLIP-115 proteins were dislocalized from the MT +ends in wild type MEFs upon EB1 depletion, whereas they were still bound to MT +ends in *TTL* knock-out cells (Fig. 23 and 35). As already stated, the C-terminal EEY/F motif of EB1 is known to interact with the CAP-Gly domains of both CLIP-170 and CLIP-115, and most of the CLIP proteins bind to MT +ends via EB1 (150, 154). Therefore it is not surprising that down-regulation of EB1 causes dissociation of CLIP-115 from MT +end in wild-type cells. Why the knock-down of EB1 did not result in dissociation of CLIP-115 from microtubule plus ends in TTL-deficient MEFs is unclear. One reason could be a possible increased number of CLIP-115 binding sites on detyrosinated microtubules by which CLIP-115 would omit EB1 protein in binding to the +ends. Hypothesizing

in this direction, the knock-down of EB1 would not have any influence on CLIP-115 plus end localization since CLIP-115 binding sites at the microtubule plus end are not affected. The possible existence of more CLIP-115 binding sites on detyrosinated MT +ends would also be consistent with previous observation, that in untransfected TTL-deficient MEFs, CLIP-115 comets at the microtubule plus ends are longer than in wild type cells (Fig. 2E and F). Data obtained by the quantification of MT +end length revealed somewhat longer CLIP-115 comets at the microtubule plus ends in untransfected TTL-deficient MEFs compared to EB1-depleted TTL-deficient cells (Fig. 23, panel B). This observation suggests that still a small portion of the CLIP-115 molecules is affected by EB1 RNAi. In EB1-depleted wild type cells the vast majority of CLIP-115 was deleted from MT +ends, however, some reminiscent CLIP-115 decorated plus ends were still detectable as small dots (Fig. 23, panel A). This would suggest that in these cells still a small portion of CLIP-115 binds to MT +ends independently of EB1. However, this remaining portion of CLIP-115 at the microtubule plus ends in EB1-depleted wild type cells could also be the result of incomplete EB1 knock-down.

The here described difference in CLIP-115 behavior can also not be simply attributed to increased availability of the CLIP-115 for microtubule binding, due to the lack of its C-terminal zinc-binding domains that are present in CLIP-170. Although the CLIP-115 resembling CLIP-170ΔC mutant indeed showed pronounced +end binding compared to CLIP-170 full length proteins (Fig. 25), it did not show any difference in MT binding in wild type and TTL-deficient cells. Additionally, also EB1 knock-down did not result in differences in mislocalization of full length CLIP-170 and CLIP170ΔC. The same CLIP-170 deletion construct also localized to microtubules in HeLa cells and this binding was also stronger than full length CLIP-170 (220). A possible role of CLIP-115 modification could also explain the observed phenotype, however, further studies are required to elucidate the kind of modifications and whether they act in concert or independently of each other. The above mentioned different phosphorylation pattern of CLIP-115 in TTL+/+ and TTL-/- MEFs needs further elaboration. Furthermore, one can not exclude possible EB1 posttranslational modifications playing a role, however, such modifications, except for EB1 phosphorylation are not known yet.

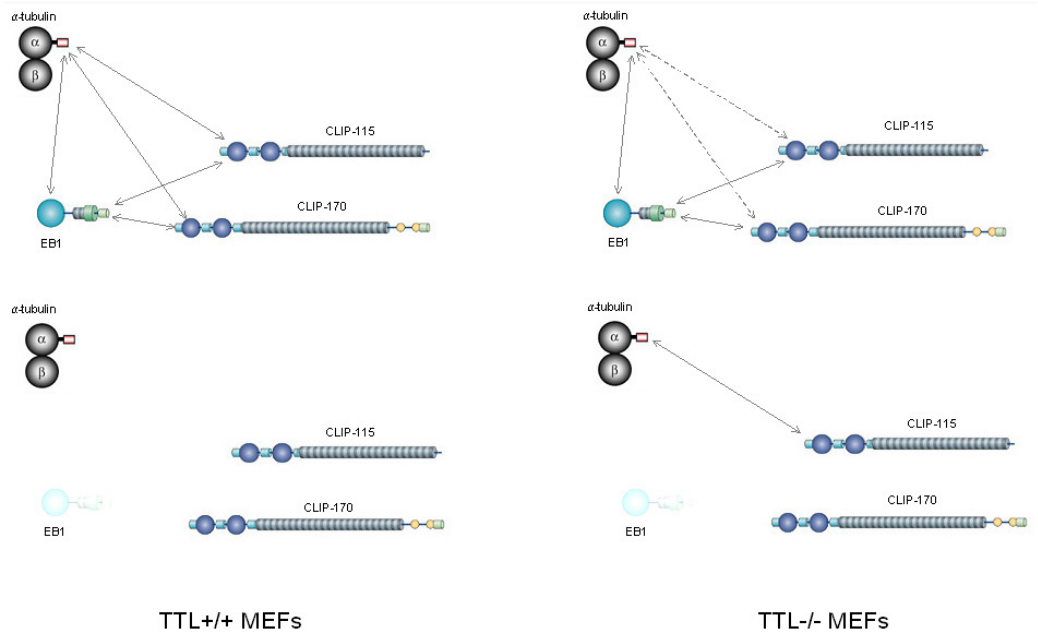

Figure 35. **Scheme showing EB1-dependent CLIP/MT binding in wild type and TTL-deficient MEFs.** In TTL+/+ and TTL-/- cells, both CLIP-170 and CLIP-115 bind to MT +ends (upper part). EB1 knock-down leads to CLIP-170 dislocalization from MT +ends in both TTL+/+ and TTL-/- cells and, in contrast, results in CLIP-115 dislocalization from MT +ends only in TTL+/+ and not TTL-/- cells (lower part). Dashed lines show the interactions of CLIPs that are in contrast to data published by Peris et al. (Ref. 128). See text for details. (*Adapted from Akhmanova & Steinmetz 2008; Nature reviews, Molecular Cell Biology*).

The CLIP-115 dissociation from microtubule plus ends observed in TTL+/+ cells after EB1 knock-down was phenocopied in TTL-/- cells that were reconstituted with the TTL enzyme and simultaneously transfected with the EB1 RNAi construct. This was also reflected in MT +end length quantification. Clearly, the CLIP-115 plus end length was decreased in TTL-deficient cells transfected with the pIRES2-EGFP-TTL construct, and drastically reduced in *TTL* knock-out cells cotransfected with the pIRES2-EGFP-TTL and EB1 RNAi constructs (Fig. 22B). These experiments confirmed that the observed distinct CLIP-115 behavior in EB1-depleted MEFs is linked to the presence of TTL enzyme.

Taken together, according to the model that we propose, CLIP-170 and CLIP-115 are localized at MT +ends mostly via EB1 and independently of MT tyrosination status (Fig. 35, upper panel). After EB1 knock-down, CLIP-170 is removed from MT +ends in both wild type and TTL-deficient cells, whereas CLIP-115 still remains bound to MT +ends in *TTL* knock-out cells (Fig. 35, lower panel).

In order to define which part of the CLIP-115 sequence specifies the distinct CLIP-115 plus end tracking behavior in TTL+/+ and TTL-/- cells, several hybrid constructs were generated. In these constructs CLIP-115 regions were exchanged with corresponding CLIP-170 fragments. Since all constructs do contain the CAP-Gly domains and the coiled coil domain involved in MT domains, all mutants localized to microtubules as expected, however in a variable mode (Fig. 28). The first five constructs contain the CLIP-170 C-terminal zinc-binding domain, which is responsible for its autoinhibition (18). This makes these fusion protein less accessible for binding to microtubules, therefore it is not surprising that the first five mutant proteins (1 – 5) conferred a weaker MT +end tracking compared to the last five mutants (6 – 10) which lack the C-terminal zinc-binding domains (Fig. 28). Interestingly, proteins 1 – 5 displayed additionally a clear perinuclear localization most probably marking the Golgi apparatus. Although CLIPs have originally been identified as cytoplasmatic linker proteins, mediating the interaction of cytoplasmic organelles (including endocytic and exocytic vesicles) with microtubules (221 – 223) there is no evidence of their direct interaction with the Golgi apparatus *in vivo*. On the other hand, CLIPs are known to interact with the C-terminus of CLASPs (18), proteins that associate with the Golgi apparatus. The apparent localization of the first five fusion proteins near or at the Golgi apparatus could thus be due to an indirect binding via CLASPs, thereby targeting CLIPs to the Golgi compartment. Moreover, CLIP-115 was cloned using an antibody that recognizes a dendritic lamellar body (DLB), an organelle that resembles the Golgi apparatus (224), which suggests its possible affinity to Golgi-like structures. CLIPR-59, another member of the CLIP protein family and thus possessing bona fide microtubule binding motifs, however, does not localize to microtubules. In contrast, CLIPR-59 binds to trans-Golgi network (225) implying a possible involvement of CLIPs in the regulation of Golgi function.

Reduced MT +end binding of the protein encoded by construct number 5, that contains the N-terminal CLIP-115 part followed by the C-terminal part of CLIP-170 (see scheme, Fig. 27), in TTL+/+ cells was observed. Also the binding of hybrid proteins 3 and 4 was a bit weakened in TTL+/+ compared to TTL-/- cells. It seems that the sequence stretch from 1476 bp to 2670 bp of CLIP-115 (Fig. 27) present in construct 5 causes decreased MT +end binding in TTL+/+ cells. On the other hand,

the sequence stretch 1462 – 2782 bp of CLIP-170, missing in construct 5 could have resulted in decreased binding of this protein to MT +ends in TTL+/+ cells. These fragments comprise three blocks that are homologous between CLIP-115 and CLIP-170 (Fig. 27), therefore the analysis of the non-homologous parts between these blocks will shed a light on the mechanism of CLIP-115/microtubule association. This region is part of the central coiled coil domain, responsible for the dimerization of CLIPs, therefore it would also be interesting to address the question of dimerization in further studies on CLIP-115 MT +end binding. To support these conclusions, further studies and deeper sequence analysis as to which amino acid residues are exactly involved in the observed differences in MT +ends binding should be constructed. Performing substitution-mutagenesis of single amino acid residues would shed some light on this issue. Furthermore, it would also be interesting to analyze the binding behavior of these hybrid proteins in EB1-depleted wild type and TTL-deficient cells.

5.2. Microtubule dynamics

Microtubule dynamics were analyzed in TTL+/+ and TTL-/- cells and some TTL-dependent changes were found. The most important observed difference was a more than two-fold reduction in microtubule shortening rate in *TTL* knock-out cells (Table X). This finding is in line with published data, as detyrosinated tubulin-containing microtubules show increased stability (119 – 121), which could be reflected by a lowered MT-shrinking rate. In addition, rescue frequencies were increased in TTL -/- MEFs as compared to TTL+/+ MEFs, which is in line with data published by Peris et al. (135). Catastrophe frequencies were comparable, though very slight decrease in TTL-/- was observed, also consistently with published results (135). Furthermore, a slight decrease in growth rate was noticed in TTL-/- MEFs and this was even more pronounced in cells that expressed the mCherry-α-tubulin-ΔY variant. These observations favor the hypothesis that the growth speed is slower for more stable microtubules. These results are in contrast to published data, where no difference in growing and shrinking MT speed was reported (135). A big decrease in the time microtubules spent growing and increase in the time microtubules spent pausing were noticed in TTL-/- cells compared to TTL+/+. This observation would be in line with the assumption that stable detyrosinated microtubules are more paused and less

growing-prone. These observations, however, are in conflict with published data, in which microtubules in TTL-null cells spent more time growing and less time pausing than microtubules in TTL wild type MEFs (135). The apparent contradictions between our study and published data might be caused by the lower number of microtubules that were analyzed in the study from Peris et al., and that in that study analyzed microtubules were mostly restricted to the ones located within 10 µm from the leading edge. In our study, almost a double amount of microtubules was analyzed and the analyzed microtubules were not temporally and spatially restrained within the cell. Furthermore, in this study a detyrosinated mCherry-α-tubulin variant was used in TTL-deficient cells that would also contribute to the observed differences. The results obtained in this study reflect then more the in vivo situation, in contrast to the study from Peris et al., where only tyrosinated mCherry-α-tubulin variant was used in experiments, resulting in TTL-deficient cells being transformed again into the wild type cells. Finally, small differences in the used cell system could have an influence on MT dynamics.

EB1 knock-down had a more prominent impact on microtubule dynamics in wild type MEFs compared to TTL-deficient cells. EB1-depletion led to a drastic reduction in shortening rate and a slight decrease in growth rate in wild type cells. In TTL-deficient cells these values were not affected. Catastrophe frequency was slightly increased in TTL+/+ cells and remarkably decreased in TTL-/- cells upon EB1 knock-down cells. Rescue frequencies remained the same in TTL+/+ cells but were decreased in TTL-/- cells upon EB1 knock-down. These observations are consistent with published data, in which YFP-CLIP-170 protein was used for analyzing microtubule dynamics in CHO-K1 cells (145). Moreover, a striking increase in time microtubules spent pausing and decrease in time microtubule spent growing was observed for TTL+/+ in EB1 knock-down conditions. These changes in MT dynamics, especially in EB1-depleted wild type cells, could be attributed to the lack of CLIP-115 and CLIP-170 on MT +ends due to EB1 depletion. CLIP-115 itself, being a rescue factor, thereby promoting microtubule growth, could play a role in the observed changes in microtubule dynamics in EB1-depleted wild type MEFs. In future experiments, it would be interesting to test whether CLIP-115 knock-down (in

combination with simultaneous EB1 or CLIP-170 depletion) in wild type MEFs can copy microtubule dynamics as observed in TTL-/- cells.

Additionally, a MBD-GFP construct, containing the microtubule-binding domain from MAP4 protein, was tested as a new tool to analyze microtubule dynamics. Although the MBD-GFP fusion protein by itself did not affect the organization and the ratio in tubulin pools in wild type and TTL-deficient cells, it caused notable changes in microtubule dynamics in both cell types in comparison to mCherry-α-tubulin. The binding of the MBD-GFP fusion protein to the microtubule lattice resulted in less dynamic microtubules in both TTL+/+ or TTL-/- MEFs. This was reflected by decreased growing and shrinking speed of microtubules and additionally by an increased time microtubules spent pausing as well as by a decreased time microtubules spent growing. This slow-down of MT dynamics might be caused by mechanical and physical confinements that could be imposed on microtubules due to MBD-GFP binding. In summary, this new MBD-GFP fusion protein can unfortunately not be used as a reliable tool for analyzing microtubule dynamics.

5.3. Actin- and microtubule-regulating proteins

The involvement of actin-regulating proteins in microtubule cytoskeletal organization in the context of the TTL cycle was tested using three different approaches. First, aluminium fluoride treatment was employed to check the general influence of unspecific activation of all GTPases on cell morphology and architecture of the microtubule cytoskeleton in wild type and TTL-deficient cells. AlF_4 induced unusual frizzy shaped microtubules in both TTL+/+ and TTL-/- MEFs. Unexpectedly, a clear colocalization of EB1, CLIP-170 and CLIP-115 was observed with these morphologically changed microtubules. These proteins decorated the entire length of those curly microtubules. Whether this colocalization is due to direct interactions of these +TIPs with the microtubules remains unknown. It is well known that +TIPs can bind to the entire microtubule lattice especially when they are ectopically expressed (220). Speculating, it could also be possible that upon microtubule structural changes some additional binding sites for the +TIPs are created, which would lead to their increased recruitment to microtubules. So far, no evidence for the direct engagement of Rho GTPases in the regulation of +TIP function and their MT-localization is

described. However, some studies showed the involvement of mDia proteins, which are effectors of the small GTPase RhoA, in binding to the +TIPs. This however, is more associated with microtubule stabilization, as it is known that EB1 binds to mDia to stabilize microtubules downstream of RhoA (33, 189).

The mDia protein pathway, involving Rho GTPase as an upstream regulator and EB1 acting downstream of mDia, is a well proven pathway that leads to the formation of common complex of mDia1 with EB1 and APC and subsequently results in microtubule stabilization (33, 189). Due to the fact that microtubules in TTL-/- MEFs are detyrosinated and confer increased stability (this study and 119 – 121), it was of interest to study the mDia proteins in TTL+/+ and TTL-/- MEFs. Two isoforms of mDia are known (i.e. mDia1 and mDia2), however the activity of these two proteins is not sufficiently dissected. Both of them are reported to play a role in MT stabilization (33, 189, 104) and furthermore, mDia1 is involved in the cross-talk of microtubules and actin cytoskeleton (58). Expression levels of both mDia1 and mDia2 in our cell system were analyzed. Since we were not able to detect mDia2, the main focus in this study was turned to mDia1. The expression of mDia1 could be confirmed in our MEFs, however the expression level was independent from TTL activity. The reason for this variation in mDia1 expression is unclear and the role of this protein in the context of tubulin tyrosination / detyrosination cycle was not studied in more detail.

The third approach in analyzing the role of actin/microtubule-regulating proteins in the context of the TTL cycle was to measure the activity levels of the small Rho GTPases RhoA, Rac1 and Cdc42. It is already described that these proteins influence the regulation and are implicated in the interplay between actin- and microtubule cytoskeleton (28, 29, 45, 54, 211). RhoA activity assays revealed increased levels of activated RhoA in TTL-/- cells. This is consistent with our expectations, since RhoA is known to trigger microtubule stabilization (33, 189, 104) and TTL-deficient cells do contain more stable microtubules (this study and 119 – 121). The observed tendency towards decreased Rac1 activity levels in TTL-deficient cells may be surprising and is in contrast to published data describing that Rac1 activity is increased in TTL-deficient neuronal cells (214). The activation of Rac1 promotes microtubule growth and stability by the inactivation of the potent microtubule destabilizer Op18/stathmin (35, 210). It is also known that microtubule growth

stimulates Rac1 activity to promote lamellipodial growth (38). In this study, decreased microtubule growth was found to be a feature of TTL-/- MEF-microtubules and considering that way, the decreased level of Rac1 in these cells would not be then surprising. Finally, we observed that the level of activated Cdc42 is slightly decreased in TTL-deficient MEFs. This would be surprising as Cdc42 is also reported to be involved in MT stabilization, triggering the GSK3β-dependent MT+ end localization of APC and the MTOC reorientation (45, 211, see chapter 2.7.).

Additionally, one should also remember the observed variability between independent experiments using several different cell lines. In the here performed assays, immortalized cells with a much faster metabolism were used. The observed insufficient serum starvation, used as a control in Rac1 and Cdc42 activation experiments, could reflect the high basal GTPase activity even after serum starvation. Thus, in further experiments a higher number of cell lines needs to be tested and the use of primary cell lines should be taken into account.

5.4. General concluding remarks

The tubulin tyrosination / detyrosination cycle has proven its importance in proper neuronal track organization in the mammalian brain, ensuring the correct function of the complete nervous system. Maintaining undisturbed neuronal differentiation and functionality, which is reflected in proper alignment of neuronal layers during embryogenesis, seems to be one of the main tasks of tyrosination / detyrosination cycle. The processes that guarantee basic neuronal activities and neuronal development in respect to the TTL cycle can also be related to proper functionality of our fibroblast system. Thus changes caused by interfering with the tubulin tyrosination / detyrosination cycle in neurons, e.g. the early-death phenotype of TTL-deficient neurons in mice, can be studied on the molecular level by analyzing similar abnormalities emerging in fibroblasts. Microtubule plus end tracking proteins have emerged as regulators of important microtubule-based processes like cell motility, intracellular transport, cell division and differentiation. In this study, a differential microtubule binding behavior of CLIP-115, a CAP-Gly domain-containing +TIPs, is reported in cells lacking the TTL enzyme and depleted from EB1 proteins. This effect was TTL-dependent, as reconstitution experiments caused reversion of this phenotype to the wild type situation. This phenotype is not dependent on a possible lack of

autoinhibition of CLIP-115, but more probably is rooted in the coiled coil domain in the central part of the protein. The lack of TTL enzyme also triggered changes in microtubule dynamics, greatly manifested in a significant decrease in microtubule shrinking speed as well as in an increase of time microtubules spent pausing and a decrease of time microtubules spent growing. The lack of TTL enzyme did not have any obvious effect on the expression of the RhoA GTPase effector mDia1 and only caused slight changes in the activation of small Rho GTPases. Further studies should focus on mapping the regions within CLIP-115 that are responsible for the difference in binding to microtubule plus ends in *TTL* knock-out cells thereby addressing the role of CLIP-115 proteins in the regulation of microtubule dynamics. The observed difference in CLIP-115 binding patterns might be the result of specific posttranslational modifications in the CLIP-115 polypeptide. Well-known modifications like phosphorylation, polyubiquitination, myristoylation or palmitoylation could potentially influence the CLIP-115 binding behavior. Future research should focus on answering the question whether CLIP-115 is differently modified in wild type and TTL-deficient cells. And if so, what kind of modifications are present and how are they coordinated. Addressing the cellular function of these modifications could provide detailed knowledge concerning the role of CLIP-115 in *TTL* knock-out cells. As mentioned before, recent observations already revealed that TTL deficiency influences the phosphorylation pattern of CLIP-115 and this probably has an impact on the MT +end tracking behavior of this protein. Further elaboration of the phosphorylation status of CLIP-115 for instance by directed mutagenesis should help in understanding the binding properties of CLIP-115 to microtubules. This, in combination with down-regulation of +TIPs like EB1 and CLIP-170 by using RNA interference in wild type as well as in TTL-deficient cells, would open a new direction in dissecting the binding hierarchy of the +TIPs at the microtubule plus ends.

Moreover, a conditional knock-out approach to generate tissue-specific TTL deletion would facilitate the investigation of the molecular mechanism(s) involved in the dramatic neurological TTL knock-out phenotype in other cell types and in adult mice. Microtubule dynamics / properties are known to play an important role in the formation of the immunological synapse, the formation of the epithelial adhesion belt and in muscle cell differentiation (139, 146, 229, 230). Analyzing the effects of a TTL deletion in for instance B- and T-lymphocytes as well as in macrophages and

dendritic cells could provide more knowledge on a possible role of TTL in basic immunological processes, such as the antigen presentation and the organization of the immunological synapse. By creating a TTL-deficient epithelial cell line it would be possible to study the role of tyrosinated / detyrosinated microtubules in epithelial cell polarization and in the regulation of intercellular junction formation (e.g. the cadherin/catenin-containing adherens junctions). Finally, the creation of a TTL-deficient myoblast cell lineage would open an interesting field towards understanding the role of the tubulin tyrosination cycle in muscle cell differentiation.

6. Abbreviations

A	Ampere
APC	adenomatous polyposis coli protein
ATP	Adenosine triphosphate
bp	base pairs
BSA	bovine serum albumin
cDNA	copy DNA
CAP-Gly	Cytoskeleton-associated protein Glycine-rich domain
CLASP	CLIP-associated protein
CLIP	CAP-Gly domain containing linker protein
Da	Dalton
DMSO	dimethylsulfoxide
DNA	desoxyribonucleic acid
EB	end binding protein
E. coli	Escherichia coli
EDTA	Ethylene diamine tetraacetic acid
EGTA	Ethylene glycol-bis(2-aminoethylether)-tetraacetic acid
ELISA	enzyme-linked immunosorbent assay
f-actin	filamentous actin
FCS	fetal calf serum
fl	full length
GDP	Guanosine diphosphate
GEF	guanine nucleotide exchange factor
EGFP	Enhanced green fluorescence protein
GAP	GTPase activating protein
GST	glutathione-S-transferase
GTP	Guanosine triphosphate
GFP	green fluorescent protein
IF	immunofluorescence
IP3	inositol triphosphate
IPTG	Isopropyl-b-D-galactopyranoside
µ	micro
m	milli
M	molar
MAP	microtubule associated protein
mc	monoclonal
MT	microtubule
MT +end	microtubules plus end
l	liter
mRFP	monomeric red fluorescent protein
mRNA	messenger RNA
Nap1	Nck associated protein1
OD	optical density
PAK1	p21 activated kinase 1
PAGE	polyacrylamide-gel electrophoresis
PBS	phosphate buffered saline
pc	polyclonal
+TIP	microtubule plus end tracking protein

PCR	polymerase chain reaction
PIP3	phosphatidylinositol (3,4,5) triphosphate
RNA	ribonucleic acid
SDS	sodium dodecyl sulphate
TAE	Tris-Acetate-EDTA-buffer
TBCB	tubulin folding cofactor B
TBCE	tubulin folding cofactor E
TBS(T)	tris buffered saline (with Tween 20)
Tris	Tris-(hydroxymethyl) aminomethane
V	Volt
v/v	volume per volume
WB	Western blot
w/v	weight per volume
x g	times gravity

7. Acknowledgments

At this point I would like to thank all the people who supported me during my PhD work.

Especially, I would like to thank my supervisor Juergen Wehland for offering me the opportunity to make this work in his Cell Biology group and for inspiration and helpful discussions throughout all research project. Special thanks go to my direct supervisor Marco van Ham for all help during entire PhD period, interesting disputes and critical reading of the script. I am very thankful to all the members of our lab, to Andreas Fischer for helping me during my first steps, to Ramona Baier for intensive scientific discussions and great academic atmosphere in the lab and to Christian Erck for sharing his great knowledge and experience. Deep gratitude goes to Hildegard Schwab-Hanisch for help with lab equipment ordering and to Amanda Muehlmann for her big help with handling administration issues. The big thanks go to the members of Cytoskeleton Dynamics and Signaling and Motility group, Jenny, Kathrin, Margit, Jan, Steffi, Marcus, Stefan, Kai who shared the same scientific fate, for their help, great atmosphere on the floor, common meeting, conferences and parties. Deepest thanks to all my friends I met during my study time in Braunschweig who made my stay very pleasant, funny and unforgettable. Thanks to Gosia for her constant help and useful advices, to Wiktor and Steve, for crazy discussions, all crazy time we had and couple of other things that made me pretty relaxed. Thanks to Asia and Gustavo for creating a nice family atmosphere that made us all feel like at home. Thanks to Zofia, Jacek, Milena, Beata, Natalia for being very helpful in solving most basic problems of everyday's life. I would also like to thank all my friends from Krakow, especially Mateusz and Lukasz who shared the same good and bad moments of scientific life.

A big gratitude and thanks go to my family. To my parents, who always believed in me and supported me for all my live. To my grandparents, without their support having my education finished would not be possible. To my brother Krzysztof and Tomasz for everything.

Finally, I would like to say special thanks to my girlfriend Monika for her endless love, unlimited support and grate motivation I always get from her.

8. References

1. Desai, A. & Mitchison, T. J. Microtubule polymerization dynamics. *Annu. Rev. Cell. Dev. Biol.* **13**, 83–117 (1997).
2. Howard, J. & Hyman, A. A. Dynamics and mechanics of the microtubule plus end. *Nature* **422**, 753–758 (2003).
3. Nogales, E. & Wang, H. W. Structural mechanisms underlying nucleotide-dependent self-assembly of tubulin and its relatives. *Curr. Opin. Struct. Biol.* **16**, 221–229 (2006).
4. Nogales, E. & Wang, H. W. Structural intermediates in microtubule assembly and disassembly: how and why? *Curr. Opin. Cell Biol.* **18**, 179–184 (2006).
5. Nogales, E. Structural insights into microtubule function. *Annu. Rev. Biochem.* **69**, 277–302 (2000).
6. Wang, H. W. & Nogales, E. Nucleotide-dependent bending flexibility of tubulin regulates microtubule assembly. *Nature* **435**, 911–915 (2005).
7. Bornens, M. Centrosome composition and microtubule anchoring mechanisms. *Curr. Opin. Cell Biol.* **14**, 25–34 (2002).
8. Desai, A. & Mitchison, T. J. Microtubule polymerization dynamics. *Annu. Rev. Cell Dev. Biol.* **13**, 83–117 (1997).
9. Chretien, D., Fuller, S. D. & Karsenti, E. Structure of growing microtubule ends: two-dimensional sheets close into tubes at variable rates. *J. Cell Biol.* **129**, 1311–1328 (1995).
10. Mandelkow, E. M., Mandelkow, E. & Milligan, R. A. Microtubule dynamics and microtubule caps: a timeresolved cryo-electron microscopy study. *J. Cell Biol.* **114**, 977–991 (1991).
11. des Georges, A. *et al.* Mal3, the *Schizosaccharomyces pombe* homolog of EB1, changes the microtubule lattice. *Nature Struct. Mol. Biol.* **15**, 1102–1108 (2008).
12. Hayden, J. H., Bowser, S. S. & Rieder, C. L. Kinetochores capture astral microtubules during chromosome attachment to the mitotic spindle: direct visualization in live newt lung cells. *J. Cell Biol.* **111**, 1039–1045 (1990).
13. Meads, T. & Schroer, T. A. Polarity and nucleation of microtubules in polarized epithelial cells. *Cell Motil. Cytoskel.* **32,** 273–288 (1995).
14. Tassin, A. & Bornens, M. Centrosome structure and microtubule nucleation in animal cells. *Biol. Cell* **91,** 343–354 (1999).
15. Mitchison, T. & Kirschner, M. Dynamic instability of microtubule growth. *Nature* **312**, 237–242 (1984).
16. Hirokawa, N. Kinesin and dynein superfamily proteins and the mechanism of organelle transport. *Science* **279,** 519–526 (1998).
17. Wittmann, T. & Waterman-Storer, C. M. Cell motility: can Rho GTPases and microtubules point the way? *J. Cell Sci.* **114,** 3795–3803 (2001).
18. Galjart, N. Clips and Clasps and cellular dynamics. *Nature reviews. Molecular cell biology* **6**, 487-498 (2005)
19. Small, J. V., Stradal, T., Vignal, E. & Rottner, K. The lamellipodium: where motility begins. *Trends Cell Biol.* **12,** 112–120 (2002).
20. Cramer, L. P. Organization and polarity of actin filament networks in cells: implications for the mechanism of myosin-based cell motility. *Biochem. Soc. Symp.* **65,** 173–205 (1999).
21. Salmon, W. C., Adams, M. C., & Waterman-Storer, C. M. Dual-wavelength fluorescent speckle microscopy reveals coupling of microtubule and actin movements in migrating cells. *J. Cell Biol.* **158,** 31–37 (2002).
22. Cramer, L. P., Siebert, M. & Mitchison, T. J. Identification of novel graded polarity actin filament bundles in locomoting heart fibroblasts: implications for the generation of motile force. *J. Cell Biol.* **136,** 1287–1305 (1997).
23. Gupton, S. L., Salmon, W. C. & Waterman-Storer, C. Converging populations of f-actin promote breakage of associated microtubules to spatially regulate microtubule turnover in migrating cells. *Curr. Biol.* **12,** 1891–1899 (2002).
24. Webb, D. J., Parsons, J. T. & Horwitz, A. F. Adhesion assembly, disassembly and turnover in migrating cells — over and over and over again. *Nature Cell Biol.* **4**, E97–E100 (2002).
25. Waterman-Storer, C. M. & Salmon, E. D. Actomyosin-based retrograde flow of microtubules in the lamella of migrating epithelial cells influences microtubule dynamic instability and turnover and is associated with microtubule breakage and treadmilling. *J. Cell Biol.* **139,** 417–434 (1997).

26. Yvon, A. M. & Wadsworth, P. Region-specific microtubule transport in motile cells. *J. Cell Biol.* **151,** 1003–1012 (2000).

27. Mikhailov, A. V. & Gundersen, G. G. Centripetal transport of microtubules in motile cells. *Cell Motil. Cytoskeleton* **32,** 173–186 (1995).

28. Etienne-Manneville, S. & Hall, A. Rho GTPases in cell biology. *Nature* **420,** 629–635 (2002).

29. Cook, T. A., Nagasaki, T. & Gundersen, G. G. Rho guanosine triphosphatase mediates the selective stabilization of microtubules induced by lysophosphatidic acid. *J. Cell Biol.* **141,** 175–185 (1998).

30. Ridley, A. J. Rho GTPases and cell migration. *J. Cell Sci.* **114,** 2713–2722 (2001).

31. Pruyne, D. *et al.* Role of formins in actin assembly: nucleation and barbed-end association. *Science* **297,** 612–615 (2002).

32. Sagot, I., Rodal, A. A., Moseley, J., Goode, B. L. & Pellman, D. An actin nucleation mechanism mediated by Bni1 and profilin. *Nature Cell Biol.* **4,** 626–631 (2002).

33. Palazzo, A. F., Cook, T. A., Alberts, A. S. & Gundersen, G. G. mDia mediates Rho-regulated formation and orientation of stable microtubules. *Nature Cell Biol.* **3,** 723–729 (2001).

34. Small, J. V., Stradal, T., Vignal, E. & Rottner, K. The lamellipodium: where motility begins. *Trends Cell Biol.* **12,** 112–120 (2002).

35. Wittmann, T., Bokoch, G. M. & Waterman-Storer, C. Regulation of leading edge microtubule and actin dynamics downstream of Rac1. *J. Cell Biol.* **161**, 845–851 (2003).

36. Daub, H., Gevaert, K., Vandekerckhove, J., Sobel, A. & Hall, A. Rac/Cdc42 and p65PAK regulate the microtubule-destabilizing protein stathmin through phosphorylation at serine 16. *J. Biol.Chem.* **276,** 1677–1680 (2001).

37. Ren, X. D., Kiosses, W. B. & Schwartz, M. A. Regulation of the small GTP-binding protein Rho by cell adhesion and the cytoskeleton. *EMBO J.* **18,** 578–585 (1999).

38. Waterman-Storer, C. M., Worthylake, R. A., Liu, B. P., Burridge, K. & Salmon, E. D. Microtubule growth activates Rac1 to promote lamellipodial protrusion in fibroblasts. *Nature Cell Biol.* **1,** 45–50 (1999).

39. Krendel, M., Zenke, F. T. & Bokoch, G. M. Nucleotide exchange factor GEF-H1 mediates cross-talk between microtubules and the actin cytoskeleton. *Nature Cell Biol.* **4,** 294–301 (2002).

40. Suter, D. M. & Forscher, P. An emerging link between cytoskeletal dynamics and cell adhesion molecules in growth cone guidance. *Curr. Opin. Neurobiol.* **8,** 106–116 (1998).

41. Schaefer, A. W., Kabir, N., & Forscher, P. Filopodia and actin arcs guide the assembly and transport of two populations of microtubules with unique dynamic parameters in neuronal growth cones. *J. Cell Biol.* **158,** 139–152 (2002).

42. Kabir, N., Schaefer, A. W., Nakhost, A., Sossin, W. S. & Forscher, P. Protein kinase C activation promotes microtubule advance in neuronal growth cones by increasing average microtubule growth lifetimes. *J. Cell Biol.* **152,** 1033–1044 (2001).

43. Zhou, F. Q., Waterman-Storer, C. M. & Cohan, C. S. Focal loss of actin bundles causes microtubule redistribution and growth cone turning. *J. Cell Biol.* **157,** 839–849 (2002).

44. Ezratty, E. J., Partridge, M. A. and Gundersen, G. G. Microtubule-induced focal adhesion disassembly ismediated by dynamin and focal adhesion kinase. *Nature Cell Biol.* **7**, 581–590 (2003)

45. Palazzo, A. F., Joseph, H.L., Chen, Y.J., Dujardin, D.L., Alberts, A.S., Pfister, K.K., Vallee, R.B., Gundersen, G.G. Cdc42, dynein, and dynactin regulate MTOC reorientation independent of Rho-regulated microtubule stabilization. *Curr. Biol.* **11,** 1536–1541 (2001).

46. Etienne-Manneville, S. & Hall, A. Integrin-mediated activation of Cdc42 controls cell polarity in migrating astrocytes through PKCzeta. *Cell* **106,** 489–498 (2001).

47. Gundersen, G. G. Evolutionary conservation of microtubule-capture mechanisms. *Nature Rev. Mol. Cell Biol.* **3,** 296–304 (2002).

48. Lansbergen, G. and Akhmanova, A. Microtubule Plus End: A Hub of Cellular Activities *Traffic* **7**, 499–507 (2006)

49. Barth, A. I. & Nelson, W. J. What can humans learn from flies about adenomatous polyposis coli? *Bioessays* **24,** 771–774 (2002).

50. Nathke, M. *et al.* The adenomatous polyposis coli tumor suppressor protein localizes to plasma membrane sites involved in active cell migration. *J. Cell Biol.* **134,** 165–179 (1996).

51. Kawasaki, Y. *et al.* Asef, a link between the tumor suppressor APC and G-protein signaling. *Science* **289,** 1194–1197 (2000).

52. Kawasaki, Y., Sato, R. & Akiyama, T. Mutated APC and Asef are involved in the migration of colorectal tumour cells. *Nature Cell Biol.* **5,** 211–215 (2003).

53. Karin Kroboth, Ian P. Newton, Katsuhiro Kita, Dina Dikovskaya, Jurg Zumbrunn, Clare M. Waterman-Storer, and Inke S. Nathke Lack of Adenomatous Polyposis Coli Protein Correlates with a Decrease in Cell Migration and Overall Changes in Microtubule Stability. *Molecular Biology of the Cell* **18**, 910 – 918 (2007).

54. Fukata, M. *et al.* Rac1 and Cdc42 capture microtubules through IQGAP1 and CLIP-170. *Cell* **109,** 873–885 (2002).

55. Watanabe, T., Wang, S., Noritake, J., Sato, K., Fukata, M., Takefuji, M., Nakagawa, M., Izumi, N., Akiyama, T., and Kaibuchi, K. Interaction with IQGAP1 Links APC to Rac1, Cdc42, and Actin Filaments during Cell Polarization and Migration. *Developmental Cell* **7**, 871– 883 (2004).

56. Lansbergen, G., Grigoriev, I., Mimori-Kiyosue, Y., Ohtsuka, T., Higa, S., Kitajima, I., Demmers, J., Galjart, N., Houtsmuller, A. B., Grosveld, F. and Akhmanova, A. CLASPs Attach Microtubule Plus Ends to the Cell Cortex through a Complex with LL5β. *Developmental Cell* **11**, 21 – 32 (2006).

57. Kodama, A., Karakesisoglou, I., Wong, E., Vaezi, A. and Fuchs, E. ACF7: An Essential Integrator of Microtubule Dynamics. *Cell* **115**, 343–354 (2003).

58. Ishizaki, T., Morishima, Y., Okamoto, M., Furuyashiki, T., Kato T., and Narumiya., S. Coordination of microtubules and the actin cytoskeleton by the Rho effector mDia1. *Nature Cell Biol.* **3**, 8–14 (2000).

59. Hirokawa, N. & Takemura, R. Kinesin superfamily proteins and their various functions and dynamics. *Exp. Cell Res.* **301**, 50–59 (2004).

60. Vallee, R. B., Williams, J. C., Varma, D. & Barnhart, L. E. Dynein: An ancient motor protein involved in multiple modes of transport. *J. Neurobiol.* **58**, 189–200 (2004).

61. Bloom, G.S., Wagner, M.C., Pfister, K.K., and Brady, S.T. Native structure and physical properties of bovine brain kinesin and identification of the ATP-binding subunit polypeptide. *Biochemistry* **27**, 3409 – 3416 (1988)

62. Fehr, A. N., Asbury, C. L., & Block, S. M. Kinesin Steps do not alternate in size. *Biophysical Journal* **94**, 20–22 (2008).

63. Verbrugge, S., Kapitein, L. C., & Peterman, E. J. Kinesin moving through the spotlight: Single-motor fluorescence microscopy with submillisecond time resolution. *Biophysical Journal* **92,** 2536–2545 (2007).

64. Endow, S. A. Determinants of molecular motor directionality. *Nature Cell Biol.* **1**, 163–167 (1999).

65. Desai, A., Verma, S., Mitchison, T. J. & Walczak, C. E. Kin I kinesins are microtubule-destabilizing enzymes. *Cell* **96**, 69–78 (1999).

66. Tai, C. Y., Dujardin, D. L., Faulkner, N. E. & Vallee, R. B. Role of dynein, dynactin, and CLIP-170 interactions in LIS1 kinetochore function. *J. Cell Biol.* **156**, 959–968 (2002).

67. Schroer, T. A. Dynactin. *Annu. Rev. Cell Dev. Biol.* **20**, 759–779 (2004).

68. Verhey, K.J., Gaertig, J. The Tubulin Code. *Cell Cycle* **6**, 2152 – 2160 (2007)

69. Westermann, S., Weber, K. Post-translational modifications regulate microtubule function. *Nat Rev Mol Cell Biol* **4,** 938 – 947 (2003).

70. Redeker, V., Levilliers, N., Vinolo, E., Rossier, J., Jaillard, D., Burnette, D., Gaertig, J., Bre, M.H. Mutations of tubulin glycylation sites reveal cross-talk between the C termini of alpha- and beta-tubulin and affect the ciliary matrix in Tetrahymena. *J Biol Chem* **280,** 596 – 606 (2005).

71. Duan, J., Gorovsky, M.A. Both carboxy-terminal tails of alpha- and beta-tubulin are essential, but either one will suffice. *Cur Biol* **12**, 313 – 316 (2002).

72. Mary, J., Redeker, V., Le Caer, J. P., Prome, J. C. & Rossier, J. Class I and IVa β-tubulin isotypes expressed in adult mouse brain are glutamylated. *FEBS Lett.* **353**, 89–94 (1994).

73. Rudiger, M., Plessman, U., Kloppel, K. D., Wehland, J. & Weber, K. Class II tubulin, the major brain β tubulin isotype is polyglutamylated on glutamic acid residue 435. *FEBS Lett.* **308**, 101–105 (1992).

74. Schneider, A., Plessmann, U., Felleisen, R. & Weber, K. Posttranslational modifications of trichomonad tubulins; ide.ntification of multiple glutamylation sites. *FEBS Lett.* **429**, 399–402 (1998).

75. Redeker, V., Rossier, J. & Frankfurter, A. Posttranslational modifications of the C-terminus of α-tubulin in adult rat brain: α4 is glutamylated at two residues. *Biochemistry* **37**, 14838–14844 (1998).

76. Janke, C., Rogowski, K., Wloga, D., Regnard, C., Kajava, A.V., Strub, J.M., Temurak, N., van Dijk, J., Boucher, D., van Dorsselaer, A., Suryavanshi, S., Gaertig, J., Eddé, B. Tubulin polyglutamylase enzymes are members of the TTL domain protein family. *Science*, **308,** 1758 – 1762 (2005).

77. van Dijk, J., Rogowski, K., Miro, J., Lacroix, B., Edde, B., Janke, C. A targeted multienzyme mechanism for selective microtubule polyglutamylation. *Mol Cell*, **26,** 437 – 448 (2007).

78. Ikegami, K., Mukai, M., Tsuchida, J., Heier, R.L., Macgregor, G.R., Setou, M. TTLL7 is a mammalian beta-tubulin polyglutamylase required for growth of MAP2-positive neurites. *J Biol Chem*, **281,** 30707 – 3071 6 (2006).

79. Schneider, A., Plessmann, U. & Weber, K. Subpellicular and flagellar microtubules of *Trypanosoma brucei* are extensively glutamylated. *J. Cell Sci.* **110**, 431–437 (1997).

80. Larcher, J. C., Boucher, D., Lazereg, S., Gros, F. & Denoulet, P. Interaction of kinesin motor domains with α- and β-tubulin subunits at a tau-independent binding site. Regulation by polyglutamylation. *J. Biol. Chem.* **271**, 22117–22124 (1996).

81. Bonnet, C., Boucher, D., Lazereg, S., Pedrotti, B., Islam, K., Denoulet, P., Larcher, J.C. Differential binding regulation of microtubule-associated proteins MAP1A, MAP1B, and MAP2 by tubulin polyglutamylation. *J. Biol. Chem.* **276**, 12839–12848 (2001).

82. Okada, Y. & Hirokawa, N. Mechanism of the single-headed processivity: diffusional anchoring between the K-loop of kinesin and the C terminus of tubulin. *Proc. Natl Acad. Sci. USA* **97**, 640–645 (2000).

83. Million, K., Larcher, J., Laoukili, J., Bourguignon, D., Marano, F., Tournier, F. Polyglutamylation and polyglycylation of α- and β-tubulins during *in vitro* ciliated cell differentiation of human respiratory epithelial cells. *J. Cell Sci.* **112**, 4357–4366 (1999).

84. Bornens, M. Centrosome composition and microtubule anchoring mechanisms. *Curr. Opin. Cell Biol.* **14**, 25–34 (2002).

85. Rudiger, M., Plessmann, U., Rudiger, A. H. & Weber, K. β tubulin of bull sperm is polyglycylated. *FEBS Lett.* **364**, 147–151 (1995).

86. Plessmann, U. & Weber, K. Mammalian sperm tubulin: an exceptionally large number of variants based on several posttranslational modifications. *J. Protein Chem.* **16**, 385–390 (1997).

87. Mary, J., Redeker, V., Le Caer, J. P., Rossier, J. & Schmitter, J. M. Posttranslational modifications of axonemal tubulin. *J. Protein Chem.* **16**, 403–407 (1997).

88. Thazhath, R., Liu, C. & Gaertig, J. Polyglycylation domain of β-tubulin maintains axonemal architecture and affects cytokinesis in *Tetrahymena*. *Nature Cell Biol.* **4**, 256–259 (2002).

89. L'Hernault, S. W. & Rosenbaum, J. L. *Chlamydomonas* α-tubulin is posttranslationally modified by acetylation on the ε-amino group of a lysine. *Biochemistry* **24**, 473–478 (1985).

90. LeDizet, M. & Piperno, G. Identification of an acetylation site of *Chlamydomonas* α-tubulin. *Proc. Natl Acad. Sci. USA* **84**, 5720–5724 (1987).

91. Sasse, R. & Gull, K. Tubulin post-translational modifications and the construction of microtubular organelles in *Trypanosoma brucei*. *J. Cell Sci.* **90**, 577–589 (1988).

92. Garvalov, B.K., Zuber, B., Bouchet-Marquis, C., Kudryashev, M., Gruska, M., Beck, M., Leis A., Frischknecht, F., Bradke, F., Baumeister, W., Dubochet, J., Cyrklaff, M. Luminal particles within cellular microtubules. *J Cell Biol* **174,** 759 – 65 (2006).

93. Nogales, E., Whittaker, M., Milligan, R. A. & Downing, K. H. High-resolution model of the microtubule. *Cell* **96**, 79–88 (1999).

94. Hubbert, C., Guardiola, A., Shao, R., Kawaguchi, Y., Ito, A., Nixon, A., Yoshida, M., Wang, X.F., Yao, T.P. HDAC6 is a microtubule-associated deacetylase. *Nature* **417,** 455 – 458 (2002).

95. Matsuyama, A., Shimazu, T., Sumida, Y., Saito, A., Yoshimatsu, Y., Seigneurin-Berny, D., Osada, H., Komatsu, Y., Nishino, N., Khochbin, S., Horinouchi, S., Yoshida, M. In vivo destabilization of dynamic microtubules by HDAC6-mediated deacetylation. *EMBO J.* **21,** 6820 – 6831 (2002).

96. North, B.J., Marshall, B.L., Borra, M.T., Denu, J.M., Verdin, E. The human Sir2 ortholog, SIRT2, is an NAD+-dependent tubulin deacetylase. *Mol Cell* **11,** 437 – 444 (2003).

97. Reed, N.A., Cai, D., Blasius, T.L., Jih, G.T., Meyhofer, E., Gaertig, J., Verhey, K.J. Microtubule acetylation promotes kinesin-1 binding and transport. *Curr Biol*, **16,** 2166 – 2172 (2006).

98. Bulinski, J.C. Microtubule modification: acetylation speeds anterograde traffic flow. *Curr Biol*, **17,** 18 – 20 (2007).

99. Haggarty, S. J., Koeller, K. M., Wong, J. C., Grozinger, C. M. & Schreiber, S. L. Domain-selective small-molecule inhibitor of histone deacetylase 6 (HDAC6)-mediated tubulin deacetylation. *Proc. Natl Acad. Sci. USA* **100**, 4389–4394 (2003).

100. Gard, D.L., Kirschner, M.W. A polymer-dependent increase in phosphorylation of beta-tubulin accompanies differentiation of a mouse neuroblastoma cell line. *J Cell Biol* **100,** 764 – 774 (1985).

101. Faruki, S., Geahlen, R.L., Asai, D.J. Syk-dependent phosphorylation of microtubules in activated B-lymphocytes. *J Cell Sci* **113,** 2557 – 2565 (2000).

102. Peters, J.D., Furlong, M.T., Asai, D.J., Harrison, M.L., Geahlen, R.L. Syk, activated by cross-linking the B-cell antigen receptor, localizes to the cytosol where it interacts with and phosphorylates alpha-tubulin on tyrosine. *J Biol Chem* **271,** 4755 – 4762 (1996).

103. Fourest-Lieuvin, A., Peris, L., Gache, V., Garcia-Saez, I., Juillan-Binard, C., Lantez, V., Job, D. Microtubule regulation in mitosis: Tubulin phosphorylation by the cyclin-dependent kinase Cdk1. *Mol Biol Cell* **17,** 1041 – 1050 (2006).

104. Bartolini, F., Moseley, J. B., Schmoranzer, J., Cassimeris, L., Goode, B. L. and Gundersen G. G. The formin mDia2 stabilizes microtubules independently of its actin nucleation activity *J Cell Biol* **181,** 523–536 (2008)

105. Caron, J. M. Posttranslational modification of tubulin by palmitoylation: I. *In vivo* and cell-free studies. *Mol. Biol. Cell* **8**, 621–636 (1997).

106. Ozols, J. & Caron, J. M. Posttranslational modification of tubulin by palmitoylation: II. Identification of sites of palmitoylation. *Mol. Biol. Cell* **8**, 637–645 (1997).

107. Caron, J. M., Vega, L. R., Fleming, J., Bishop, R. & Solomon, F. Single site α-tubulin mutation affects astral microtubules and nuclear positioning during anaphase in *Saccharomyces cerevisiae*: possible role for palmitoylation of α-tubulin. *Mol. Biol. Cell* **12**, 2672–2687 (2001).

108. Preston, S. F., Deanin, G. G., Hanson, R. K. & Gordon, M. W. The phylogenetic distribution of tubulin tyrosine ligase. *J Mol Evol* **13,** 233–244 (1979)

109. Barra, H.S., Arce, C.A. and Argarana, C.E. Posttranslational tyrosination / detyrosination of tubulin. *Mol Neurobiol* **2,** 133–153 (1988).

110. Argarana, C. E., Barra, H. S. & Caputto, R. Release of [14C]tyrosine from tubulinyl-[14C]tyrosine by brain extract. Separation of a carboxypeptidase from tubulin-tyrosine ligase. *Mol Cell Biochem* **19**, 17–21 (1978).

111. Westermann, S., Weber, K., Post-translational modifications regulate microtubule function. *Nat Rev Mol Cell Biol* **4,** 938 – 947 (2003).

112. Kalinina, E., Biswas, R., Berezniuk, I., Hermoso, A., Aviles, F.X., Fricker, L.D. A novel subfamily of mouse cytosolic carboxypeptidases. *Faseb J* **21,** 836 – 850 (2007).

113. Ersfeld, K., Wehland, J., Plessmann, U., Dodemont, H., Gerke, V., Weber, K. Characterization of the tubulin-tyrosine ligase. *J Cell Biol* **120,** 725 – 732 (1993).

114. Arce, C. A., Hallak, M. E., Rodriguez, J. A., Barra, H. S. and Caputto, R. Capability of tubulin and microtubules to incorporate and to release tyrosine and phenylalanine and the effect of the incorporation of these amino acids on tubulin assembly. *J Neurochem* **31,** 205 – 210 (1978).

115. Janke, C., Rogowski, K., Wloga, D., Regnard, C., Kajava, A.V., Strub, J.M., Temurak, N., van Dijk, J., Boucher, D., van Dorsselaer, A., Suryavanshi, S., Gaertig, J., Edde, B. Tubulin polyglutamylase enzymes are members of the TTL domain protein family. *Science* **308,** 1758 – 1762 (2005).

116. Paturle-Lafanechere, L., Edde, B., Denoulet, P., Van Dorsselaer, A., Mazarguil, H., Le Caer, J. P., Wehland, J. & Job, D. Characterization of a major brain tubulin variant which cannot be tyrosinated. *Biochemistry* **30,** 10523–10528 (1991).

117. Rudiger, M., Wehland, J. & Weber, K. The carboxy-terminal peptide of detyrosinated α tubulin provides a minimal system to study the substrate specificity of tubulin-tyrosine ligase. *Eur J Biochem* **220**, 309–320 (1994).

118. Paturle-Lafanechere, L., Manier, M., Trigault, N., Pirollet, F., Mazarguil, H. & Job, D. Accumulation of delta 2-tubulin, a major tubulin variant that cannot be tyrosinated, in neuronal tissues and in stable microtubule assemblies. *J Cell Sci* **107,** 1529–1543 (1994).

119. Gundersen G. G., Kalnoski, M. H. & Bulinski, J. C. Distinct populations of microtubules: tyrosinated and nontyrosinated alpha tubulin are distributed differently in vivo *Cell* **38,** 779–789 (1984).

120. Kreis, T. E. Microtubules containing detyrosinated tubulin are less dynamic. *EMBO J* **6,** 2597–2606 (1987).

121. Wehland, J. & Weber, K. Turnover of the carboxy-terminal of alpha-tubulin and means of reaching elevated levels of detyrosination in living cells. *J Cell Sci* **88,** 185–203 (1987).

122. Webster, D. R., Wehland, J., Weber, K. & Borisy, G. G. Detyrosination of alpha-tubulin does not stabilze microtubules in vivo. *J Cell Biol* **111,** 113–122 (1990).

123. Banerjee, A. Coordination of posttranslational modifications of bovine brain α-tubulin. Polyglycylation of δ2 tubulin. *J Biol Chem* **277**, 46140–46144 (2002).

124. Mialhe, A., L. Lafanechere, I. Treilleux, N. Peloux, C. Dumontet, A. Bremond, M.H. Panh, R. Payan, J. Wehland, R.L. Margolis, and D. Job. Tubulin detyrosination is a frequent occurrence in breast cancers of poor prognosis. *Cancer Res* **61,** 5024–5027 (2001).

125. Erck, C., L. Peris, A. Andrieux, C. Meissirel, A.D. Gruber, M. Vernet, A. Schweitzer, Y. Saoudi, H. Pointu, C. Bosc, et al. A vital role of tubulin-tyrosine-ligase for neuronal organization. *Proc Natl Acad Sci USA* **102,** 7853–7858 (2005).

126. Murofushi, H. Purification and characterization of tubulintyrosine ligase from porcine brain *J Biochem* **87**, 979–984 (1980).

127. Galperin, M. Y. & Koonin, E. V. A diverse superfamily of enzymes with ATP-dependent carboxylate-amine/thiol ligase activity. *Protein Sci* **6**, 2639–2643 (1997).

128. Peris, L., M. Thery, J. Fauré, Y. Saoudi, L. Lafanechère, J.K. Chilton, P. Gordon- Weeks, N. Galjart, M. Bornens, L. Wordeman, Wehland, J., Andrieux, A., Job, D. Tubulin tyrosination is a major factor affecting the recruitment of CAP-Gly proteins at microtubule plus ends. *J Cell Biol* **174,** 839–849 (2006).

129. Reed, N.A., Cai, D., Blasius, T.L., Jih, G.T., Meyhofer, E., Gaertig, J., Verhey, K.J. Microtubule acetylation promotes kinesin-1 binding and transport. *Curr Biol* **16,** 2166 – 2172 (2006).

130. Liao, G., Gundersen, G.G. Kinesin is a candidate for crossbridging microtubules and intermediate filaments. Selective binding of kinesin to detyrosinated tubulin and vimentin. *J Biol Chem* **273,** 9797 – 9803 (1998).

131. Kreitzer, G., Liao, G., Gundersen, G.G. Detyrosination of tubulin regulates the interaction of intermediate filaments with microtubules in vivo via a kinesin-dependent mechanism. *Mol Biol Cell* **10,** 1105 – 1118 (1999).

132. Lin, S.X., Gundersen, G.G., Maxfield, F.R. Export from pericentriolar endocytic recycling compartment to cell surface depends on stable, detyrosinated (glu) microtubules and kinesin. *Mol Biol Cell* **13,** 96 – 109 (2002).

133. Arce, C.A., Rodriguez, J.A., Barra, H.S., Caputo, R,. Incorporation of L-tyrosine, L-phenylalanine and L-3,4-dihydroxyphenylalanine as single units into rat brain tubulin. *Eur J Biochem* **59,** 145–149 (1975).

134. Joniau, M., Coudijzer, K., De Cuyper, M. Reaction of alpha-tubulin with iodotyrosines catalyzed by tubulin:tyrosine ligase: carboxy- terminal labeling of tubulin with [125I]monoiodotyrosine. *Anal Biochem* **184,** 325–329 (1990).

135. Peris, L., Wagenbach, M., Lafanechère, L., Brocard, J., Moore, A.T., Kozielski, F., Job, D., Wordeman, L. and Andrieux, A. Motor-dependent microtubule disassembly driven by tubulin tyrosination. *J Cell Biol* **185,** 1159–1166 (2009).

136. Eiserich, J. P., Estévez, A.G., Bamberg, T.V., Ye, Y.Z., Chumley, P.H., Beckman, J.S., Freeman, B.A. Microtubule dysfunction by posttranslational nitrotyrosination of α-tubulin: a nitric oxide-dependent mechanism of cellular injury. *Proc Natl Acad Sci USA* **96**, 6365–6370 (1999).

137. Kalisz, H. M., Erck, C., Plessmann, U. & Wehland, J. Incorporation of nitrotyrosine into α-tubulin by recombinant mammalian tubulin-tyrosine ligase. *Biochim Biophys Acta* **1481**, 131–138 (2000).

138. Chang, W. Webster, D.R., Salam, A.A., Gruber, D., Prasad, A., Eiserich, J.P., Bulinski, J.C. Alteration of the C-terminal amino acid of tubulin specifically inhibits myogenic differentiation. *J Biol Chem* **277**, 30690–30698 (2002).

139. Zhang, T., Zaal, K. J. M., Sheridan, J., Mehta, A., Gundersen, G. G.and Ralston, E. Microtubule plus-end binding protein EB1 is necessary for muscle cell differentiation, elongation and fusion *Journal of Cell Science* **122,** 1401 – 1409 (2009).

140. Saitoh, O., Arai, T. and Obinata, T. Distribution of microtubules and other cytoskeletal filaments during myotube elongation as revealed by fluorescence microscopy. *Cell Tissue Res* **252,** 263 – 273 (1988).

141. Tirnauer, J.S., Bierer, B.E. EB1 proteins regulate microtubule dynamics, cell polarity, and chromosome stability. *J Cell Biol* **149,** 761–766 (2000).

142. Morrison, E.E., Wardleworth, B.N., Askham, J.M., Markham, A.F., Meredith, D.M. EB1, a protein which interacts with the APC tumour suppressor, is associated with the microtubule cytoskeleton throughout the cell cycle. *Oncogene* **17,** 3471–3477 (1998).

143. Rogers, S.L., Rogers, G.C., Sharp, D.J., Vale, R.D. Drosophila EB1 is important for proper assembly, dynamics, and positioning of the mitotic spindle. *J Cell Biol* **158,** 873–884 (2002).

144. Tirnauer, J.S., O'Toole, E., Berrueta, L., Bierer, B.E., Pellman, D. Yeast Bim1p promotes the G1-specific dynamics of microtubules. *J Cell Biol* **145,** 993–1007 (1999).

145. Komarova, Y., De Groot, C. O., Grigoriev, I., Montenegro Gouveia, S., Munteanu, E. L., Schober J. M., Honnappa, S., Buey, R. M., Hoogenraad, C. C., Dogterom, M., Borisy, G. G., Steinmetz, M.O., and Akhmanova, A.. Mammalian end binding proteins control persistent microtubule growth. *The Journal of Cell Biology* **184,** 691-706 (2009)

146. Straube , A., and Merdes, A. EB3 regulates microtubule dynamics at the cell cortex and is required for myoblast elongation and fusion. *Curr. Biol* **17,** 1318 – 1325 (2007).

147. Hayashi, I., and Ikura, M. Crystal structure of the amino-terminal microtubule-binding domain of end-binding protein 1 (EB1). *J Biol Chem* ***278*****,** 36430–36434 (2003).

148. Honnappa, S., John, C. M., Kostrewa, D., Winkler, F. K., and Steinmetz, M. O. Structural insights into the EB1-APC interaction. *EMBO J* ***24*****,** 261–269 (2005).

149. Slep, K. C., Rogers, S. L., Elliott, S. L., Ohkura, H., Kolodziej, P. A., and Vale, R. D. Structural determinants for EB1-mediated recruitment of APC and spectraplakins to the microtubule plus end. *J Cell Biol* **168,** 587–598 (2005).

150. Komarova, Y., Lansbergen, G., Galjart, N., Grosveld, F., Borisy, G. G. and Akhmanova, A. EB1 and EB3 control CLIP dissociation from the ends of growing microtubules. *Mol Biol Cell* **16,** 5334–5345 (2005).

151. Bu, W. and Su, L. K. Characterization of functional domains of human EB1 family proteins. *J Biol Chem* **278,** 49721–49731 (2003).

152. Akhmanova , A. and M.O. Steinmetz. Tracking the ends: a dynamic protein network controls the fate of microtubule tips. *Nat Rev Mol Cell Biol* **9,** 309 – 322 (2008).

153. Miller, R. K., D'Silva, S., Moore, J. K. & Goodson, H. V. The CLIP-170 orthologue Bik1p and positioning the mitotic spindle in yeast. *Curr Top Dev Biol* **76**, 49–87 (2006).

154. Weisbrich, A., Honnappa, S., Jaussi, R., Okhrimenko, O., Frey, D., Jelesarov, I., Akhmanova, A., Steinmetz, M.O. Structure-function relationship of CAP-Gly domains. *Nature Struct Mol Biol* **14**, 959–967 (2007).

155. Su, L-K., Burrell, M., Hill, D. E., Gyuris, J., Brent, R., Wiltshire, R., Trent, J., Vogelstein, B. and Kinzler, K. W. APC binds to the novel protein EB1. *Cancer Res* **55,** 2972– 2977 (1995).

156. Schroder, J.M., Schneider, L., Christensen, S .T. and Pedersen, L .B. EB1 is required for primary cilia assembly in fibroblasts. *Curr Biol* **17,** 1134 – 1139 (2007).

157. Bienz, M. Spindles cotton on to junctions, APC and EB1. Nat Cell Biol **3,** 67–68 (2001).

158. Green, R. A., Wollman, R. and Kaplan, K. B. APC and EB1 function together in mitosis to regulate spindle dynamics and chromosome alignment. *Mol Biol Cell* **16,** 4609–4622 (2005).

159. Rehberg, M. and Graf, R. *Dictyostelium* EB1 is a genuine centrosomal component required for proper spindle formation. *Mol Biol Cell* **13,** 2301 – 2310 (2002).

160. Maiato, H., DeLuca, J., Salmon, E. D. and Earnshaw, W. C. (2004) The dynamic kinetochore-microtubule interface. J. Cell Sci. **117,** 5461–5477.

161. Goodson, H. V., Skube, S.B., Stalder, R., Valetti, C., Kreis, T.E., Morrison, E.E., Schroer,T.A. CLIP-170 interacts with dynactin complex and the APC-binding protein EB1 by different mechanisms. *Cell Motil Cytoskeleton* **55**, 156–173 (2003).

162. Lansbergen, G., Komarova, Y., Modesti, M., Wyman, C., Hoogenraad, C.C., Goodson, H.V., Lemaitre, R.P., Drechsel, D,N., van Munster, E., Gadella, T.W. Jr, Grosveld, F., Galjart, N., Borisy, G.G., Akhmanova, A. Conformational changes in CLIP-170 regulate its binding to microtubules and dynactin localisation. *J Cell Biol* **166**, 1003–1014 (2004).

163. Hayashi, I., Plevin, M. J. & Ikura, M. Autoinhibitory interactions within CLIP-170 mimic the intermolecular binding modes of $p150^{Glued}$ and EB1, providing a structural basis for the regulation of microtubule dynamics. *Nature Struct Biol* **14**, 980–981 (2007).

164. De Zeeuw, C. I., Hoogenraad, C.C., Goedknegt, E., Hertzberg, E., Neubauer, A., Grosveld, F., Galjart, N. CLIP-115, a novel brain-specific cytoplasmic linker protein, mediates the localization of dendritic lamellar bodies. *Neuron* **19**, 1187–1199 (1997).

165. Pierre, P., Scheel, J., Rickard, J.E., Kreis, T.E. CLIP-170 links endocytic vesicles to microtubules. *Cell* **70,** 887–900 (1992)

166. Perez, F., Diamantopoulos, G.S., Stalder, R., Kreis, T.E. CLIP-170 highlights growing microtubule ends in vivo. *Cell* **96,** 517–527 (1999)

167. Steinmetz, M.O. and Akhmanova, A. Capturing protein tails by CAP-Gly domains *Trends in Biochemical Sciences* **33,** 535-545 (2008)

168. Bieling, P., Laan, L., Schek, H., Munteanu, E.L., Sandblad, L., Dogterom, M., Brunner, D., Surrey, T. Reconstitution of a microtubule plus-end tracking system in vitro. *Nature* **450,** 1100–1105 (2007).

169. Komarova, Y.A., Akhmanova, A.S., Kojima, S., Galjart, N., Borisy, G.G. Cytoplasmic linker proteins promote microtubule rescue in vivo. *J Cell Biol* **159,** 589–599 (2002).

170. Watson, P. and Stephens, D.J. Microtubule plus-end loading of $p150^{Glued}$ is mediated by EB1 and CLIP-170 but is not required for intracellular membrane traffic in mammalian cells. J Cell Sci **119,** 2758–2767 (2006).

171. Tanenbaum, M.E., Galjart, N., van Vugt, M.A., Medema, RH. CLIP-170 facilitates the formation of kinetochore-microtubule attachments. *EMBO J* **25,** 45–57 (2006)

172. Dujardin, D., Wacker ,U.I., Moreau, A., Schroer, T.A., Rickard, J.E., De Mey, J.R. Evidence for a role of CLIP-170 in the establishment of metaphase chromosome alignment. *J Cell Biol* **141**, 849–862 (1998).

173. Xiang, X. LIS1 at the microtubule plus end and its role in dynein-mediated nuclear migration. *J. Cell Biol* **160**, 289–290 (2003).

174. Lallemand-Breitenbach, V. et al. CLIPR-59 is a lipid raftassociated protein containing a cytoskeleton-associated protein glycine-rich domain (CAP-Gly) that perturbs microtubule dynamics. *J Biol Chem* **279,** 41168–41178 (2004).

175. Ota, T. et al. Complete sequencing and characterization of 21,243 full-length human cDNAs. *Nat Genet* **36,** 40–45 (2004)

176. Lopez-Fanarraga, M., Avila, J., Guasch, A., Coll, M., Zabala, J.C. Review: postchaperonin tubulin folding cofactors and their role in microtubule dynamics. *J Struct Biol* **135,** 219–229 (2001).

177. Courtois, G. Tumor suppressor CYLD: negative regulation of NF-kB signaling and more. Cell. *Mol Life Sci* **65,** 1123–1132 (2008)

178. Hoppeler-Lebel, A., Celati, C., Bellett, G., Mogensen, M.M., Klein-Hitpass, L., Bornens, M., Tassin, A.M. Centrosomal CAP350 protein stabilises microtubules associated with the Golgi complex. *J Cell Sci* **120,** 3299–3308 (2007)

179. Asaba, N., Hanada, T., Takeuchi, A., Chishti, A.H. Direct interaction with a kinesin-related motor mediates transport of mammalian discs large tumor suppressor homologue in epithelial cells. J Biol Chem **278,** 8395–8400 (2003)

180. Akhmanova, A., Hoogenraad, C.C., Drabek, K., Stepanova, T., Dortland, B., Verkerk, T., Vermeulen, W., Burgering, B.M., De Zeeuw, C.I., Grosveld, F., Galjart, N. CLASPs are CLIP-115 and-170 associating proteins involved in the regional regulation of microtubule dynamics in motile fibroblasts. *Cell* **104**,923–935 (2001).

181. Mimori-Kiyosue, Y., I. Grigoriev, G. Lansbergen, H. Sasaki, C. Matsui, F. Severin, N. Galjart, F. Grosveld, I. Vorobjev, S. Tsukita, and A. Akhmanova. CLASP1 and CLASP2 bind to EB1 and regulate microtubule plus-end dynamics at the cell cortex. *J Cell Biol* **168,** 141–153 (2005).

182. Maiato, H., Fairley, E.A., Rieder, C.L., Swedlow, J.R., Sunkel, C.E., Earnshaw, W.C. Human CLASP1 is an outer kinetochore component that regulates spindle microtubule dynamics. *Cell* **113**, 891–904 (2003).

183. Wittmann, T., and Waterman-Storer, C.M. Spatial regulation of CLASP affinity for microtubules by Rac1 and GSK3beta in migrating epithelial cells. *J Cell Biol* **169,** 929 939 (2005).

184. Drabek, K., van Ham, M., Stepanova, T., Draegestein, K., van Horssen, R., Sayas, C.L., Akhmanova, A., Ten Hagen, T., Smits, R., Fodde, R., Grosveld F., and Galjart, N. Role of CLASP2 in microtubule stabilization and the regulation of persistent motility. *Curr Biol* **16**, 2259 – 2264 (2006).

185. Nathke, I. S. The Adenomatous Polyposis Coli protein: the Achilles heel of the gut epithelium. *Annu Rev Cell Dev Biol* ***20,*** 337–366 (2004).

186. Kaplan, K. B., Burds, A., Swedlow, J. R., Bekir, S. S., Sorger, P. K., and Nathke, I. S. A novel role for the APC tumour suppressor in chromosome segregation. *Nat Cell Biol* ***3,*** 429–432 (2001).

187. Mogensen, M. M., Tucker, J. B., Mackie, J. B., Prescott, A. R., and Nathke, I. S. The adenomatous polyposis coli protein unambiguously localizes to microtubule plus ends and is involved in establishing parallel arrays of microtubule bundles in highly polarized epithelial cells. *J Cell Biol* ***157,*** 1041–1048 (2002).

188. Zumbrunn, J., Inoshita, K., Hyman, A. A., and Nathke, I. S. Binding of the Adenomatous Polyposis Coli protein to microtubules increases microtubule stability and is regulated by GSK3β phosphorylation. *Curr Biol* **11**, 44–49 (2001).

189. Wen, Y., Eng, C. H., Schmoranzer, J., Cabrera-Poch, N., Morris, E. J., Chen, M., Wallar, B. J., Alberts, A. S., and Gundersen, G. G. EB1 and APC bind to mDia to stabilize microtubules downstream of Rho and promote cell migration. *Nat Cell Biol* **6,** 820–830 (2004).

190. Nathke, I. APC at glance. *Journal of cell science* **117**, 4873-4875 (2004)

191. Dikovskaya, D., Zumbrunn, J., Penman, G. A. and Näthke, I. S. The Adenomatous Polyposis Coli protein, in the limelight out at the edge. *Trends Cell Biol* **11**, 378-384 (2001).

192. Grigoriev, I., Gouveia, S.M., van der Vaart, B., Demmers, J., Smyth, J.T., Honnappa, S., Splinter, D., Steinmetz, M.O., Putney, J.W. Jr, Hoogenraad, C.C., Akhmanova, A. STIM1 is a microtubule plus end tracking protein involved in remodeling of the endoplasmic reticulum. *Curr Biol* **18**, 177–182 (2008).

193. Gard, D. L., Becker, B. E. & Josh Romney, S. MAPping the eukaryotic tree of life: structure, function, and evolution of the MAP215/Dis1 family of microtubuleassociated proteins. *Int. Rev. Cytol* **239**, 179–272 (2004).

194. Al-Bassam, J., Larsen, N. A., Hyman, A. A. & Harrison, S. C. Crystal structure of a TOG domain: conserved features of XMAP215/Dis1-family TOG domains and implications for tubulin binding. *Structure* **15**, 355–362 (2007).

195. Kim, M. H., Cooper, D.R., Oleksy, A., Devedjiev, Y., Derewenda, U., Reiner, O., Otlewski, J., Derewenda, Z.S. The structure of the N-terminal domain of the product of the lissencephaly gene Lis1 and its functional implications. *Structure* **12**, 987–998 (2004).

196. Dragestein, K. A., van Cappellen, W. A., van Haren, J.,Tsibidis, G. D., Akhmanova, A., Knoch, T. A., Grosveld, F., and Galjart N. Dynamic behavior of GFP – CLIP-170 reveals fast protein turnover on microtubule plus ends *The Journal of Cell Biology* **180,** 729-37 (2008).

197. Dujardin, D.L., Vallee, R.B. Dynein at the cortex. *Curr Opin Cell Biol* **14,** 44–49 (2002).

198. Jimbo, T., Kawasaki, Y., Koyama, R., Sato, R., Takada, S., Haraguchi, K., Akiyama, T. Identification of a link between the tumour suppressor APC and the kinesin superfamily *Nature cell boil* **4,** 323 – 327 (2002)

199. Fukata, M., Watanabe, T., Noritake, J., Nakagawa, M., Yamaga, M., Kuroda, S., Matsuura, Y., Iwamatsu, A., Perez, F., Kaibuchi, K. Rac1 and Cdc42 capture microtubules through IQGAP1 and CLIP-170. *Cell* **109,** 873–885 (2002).

200. Etienne-Manneville, S., Manneville, J.B., Nicholls, S., Ferenczi, M.A., Hall, A. Cdc42 and Par6-PKC{zeta} regulate the spatially localized association of Dlg1 and APC to control cell polarization. *J Cell Biol* **170,** 895–901 (2005).

201. Xiao, H., El Bissati, K., Verdier-Pinard, P., Burd, B., Zhang, H., Kim, K., Fiser, A., Hogue, R. Angeletti, and. Weiss, L. M. Post-Translational Modifications to Toxoplasma gondii α- and β-Tubulins Include Novel C-Terminal Methylation *Journal of Proteome Research,* **9,** 359–372(2010).

202. Bershadsky, A.D., Vaisberg, E.A., and Vasiliev, J.M. Pseudopodial activity at the active edge of migrating fibroblast is decreased after drug-induced microtubule depolymerization. *Cell Motil Cytoskeleton* **19,** 152–158 (1991).

203. Mataraza, J.M., Briggs, M.W., Li, Z., Entwistle, A., Ridley, A.J., and Sacks, D.B. IQGAP1 promotes cell motility and invasion. *J Biol Chem* **278,** 41237–41245 (2003).

204. Siegrist, S.E. and Doe, C.Q. Microtubule-induced cortical cell polarity. *Genes and development* **21,** 483–496 (2007).

205. Benais-Pont, G., Punn, A., Flores-Maldonado, C., Eckert, J., Raposo, G., Fleming, T.P., Cereijido, M., Balda, M.S., and Matter, K. Identification of a tight junction-associated guanine nucleotide exchange factor that activates Rho and regulates paracellular permeability. *J Cell Biol* **160:** 729– 740 (2003).

206. Callow, M.G., Zozulya, S., Gishizky, M.L., Jallal, B., and Smeal, T. 2005. PAK4 mediates morphological changes through the regulation of GEF-H1. *J Cell Sci* **118:** 1861 1872.

207. Ren, Y., Li, R., Zheng, Y., and Busch, H. Cloning and characterization of GEF-H1, a microtubule-associated guanine nucleotide exchange factor for Rac and Rho GTPases. *J Biol Chem* **273,** 34954–34960 (1998).

208. Blangy, A., Vignal, E., Schmidt, S., Debant, A., Gauthier-Rouviere, C., and Fort, P. TrioGEF1 controls Rac- and Cdc42-dependent cell structures through the direct activation of rhoG. *J Cell Sci* **113,** 729–739(2000).

209. Shpetner, H.S. and Vallee, R.B. Dynamin is a GTPase stimulated to high levels of activity by microtubules. *Nature* **355,** 733–735 (1992).

210. Wittmann, T., Bokoch, G.M., and Waterman-Storer, C.M. Regulation of microtubule destabilizing activity of Op18/ stathmin downstream of Rac1. *J Biol Chem* **279,** 6196– 6203 (2004).

211. Etienne-Manneville, S. and Hall, A. Cdc42 regulates GSK- 3β and adenomatous polyposis coli to control cell polarity. *Nature* **421,** 753–756 (2003).

212. Kumar, P., Lyle, K.S, . Gierke, S., Matov, A., Danuser, G. and Wittmann T. GSK3β phosphorylation modulates CLASP – microtubule association and lamella microtubule attachment *J Cell Biol* **184**, 895–908 (2009).

213. Li, R. and Gundersen, G. G., Beyond polymer polarity: how the cytoskeleton builds a polarized cell. *Nature Rev Mol cell biol* **9,** 860 – 873 (2008).

214. Marcos, S., Moreau, J., Backer, S., Job, D., Andrieux, A., Bloch- Gallego, E. Tubulin Tyrosination Is Required for the Proper Organization and Pathfinding of the Growth Cone *PLoS ONE* **4,** 1 – 16 (2009).

215. Juwana, J.P., Hendrikx, P., Mischo, A., Wadle, A., Fadle, N., Gerlach, K., Arends, J.M, Hoogenboom, H., Pfreundschuh, M. and Renner, C. *EB/RP* Gene family encodes tubulin binding proteins *Int J Cancer:* **81,** 275–284 (1999).

216. van Hagen, J. M., van der Geest, J. N., van der Giessen, R. S., Lagers-van Haselen, G. C., Eussen, H. J., Gille, J. J., et al. Contribution of CYLN2 and GTF2IRD1 to neurological and cognitive symptoms in Williams Syndrome. *Neurobiology of Disease **26,*** 112–124 (2007).

217. Hoogenraad, C. C., Akhmanova, A., Galjart, N., & De Zeeuw, C. I. LIMK1 and CLIP-115: Linking cytoskeletal defects to Williams syndrome. *Bioessays **26,*** 141–150 (2004).

218. Hoogenraad, C. C., Koekkoek, B., Akhmanova, A., Krugers, H., Dortland, B., Miedema, M., et al. Targeted mutation of Cyln2 in the Williams syndrome critical region links CLIP-115 haploinsufficiency to neurodevelopmental abnormalities in mice. *Nature Genetics* **32,** 116–127 (2002).

219. Hoogenraad, C.C., Akhmanova, A., Grosveld, F., De Zeeuw, C. I., and Galjart, N., Functional analysis of CLIP-115 and its binding to microtubules *Journal of Cell Science* **113,** 2285-2297 (2000).

220. Pierre, P., Pepperkok, R., and Kreis, T. E. Molecular characterization of two functional domains of CLIP-170 in vivo *Journal of Cell Science* **107,** 1909-1920 (1994).

221. van der Sluijs, P., Bennet, M. K., Antony, C., Simons, K. and Kreis, T. E. Binding of exocytic vesicles from MDCK cells to microtubules in vitro. *J. Cell Sci.* **95**, 545-553 (1990).

222. Karecla, P. I. and Kreis, T. E. Interaction of membranes of the Golgi complex with microtubules in vitro. *Eur J Cell Biol* **57,** 139 – 146 (1992).

223. Pierre, P., Scheel, J., Rickard, J. E. and Kreis, T. E. CLIP-170 links endocytic vesicles to microtubules. *Cell* **70,** 887-900 (1992).

224. De Zeeuw, C. I., Hertzberg, E. L. & Mugnaini, E. The dendritic lamellar body: a new neuronal organelle putatively associated with dendrodendritic gap junctions. *J Neurosci* **15**, 1587–1604 (1995).

225. Perez, F., Pernet-Gallay, K., Nizak, C., Goodson, H.V., Kreis, T.E., Goud, B. CLIPR-59, a new *trans*-Golgi/TGN cytoplasmic linker protein belonging to the CLIP-170 family. *J Cell Biol* **156**, 631–642 (2002).

226. Gupta, K. K., Joyce, M. V., Slabbekoorn, A. R , Zhu, Z. C., Paulson, B. A., Boggess, B. and Goodson, H. V., Probing Interactions between CLIP-170, EB1, and Microtubules. *J Mol Biol* **395,** 1049–1062 (2010)

227. Ikegami, K., Setou, M., TTLL10 can perform tubulin glycylation when co-expressed with TTLL8. *FEBS Lett* **12,** 1957 – 1953 (2009)

228. Wloga, D., Webster, D.M., Rogowski, K., Bre, M.H., Levilliers, N., Jerka-Dziadosz, M, Janke, C., TTLL3 is a tubulin ligase that regulates the assembly of cilia. *Dev Cell* **16**, 867 – 876 (2009)

229. Bellett, G., Carter, J.M., Keynton, J., Goldspink, D., James, C., Moss, D.K., Mogensen, M.M., Microtubule plus-end and minus-and capture at adherens junctions is involved in assembly of apico-basal arrays in polarized epithelial cells. *Cell Motil Cyt* oskeleton **66,** 893 – 908 (2009)

230. Billadeau, D.D., Nolz, J.C., Gomez, T.S., Regulation of T-cell activation by the cytoskeleton. *Nat Rev Immunol* **7,** 131 – 143 (2007)